A STUDY OF THE BERG AUKAS-TYPE Pb-Zn-V DEPOSITS IN THE OTAVI MOUNTAIN LAND, NAMIBIA

by

Peter J Chadwick

Submitted in fulfillment
for the degree of Master
of Science (Geology) at the
University of Cape Town.

January. 1993

All arguments and interpretations presented in this thesis are my own except where referenced.

Signed by candidate

Peter J Chadwick

ABSTRACT

This study is focussed on the petrographic and isotopic aspects of the crystallization processes, taking place in carbonate-hosted Berg Aukas-type Zn-Pb-V deposits of the Otavi Mountain Land in Northern Namibia. Numerous studies have shown that ore formation in Mississippi Valley-type deposits, bears a close relationship with carbonate diagenesis and basin evolution. The application of isotope (Sr, O, C) techniques as regards to timing and mechanisms of ore-forming processes, as a possible tool in exploration, is especially emphasized in this study.

Detailed petrographic and isotope-geochemical investigations were carried out in the Late Precambrian deposits of Berg Aukas, situated just north of the town of Grootfontein, in addition to the Odin Prospect situated to the east of Kombat Mine. Both ore deposits display many similarities, but also show differences concerning the facies-bound character of the host rock, which is related to the paleogeographic position and the tectonic framework. In spite of these differences, similar complex diagenetic textures and structures suggest a comparable diagenetic evolution.

Isotope-geochemical analyses have been performed on samples of consecutive crystallization generations, or dolomite types. This was checked petrographically using cathodoluminescence, and sample homogeneity was monitored by means of X-ray diffraction. The results reveal significant isotopic trends, which are interpreted to reflect the diagenetic evolution of the respective basin.

A consistent strontium isotope trend is noted, and in both cases studied the later crystallization generations are enriched in radiogenic strontium, as compared to the earlier ones, which tend to approximate the strontium isotope composition of contemporaneous seawater. The increase in $^{87}Sr/^{86}Sr$ ratios in subsequent diagenetic generations is explained with the pore fluids evolving towards more radiogenic compositions with advancing diagenetic stages. The influence of basinal brines enriched in radiogenic strontium as a consequence of the reaction with Rb-bearing phases, especially detrital (clay) minerals hosted by underlying basement rocks, is considered to be most likely.

Stable isotope investigations carried out on identical samples also show certain trends, though these are less pronounced compared to the strontium studies. In general, the later crystallization generations are depleted in the heavy isotope of carbon and oxygen, which is explained in terms of changing physico-chemical conditions of the system, in combination with changing fluid compositions during the coarse of diagenetic evolution.

By combining petrographic and isotopic observations, the genetic hypothesis for the ore deposits at Berg Aukas and Odin can be significantly constrained. In both cases, a model is proposed based on basinal brine migration during advanced diagenetic stages. These brines were enriched in radiogenic strontium due to the interaction with basement rocks.

Thus, the combination of petrographic and isotope-geochemical methods has proved to constitute a powerful tool in tracing the diagenetic evolution, and in an exploration sense may be used to identify imprints of fluid circulation, which mobilized and concentrated metals during various stages of basin evolution.

CONTENTS

		Page
1.	**INTRODUCTION**	1
	1.1 Preface	1
	1.2 Carbonate-hosted, Stratabound Base Metal Deposits	4
	1.3 Dolomitization Models and Recrystallization	5
	1.3.1 Hypersaline Basin and Seepage Reflux Model	6
	1.3.2 Burial Compaction Model	8
	1.3.3 Coorong Model	9
	1.3.4 Sabkha Model	9
	1.3.5 Mixed-Water Model	10
	1.3.6 Solution Cannibalization and Pressure Solution Dolomite	11
	1.3.7 Tectonic or Hydrothermal Dolomite	12
	1.3.8 Recrystallization	12
	1.4 Material and Methods	13
	1.4.1 Sr	14
	1.4.2 C	16
	1.4.3 O	17
	1.5 Regional Geology, Evolution of the Otavi Mountain Land During the Pan-African Cycle	19
	1.5.1 The Damara Province	19
	1.5.2 Geology of the Otavi Mountain Land	23
	1.6 Review of Genetic Models	25
	1.6.1 Magmatic Origin Model	26
	1.6.2 Basin Dewatering Model	26
	1.6.3 Mixing Model	27
	1.6.4 Berg Aukas Model	27
2.	**GEOLOGICAL AND PETROGRAPHIC INVESTIGATIONS IN THE VICINITY OF THE BERG AUKAS MINE**	29
	2.1 Introduction - Field Work and Sampling	29
	2.2 Surface Geology	30
	2.2.1 Lithostratigraphy	31
	2.2.2 Structure	34
	2.2.3 Alteration	40
	2.2.4 Types of Brecciation	43
	2.3 Types of Ore Bodies	45

2.3.1 The Northern Ore Horizon 46
2.3.2 The Central Ore Body 47
2.3.3 The Hanging Wall Ore Body 47
2.4 Types of Mineralization 48
2.4.1 Hypogene Mineralization 48
2.4.2 Supergene Mineralization 48
2.5 Petrographical Studies 50
2.6 Host Rock Mineralogy 54
2.7 Cathodoluminescence 63

3. **ISOTOPE - GEOCHEMICAL STUDIES (Sr, C, O)** 69
3.1 Introduction and Sample Description 69
3.2 Geochemistry of Carbonates 72
3.3 Sr Isotope Studies 73
3.4 C and O Isotope Studies 77

4. **COMPARATIVE ISOTOPE STUDIES IN THE ODIN PROSPECT** 80
4.1 Introduction and Local Geology 80
4.1.1 Lithology 81
4.1.2 Structure 82
4.1.3 Alteration 83
4.2 Sample Description 83
4.3 Results 84
4.3.1 Petrographical Studies 84
4.3.2 Host Rock Mineralogy 85
4.3.3 Isotope - Geochemical Studies (Sr, C, O) 87

5. **POST DEPOSITIONAL ALTERATION** 92
5.1 Dolomitization 92
5.2 Formation of Colloforms 96
5.3 Fluid/Rock Ratio During Mineralization 102
5.3.1 Sr Isotope Shift 103
5.3.2 O and C Isotope Shift 108
5.4 Source of Mineralizing Fluid 112

6. **GENETIC MODEL** 114
6.1 Genetic Model for Berg Aukas 115
6.2 Comparison with MVT Deposits 117
6.3 Implications for Further Prospecting 121

7. SUMMARY and CONCLUSIONS 124

ACKNOWLEDGEMENTS 130

REFERENCES 131

Appendices

I - Geological map of the Berg Aukas area - scale 1:10 000.
II - A series of cross-sections of the Berg Aukas area.
III - Detailed sample localities.
IV - X-ray diffraction - analytical techniques.
V - AAS - analytical technique.
VI - Sr isotopes - analytical technique.
VII - Stable isotopes - analytical techniques and terminology.

LIST OF FIGURES

		Page
1.1	Locality plan of the OML	1
1.2	Major dolomitization models as summarized in generalized representative cross sections	7
1.3	Tectonostratigraphic zones of the Damara orogen	19
1.4	Supposed rift systems of the Damara orogen ..	20
1.5	Geological plan of the OML	24
1.6	Geological cross-section of the OML	25
2.1	Genetic stratigraphy of the Berg Aukas area	32
2.2	Geological interpretation of Berg Aukas	35
2.3	A series of cross-sections based on the inferred surface/structural geology	36
2.4	Carbonate coastal/shelf half-graben showing the associated carbonate facies	37
2.5	Structures developed above basement extension faults	38
2.6	Sketch of hangingwall basins developed during extensional and compressional tectonics	39
2.7	Sketch to illustrate the development of thrusts as a results of continued compression	39
2.8	Cross-section across the Berg Aukas Syncline - a comparison with earlier interpretation ..	39

2.9 Alteration map of the Berg Aukas area 41

2.10 Composite underground plan of the Berg Aukas deposit 45

2.11 Simplified north-south section through the Berg Aukas deposit 46

2.12 Examples of diffractograms to illustrate different dolomite-calcite-quartz assemblages 57

2.13 A plot of peak intensities for the dolomite 110 versus the dolomite 015 peaks 61

3.1 Selected element concentrations with respect to Sr concentration for different dolomite types 73

3.2 $^{87}Sr/^{86}Sr$ ratios with respect to Sr concentration for the different dolomite types in Berg Aukas 75

3.3 $^{87}Sr/^{86}Sr$ ratios with respect to fabric types in Berg Aukas carbonates 76

3.4 Results of C and O isotope with respect to fabric types at Berg Aukas 77

3.5 A plot of $\delta^{18}O$ versus $\delta^{13}C$ for Berg Aukas carbonates 78

4.1 Locality map of the Odin and Clubhead Prospects 80

4.2 Geological plan of the Odin Prospect 81

4.3 Dolomite crystallinity as determined by XRD for both Odin and Berg Aukas samples 86

4.4 $^{87}Sr/^{86}Sr$ ratios with respect to Sr concentration for different dolomite types at Odin, compared to Berg Aukas data 88

4.5 $^{87}Sr/^{86}Sr$ ratios with respect to fabric types at Odin, compared to Berg Aukas data 88

4.6 Plot of $\delta^{18}O$ versus $\delta^{13}C$ for different fabric types at Odin 89

4.7 Results of C and O isotope with respect to fabric types at Odin 90

5.1 Bar graphs for $\delta^{13}C$ and $\delta^{18}O$ comparing Berg Aukas dolomites with other species of dolomite 93

5.2 C and O isotope values for Berg Aukas dolomites compared with other varieties of dolomite 94

5.3 Ranges of $^{87}Sr/^{86}Sr$ ratios and Sr concentrations for Berg Aukas dolomites 104

5.4 Ranges of $^{87}Sr/^{86}Sr$ ratios showing the isotopic shifts 106

5.5 Relationship between Sr-content in 2 different fluids and calculated F/R ratio (open system) 107

5.6 Ranges of $\delta^{18}O$ and $\delta^{13}C$ values for Berg Aukas dolomites 110

5.7 Changes in $\delta^{18}O_i$ (fluid) as a function of temperature 111

6.1 Variation ranges of Sr isotope compositions in Berg Aukas compared to data for other MVT districts 118

7.1 Comparison of the variation ranges of the Sr isotope ratios for the different dolomite generations, as sampled from Berg Aukas and Odin 126

LIST OF TABLES

		Page
1.1	Litho-stratigraphy of the OML	2
1.2	Geochronological evolution of the Damara Oregon	21
2.1	Lithotypes and associated depositional environments of Berg Aukas carbonates	30
2.2	Relationship of Abenab sub-group formations to previously described units	33
2.3	Hypogene Mineralogy of Berg Aukas	48
2.4	Supergene Mineralogy of Berg Aukas	49
2.5	Characteristics of dolomite types	50
2.6	Semi-quantitative evaluation of Berg Aukas samples determined by XRD	56
2.7	Mole % of $CaCO_3$ in Berg Aukas samples as determined by XRD	59
2.8	Dolomite crystallinity of Berg Aukas samples based on XRD peak intensity ratios	60
2.9	Mean values of $I_{(015)}/I_{(110)}$ peaks for different dolomite types	62
2.10	The different colours observed in CL associated with various mineral types	63
3.1	Carbonate samples from Berg Aukas used for isotope studies	70
3.2	Results of AAS analyses on Berg Aukas samples	71

3.3 Isotopic results (Sr, C, O) on carbonate samples from the Berg Aukas area 74

4.1 Carbonate samples from the Odin and Clubhead Prospects used for isotope studies 84

4.2 Semi-quantitative evaluation of Odin and Clubhead samples determined by XRD 85

4.3 Dolomite crystallinity of Odin and Clubhead samples based on XRD peak intensity ratios 86

4.4 Isotopic results (Sr, C, O) on carbonate samples from the Odin and Clubhead Prospects 87

5.1 Average concentrations (ppm) of Sr, and mean values of C, O and Sr isotopes for Berg Aukas dolomites 92

5.2 Isotopic analyses of discrete samples taken from a typical colloform texture (specimen K1-1) 98

6.1 Comparison of Berg Aukas with other MVT deposits 119

LIST OF PLATES

		Page
2.1	Types of brecciation as found at Berg Aukas	44
2.2	A series of photomicrographs depicting the different dolomite types	52
2.3	A series of photomicrographs of dolomite, as seen in cathodoluminescence	64
5.1	A polished surface showing colloform texture including sample sites for isotopic analysis	98
5.2	A photomicrograph of part of a colloform texture in contact with micritic dolomite as seen in cathodoluminescence	99

1. INTRODUCTION

1.1 Preface

The Otavi Mountain Land (OML) is an approximate 10 000 km² ore province, located at the eastern extremity of the exposed carbonate platform in the south of the Congo craton. The carbonates were deposited between 830 - 760 Ma (Miller, 1983) and were later affected by the Pan African orogeny, to form the northern foreland of the Damara orogenic belt. The region encompasses the settlements of Otavi, Tsumeb and Grootfontein, which are situated in the north-eastern part of Namibia (Fig. 1.1).

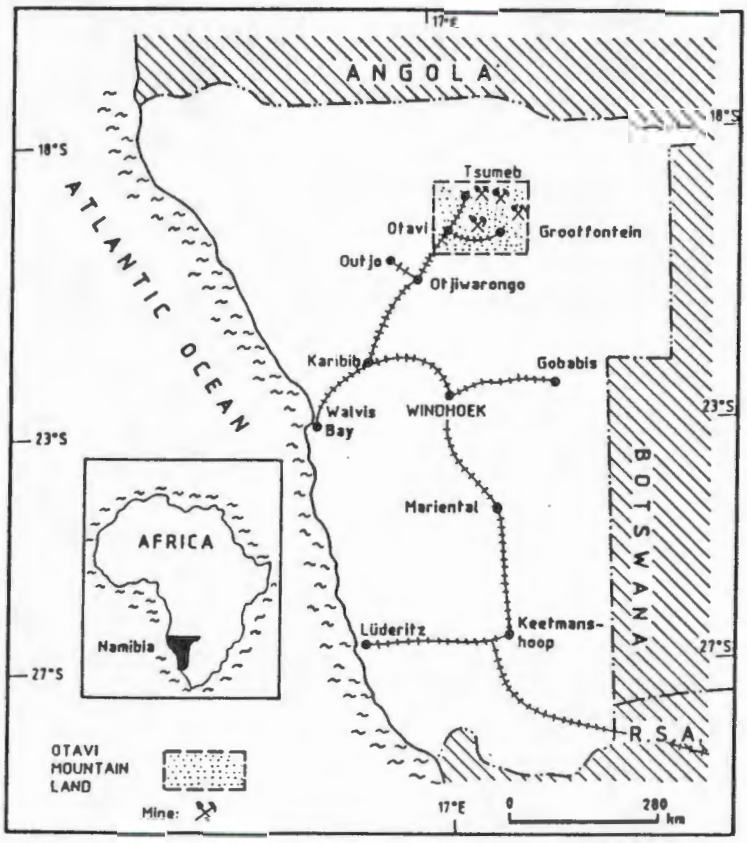

Figure 1.1: Locality map showing the regional setting of the OML.

Stratigraphically, this carbonate platform has been subdivided into three groups, the Nosib, Otavi and Mulden Groups (SACS, 1980), as illustrated in Table 1.1.

Exploitation of the Cu-Pb-Zn-V province has been on-going since 1890, with production having been centered around Tsumeb, Kombat, Berg Aukas and Abenab. Two major styles of mineralization known as the Tsumeb-type and the Berg Aukas-type, can be distinguished in the OML. The Tsumeb-type is a mineralogically complex, cupriferous, polymetallic mineralization confined to the upper Tsumeb Subgroup (Tab. 1.1). A similar style of mineralization known as Tschudi-type, occurs in the overlying Mulden Group. This is a mineralogically simple, stratiform, Cu mineralization.

Table 1.1: Stratigraphy of the OML (SACS, 1980).

Sequence	Group	Subgroup	Formation	Informal Lithozone	Lithology	Average thickness (m)
Damara	Mulden		Kombat and Tschudi		Kombat Formation: slate; sub-arkose and pebbly sandstone near base Tschudi Formation: feldspathic sandstone, sub-greywacke; argillite and conglomerate interbeds in basal portion	> 700
			Disconformity			
	Otavi	Tsumeb	Hüttenberg	T8	Dolomite, bedded light to medium grey; oolitic chert and stromatolite layers near top	240
				T7	Dolomite, bedded dark grey; limestone, shale and chert interbeds	300
				T6	Dolomite, bedded light grey; abundant chert; stromatolite interbeds in lower part	300
			Elandshoek	T5	Dolomite, bedded and massive light grey	1 200
				T4	Dolomite, massive light grey	
			Maieberg	T3	Dolomite, thinly bedded light and dark grey	180
				T2	Limestone, bedded light and dark grey	700
			Chuos	T1	Tillite, quartzite, shale, minor dolomite and limestone	200
			Disconformity			
		Abenab	Auros		Dolomite, bedded and massive light to medium grey; limestone, marl, shale, oolite and stromatolite interbeds	350
			Gauss		Dolomite, massive light to dark grey; local oolite and stromatolite interbeds	750
			Berg Aukas		Dolomite, laminated and massive light and dark grey; black limestone, shale	550
			Disconformity			
	Nosib		Varianto		Quartzite, conglomerate, arkosic mixtite, dolomite, ferruginous shale	
			Askevold		Phyllitic agglomerate, tuff; epidosite	750
			Nabis		Feldspathic quartzite, arkose, conglomerate	
			Unconformity			
Grootfontein Basement Complex					Granite, gneiss, mafic schist	

The Berg Aukas-type is a Zn-Pb-V variety, and has been compared previously with Mississippi Valley-Type (MVT) deposits (Misiewicz, 1988). Mineralization of this type is confined to the lower parts of the Abenab Subgroup.

To date, the basic exploration strategy has been to concentrate around old workings in order to evaluate known deposits, and to locate possible extensions to these. Exploration techniques have included various geophysical methods in addition to surface sampling geochemistry. Success of such methods have been hindered, however, due partly to the karstic nature of the country rock, as well as the abundance of surficial calcrete.

The aim of this thesis is to characterize mineralizing fluids and to quantify fluid-rock interaction, in order to improve the chances of discovering additional base metal deposits in the OML. To concentrate the effectiveness of this research, only Berg Aukas-type mineralization was considered. For this reason, study sites have been restricted primarily to the immediate vicinity of the Berg Aukas mine. However, a lesser number of samples have been collected from two other mineral occurrences found within the Abenab Subgroup carbonates, namely the Odin and Clubhead Prospects.

Previous studies on base metal mineralization (Frimmel, 1988; Gorzawski, 1989; Gorzawski et al., 1990; Frimmel & Niedermayer, 1991) have shown that O, C and Sr isotopic ratios are particularly useful to monitor the interaction between mineralizing fluid and carbonate host rock. For instance, Gorzawski (1989, 1990) makes use of O, C and Sr isotope ratios to reconstruct the diagenetic evolution of carbonate rocks, whilst Frimmel (1988) succeeded in differentiating between syngenetic and epigenetic mineralization based on $^{87}Sr/^{86}Sr$ ratios.

The prime objectives of the project are threefold. Firstly, to investigate the isotopic characteristics of the different carbonate generations associated with various infiltration events. Secondly, to establish the source and type of these fluids, and thirdly to recognize possible isotopic alteration haloes around sites of mineralization. One of the fluids that infiltrated the carbonate host sediment, must have been responsible for the dolomitization, therefore a special focus will be on the various dolomitization models.

Assuming Berg Aukas-type mineralization to be epigenetic, isotopic disequilibrium with the host rock should be expected. An attempt will thus be made to establish the spatial distances over which

fluid-rock interaction has taken place. With a sufficiently large database, the differences in isotopic composition of mineralized and non-mineralized host rocks may then be used, not only to model fluid-rock ratios, but in an attempt to measure the proximity to an ore body.

1.2 Carbonate-hosted, Stratabound Base Metal Deposits

The term "carbonate-hosted stratabound base metal deposits" refers worldwide to a large number of economically important ore deposits. The largest part of these occurrences include the so-called MVT deposits.

MVT deposits owe their commonly accepted name to the fact that several classical districts occur within the drainage basin of the Mississippi River, central U.S.A., and have traditionally supplied the major portion of that country's Pb and Zn production, currently among the largest in the world. Many attempts have been made to characterize the main geological features of this enigmatic type of deposit. Among the better known are those of Ohle (1959, 1980), Callahan (1964), Hoagland (1976), Anderson and Macqueen (1982), and Sverjensky (1986).

MVT Pb-Zn deposits are often hosted in carbonate rocks, which are usually platformal in origin and almost invariably dolostone. The major control in a vast majority of districts is irregular discordant or tabular breccia bodies (Ohle, 1985; Sangster, 1988). Deposits are consequently discordant and strata-bound but not stratiform. They are not obviously related to igneous intrusions.

Ore mineralogy is simple with pyrite, marcasite, sphalerite and galena being the most common, although the relative mineral abundances may vary between deposits and districts. Barite and/or fluorite are accessory minerals in some districts, but, in a majority of cases, these minerals are entirely absent. The minerals are commonly, but not invariably, coarse-grained. Sulphide textures in MVT deposits are extremely varied and range from massive to disseminated. A very common texture consists of coarse-grained clusters or individual crystals of sulphides, together with sparry white dolomite, occurring as cement between

angular carbonate breccia fragments. The large crystal size of MVT sulphides is usually taken to indicate slow precipitation and crystal growth.

Pb and Zn are the most common elements that determine economic viability. In some districts silver is an important by-product, but in most deposits it is negligible. Barite and fluorite may also been found in some deposits (Sangster, 1990), in addition to the elements cadmium and germanium.

The ore-hosting breccias are considered to have resulted from dissolution of the more soluble sedimentary layers, with subsequent collapse of overlying beds (Ohle, 1985; Sangster, 1988). The major mineralizing processes appear to have been open-space filling between breccia fragments and replacement of fragments or wall rock, although the relative importance of these processes varies widely between deposits.

1.3 Dolomitization Models and Recrystallization

The correct interpretation of isotopic data from dolomites is ultimately linked to the understanding of the process of dolomitization.

The "dolomite problem" has often been cited as a major conundrum of sedimentary geology (Fairbridge, 1957; Lippman, 1973; Morrow, 1982a; Ricketts, 1983). Precambrian carbonates in particular have been singled out as an important part of this problem, because they consist predominantly of dolostones. The hypothesis that Precambrian dolostone represents the direct (primary) precipitation of dolomite from seawater was popularized by Chilingar (1956), and more recently by Tucker (1982).

Based on sedimentary fabrics and stable isotope criteria, Tucker (1982) further suggested that dolomite precipitated in a manner that was analogous to calcite and aragonite. That is to say that dolomite precipitated in fibrous, bladed, and rhombohedral crystal forms, as dolomite sediment and dolomite cement. However, it is the view of Ricketts (1983) that most Precambrian dolostones represent replacement of original limestone or calcareous sediment,

and that such dolostone sequences can be interpreted in much the same way as Phanerozoic dolostone sequences.

It is not the authors intention to resolve which of these views is correct, but more to present a brief inventory of current ideas and models pertaining to dolostones and the process of dolomitization.

Prior to presenting a brief description of published dolomitization models, it is important to note that several conditions must be satisfied for any of these models to be applicable for a particular type of dolomite. According to Morrow (1982a) these conditions, in their simplest form are as follows:

a) The amount of Mg^{2+} available for dolomitization must be adequate to form a given mass of dolostone (i.e. source of Mg^{2+}).

b) A mechanism is required to deliver the available Mg^{2+} to the dolomitization site. This mechanism may also be required to deliver a small amount of CO_3^{2-} ions to the dolomitization site and carry away Ca^{2+} ions.

c) The composition of a proposed dolomitizing solution must be conducive to dolomitization.

1.3.1 Hypersaline Basin and Seepage Reflux Model

One of the first models proposed for dolomitization on a large scale was the Seepage Refluxion or more simply, the Reflux Model (Adams and Rhodes, 1960). In this model (Fig. 1.2) open marine water evaporates as it passes landward across a hypersaline shelf lagoon. The resulting increase in density of these evaporated waters causes them to infiltrate the underlying sediment and to move seaward by seepage, through the seaward-dipping beds. The cycle of fresh marine replenishment of lagoon waters and seaward seepage of brines is the mechanism by which Mg^{2+} is continually transported to the sediment, the source of Mg^{2+} being the sea water itself.

1. SEEPAGE REFLUXION or REFLUX MODEL

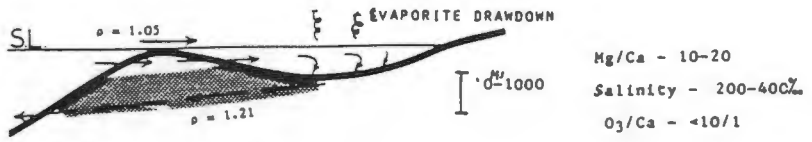

2. BURIAL - COMPACTION MODEL

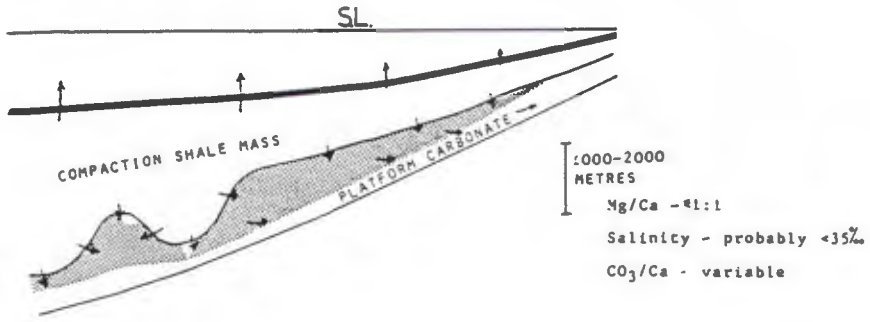

3. COORONG MODEL (variant of mixed-water model)

4. SABKHA MODEL (variant of reflux model)

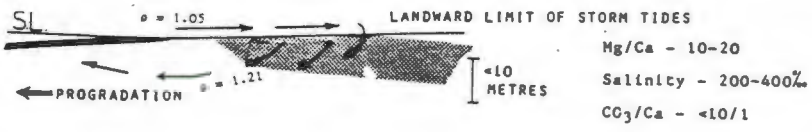

5. MIXED - WATER MODEL

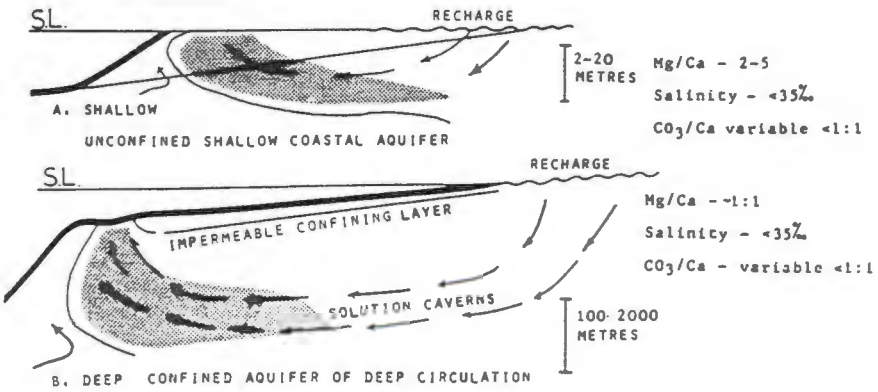

Figure 1.2: Major dolomitization models summarized in generalized representative cross sections (after Morrow, 1982b). Shaded areas represent zones of active dolomitization.

The dolomitization reaction probably occurs after a large amount of gypsum (or anhydrite) has precipitated and the Mg/Ca ratio approaches 9.0, sufficiently high to inhibit the effect of salinity. Furthermore, the increase of the CO_3^{2-}/Ca^{2+} ratio that occurs during gypsum or anhydrite precipitation may also aid dolomitization.

1.3.2 Burial Compaction Model

Compaction of fine-grained sediments during burial involves the progressive expulsion of pore water. Commonly large shale masses contain carbonate reef bodies and are either underlain or bordered by thick shelf carbonate sequences. A part of the Mg^{2+}-bearing compaction water may pass through adjacent limestones and cause dolomitization (Fig. 1.2). The Mg^{2+} required for dolomitization is derived primarily from the pore water (Jodry, 1969; Mattes and Mountjoy, 1980).

Kinetic inhibitions associated with the formation of dolomite at near-surface conditions are greatly reduced in deep burial environments, largely due to the increase of temperature with depth. Furthermore, the time available for dolomitization is much greater in deep subsurface environments than in the near-surface environments of early dolomitization (Mattes and Mountjoy, 1980).

However, it should be noted that the problem of the supply of Mg^{2+} for dolomitization is an important constraint in deep burial environments. Morrow (1982b) reported that on a basinwide scale, the order of hundreds of cm^3 of compacted shale are required for the dolomitization of 1 cm^3 of laterally adjacent limestone. In burial environments greater than 2000 m, the transformation of montmorillonitic clays to illite is accompanied by the release of Si^{4+}, Fe^{2+}, Ca^{2+} and Mg^{2+} ions to pore solution, thus allowing authigenic ankerite, ferroan dolomite and chlorite to precipitate as cements in some sand-shale sequences (Boles, 1981).

According to Morrow (1982b) it is unlikely that there is sufficient volume of fluid at such depths, to move these ions laterally and so participate in the solution of large amounts of limestone and contemporaneous precipitation of dolomite. Although small amounts

of dolomite may be associated with this model, the ease of dolomitization at the higher temperatures of deeper burial is countered by the progressive loss of the raw materials for dolomitization (i.e. pore fluids and their ions), as burial compaction proceeds.

1.3.3 Coorong Model

The Coorong Lagoon in southern Australia was known to be an area of dolomite formation since the later 1920s. Past work (Von der Borch, 1976; Muir et al., 1980) has established the Coorong Lagoon as a model for early dolomitization in many ancient sequences of aphanitic dolomite that are not associated with evaporites (Fig. 1.2).

Ephemeral lakes are filled during the humid winter months by groundwater seepage and are evaporated to partial or complete dryness during the summer months. Extremely fine-grained calcian dolomite mud and magnesite forms in the landward ephemeral lakes, under the influence of continental groundwater or in the zone of mixing between sea water and continental water. Such dolomite (and magnesite) precipitation is aided by groundwater dilution and by the high CO_3^{2-} concentration of the alkaline groundwater (Morrow, 1982a). Though the source of Mg^{2+} ions has not been identified with certainty, dolomite forming close to the coast may have derived their Mg^{2+} directly from sea water, whilst dolomites forming further inland retained Mg^{2+} ions from the groundwater, which in turn had been derived from the possible weathering of basic volcanic rocks.

Due to the predominant role of fresh groundwater, the Coorong Lagoon Model may be regarded as a specific type of the more generalized mixed-water or dilution model.

1.3.4 Sabkha Model

Another well-documented setting for penecontemporaneous dolomite, the sabkha environment, is restricted to those dolomites with

accompanying evaporite minerals. Illing et al. (1965) provided the first comprehensive report on the Holocene intertidal and supratidal dolomite that had replaced aragonitic sediments exposed on sabkha surfaces bordering the Qatar Peninsula on the Persian Gulf.

In essence, the dense Mg^{2+}-bearing hypersaline floodwater brines sink downward and flow seaward through the sediment by seepage refluxion (Fig. 1.2). Dolomitization of the underlying intertidal and subtidal sediments occurs to a depth of 2 to 3 m beneath the sabkha surface, in regions landward of the continuous algal mat (Bush, 1973). McKenzie et al. (1980) have developed an alternative model for sabkha dolomitization based on a process which they termed "evaporative pumping". In this process, a continual flow of seawater moves landward through the sabkha sediments to replace groundwater lost by evaporation at, or near the sabkha surface.

Regrettably, this mechanism does not provide the volume of flow of ion-bearing groundwater necessary for extensive dolomitization. The Sabkha Model may be regarded as a specific example of the Reflux Model modified slightly by the process of evaporative pumping (Morrow, 1982b).

1.3.5 Mixed-Water Model

The Mixed-Water or Dilution Model was first proposed by Hanshaw et al. (1971), who documented the first large-scale system of deep burial dolomitization under the influence of fresh groundwater, in the deep confined Tertiary carbonate aquifer of Florida (Fig. 1.2). They emphasized the role of active groundwater circulation in supplying marine-derived Mg^{2+} for dolomitization.

It has since been argued (Land et al., 1975) that such carbonates were dolomitized penecontemporaneously by the interaction of marine and fresh groundwater in a shallow coastal aquifer, and suggested that many ancient platform dolomites which lack evaporites and are depleted in both trace elements (e.g. Na^{+}, Sr^{2+}) and the relatively heavier stable isotopes (^{18}O, ^{13}C), may have formed in a similar manner. However, vast differences in the chemical and isotopic composition between dolomites that have formed under the influence

of freshwater and those formed from hypersaline brines, has led to an emphasis on these types of data as criteria in choosing between the Mixed-Water Model and other models (Morrow, 1982b). It should be stressed that uncertainties in the interpretation of chemical and isotopic data preclude their use in model discrimination in the absence of other data.

In the Mixed-Water Model, dolomitization occurs within the zone of mixing of fresh groundwater with phreatic seawater. The Mg^{2+} ions for dolomitization are derived primarily from seawater, and the delivery mechanism is the continual circulation of seawater induced by the flow of fresh groundwater. Dilution of saline solutions causes slow precipitation which favours dolomite precipitation (Folk and Land, 1975), and the high CO_3^{2-} concentration in many dilute continental groundwaters may also promote the precipitation of dolomite.

1.3.6 Solution Cannibilization and Pressure Solution Dolomite

Solution Cannibilization (Goodell and Garman, 1969) refers to the derivation of Mg^{2+} for dolomitization from the dissolution of magnesian calcite and reprecipitation of low-magnesian calcite. Though some examples of partial dolomitization, such as dolomitized burrow fillings, have been explained by solution cannibilization, but for more complete dolomitization other sources of Mg^{2+} are required (Morrow, 1982b).

More recently, the phenomenon of pressure solution along solution seams and stylolites has been cited as a major cause of dolomitization (Wanless, 1979). The source of Mg^{2+} ions in pressure solution dolomitization is by solution cannibilization of Mg^{2+} from pre-existing magnesian calcite during pressure solution (Wanless, 1979). Complete dolomitization is thought to result from the concentration of dolomite along solution seams as a relatively insoluble residue. Unfortunately, this model suffers from the difficulty in reconciling the deep burial setting of most stylolites with the common pre-burial conversion of magnesian calcite to low-magnesian calcite (Morrow, 1982b). For large amounts of dolomite other sources of Mg^{2+} are required.

1.3.7 Tectonic or Hydrothermal Dolomite

Many coarsely crystalline, white sparry dolostones that have cross-cutting relationships with the enclosing strata have been designated as "tectonic" or "hydrothermal" dolomites in older studies (Stanford, 1962). However, the common absence of other hydrothermal minerals implies that many of these dolostones have other origins. The relationship of some dolostone masses to faults may merely reflect the fact that groundwater movement in aquifers tends to be much more rapid along subsurface fault zones, enhancing diagenesis.

1.3.8 Recrystallization

In 1965 Folk proposed the word "neomorphism" as a "comprehensive term of ignorance" to embrace "all transformations between one mineral and itself or a polymorph ... whether the new crystals are larger or smaller or simply differ in shape from the previous ones. It does not include simple pore-space filling; older crystals must have gradually been consumed, and their place simultaneously occupied by new crystals of the same mineral or a polymorph" (Folk, 1965, p21).

The term includes two in situ processes: polymorphic transformation, and recrystallization. It is valuable because it can be used when it is certain that a carbonate fabric has been modified in situ, but it is not known whether polymorphic transformation or recrystallization or both were involved (Bathurst, 1971).

Recrystallization includes any changes in the fabric of a mineral or a monomineralic sediment (Folk, 1965). Several changes are known to occur with this process, which include crystal volume, crystal shape and crystal lattice orientation. In the context of this study, the term recrystallization shall primarily be restricted to the mineral dolomite, and will include the various fabrics of neomorphic dolospar observed during this study. An attempt will thus be made to determine different recrystallization events, based on petrographic and isotopic data.

1.4 Material and Methods

The main part of the work for this study was carried out on the Zn-Pb-V mine at Berg Aukas, some 20 km north-east of the town of Grootfontein. The mine itself ceased operations in 1978 as a result of poor metal prices and underground water problems. Whilst operating, Berg Aukas mine was a high grade, low tonnage mine with a small scale of operations, milling only 11 000 tons of ore monthly. The mine had an average grade of 22% comprising 17% Zn, 5% Pb and 0.6% V_2O_5.

This study is based on a period of 18 months of geological exploration conducted by the author at Berg Aukas, on behalf of Gold Fields Namibia Limited. The studies in the area include detailed mapping, sampling and carbonate petrography. In a second stage XRD, AAS and isotope determinations (Sr, O, C) were carried out on distinct mineral phases of petrographically well characterized samples in order to trace geochemically the post-depositional history of the Berg Aukas area.

Another aspect of this study involved the sampling and isotopic investigation (Sr, C, O) of the gangue and host carbonates at the Clubhead and Odin Prospects. Though similar in mineralogy compared to Berg Aukas, the ore associated with both of these prospects lies stratigraphically higher in the sedimentary succession.

In all the selected localities, similar textures and structures suggest a partially comparable diagenetic history. In each area petrographic analysis permits the classification of different mineral generations according to their position in the crystallization sequence. Preferred objects for sampling have been the different generations of recrystallized dolomite and sparry dolomite. Furthermore, samples were collected which exhibit different dolomite generations; one of them appears to have a close association with ore mineralization. Care was taken that only those dolomite fabrics were sampled, whose diagenetic crystallization generations were megascopically visible. Each sample was checked for mineral contamination by microscopy and XRD, and subsequently analyzed for their isotopic composition. In order to avoid cross-contamination between different dolomite generations

in one sample, each sample used for the isotopic studies was checked by means of cathodoluminescence.

Isotopic studies of Sr, C and O constitute an important part of this study, and therefore a brief overview of the isotope geochemistry of these elements will follow, as taken from Faure (1986) and Gorzawski (1989). Special emphasis will be placed upon isotopic modifications during diagenesis, and the application of these techniques in an attempt to characterize mineralizing fluids and to quantify fluid-rock interaction. The analytical procedures used for the measurement of isotopic ratios of Sr, C and O appear as appendices of this thesis.

1.4.1 Strontium

Sr has four stable isotopes: ^{84}Sr, ^{86}Sr, ^{88}Sr, and ^{87}Sr. Whilst geological processes do not cause any isotope fractionation, the variation of the isotopic composition result from the decay of ^{87}Rb to ^{87}Sr. Natural variations of ^{87}Sr are very small due to the low Rb content and the relatively low proportion of ^{87}Rb in naturally occurring Rb, as well as the long half-life period (50×10^9 years) of ^{87}Rb.

Significant differences in the Sr isotopic compositions exist between the earth's mantle and the crust, and are usually presented as the ratio $^{87}Sr/^{86}Sr$. Young ocean basalts with a Rb/Sr ratio of normally < 0.1, typically have $^{87}Sr/^{86}Sr$ which range from 0.701 (tholeites) to 0.706 (alkali-basalts), whereas crustal material (Rb/Sr = 0.25-0.35) is characterized by higher $^{87}Sr/^{86}Sr$ ratios from 0.720 to 0.730 (Faure & Powell, 1972; Hedge, 1974).

As regards to Sr isotopes in carbonate rocks, two fundamental aspects should be considered: Firstly, the seawater Sr isotope composition during sedimentation, and secondly, the influence of the diagenetic evolution on the $^{87}Sr/^{86}Sr$ ratios.

As reported by Burke et al. (1982), temporal variations of the $^{87}Sr/^{86}Sr$ ratio of seawater throughout geological times have been recognized. Such Sr isotope variations result from changes in the relative proportions contributed to the marine Sr from different

sources, such as old crustal rocks, young basic and intermediate volcanic rocks, and marine carbonates.

Since most of the results obtained in this study are Sr ratios characterizing different diagenetic stages, the possibilities of diagenetic changes on the $^{87}Sr/^{86}Sr$ ratios should be described. Veizer and Compston (1974) reported that for an open diagenetic system, marine influence would not alter the $^{87}Sr/^{86}Sr$ ratios, whereas an input of volcanic rocks or hydrothermal solutions with a lower Sr isotope ratio could cause a diminution of the $^{87}Sr/^{86}Sr$ ratios. Conversely, a continental influence would increase the Sr ratios due to the higher content of radiogenic Sr in continental waters. In most of the known cases, diagenetic effects tend to increase the Sr isotope ratios (Veizer and Compston, 1974; Gorzawski et al., 1989).

In general, an increase in Sr isotopic ratios during diagenesis can be attributed to the Rb-content of the host rock. But, the Rb contents of carbonate rocks are generally low. Veizer and Compston (1974) discussed the possibility that element exchange in situ between silicate and carbonate phases, can take place during late burial diagenesis, initiated by load pressure. Such an exchange would depend on the abundance of clay minerals present within the sediment.

As in the case of the present study, where phyllosilicate-free samples were selected, an alternate process is sort to account for increased Sr ratios in diagenetic carbonate minerals. Such a process is the equilibration of the minerals with diagenetic fluids enriched at different degrees in radiogenic Sr. The level of enrichment would depend on the source of such fluids, in addition to the media through which they have been transported.

An attempt will be made in this study to apply this theory, in an effort to characterize the various carbonate generations associated with hydrothermal infiltration events, in particular those fluids associated with Pb-Zn mineralization.

1.4.2 Carbon

C has two stable isotopes, ^{12}C and ^{13}C, with relative abundances of 98.89% and 1.11% respectively. The ratios of these isotopes are reported in the form of the δ notation in per mil, and the international standard used is calcium carbonate of the Peedee Belemnite (PDB). All δ-values (see Appendix VII) given in this thesis are based on the PDB standard.

C occurs in the oxidized state, mainly as CO_2, carbonate ions in aqueous solution, and as carbonate minerals. The reduced form of C occurs in organic compounds and in coal. This distribution accounts for a large isotope fractionation in nature, which results in a natural variation range of C isotopic compositions.

Organic matter and sedimentary carbonates are the two main sources of C, but are quite different from each other due to the existence of two different reaction mechanisms: The first being a kinetic isotope effect during photosynthesis, resulting in a concentration of light ^{12}C in organic material; The second mechanism involves a chemical exchange effect between atmospheric CO_2 and dissolved HCO_3^{--}, which leads to an enrichment of ^{13}C in the bicarbonate.

The $\delta^{13}C$ of recent marine carbonate sediments ranges between +4 and -2 per mil, and the temperature dependence of the C isotope fractionation between calcium carbonate and dissolved bicarbonate was determined by Emrich et al. (1970) as 0.035 per mil per °C. As a result of this, the C isotope composition in the crystallizing carbonate should become heavier with increasing temperature. Due to the fact that dolomite has yet to be synthesized at 25°C, it is presently not possible to determine the exact isotopic fractionation between dolomite and water at sedimentary temperatures.

As CO_2 is relatively insoluble at diagenetic P - T conditions, the C isotopic composition of carbonate sediment remains very close to its initial value (Land, 1980). However, diagenetic processes may cause a shift in the isotopic composition of newly formed (recrystallized) carbonates, often towards lighter $\delta^{13}C$ values. Such shifts in the isotopic composition may be the result of any of the following three mechanisms:

a) The oxidation of organic matter to release light C, which would then contribute to the total HCO source for carbonate precipitation.

b) Progressive in situ depletion of the heavier isotopic components in carbonate reservoirs during crystallization. For a system closed to fluid migration, concentration of the heavier isotope in earlier formed carbonates would deplete the residual fluid, and hence the source for later crystallizing carbonates in ^{13}C.

c) Recrystallization in the presence of depleted pore fluids, as a result of the aforementioned process.

1.4.3 Oxygen

O has three stable isotopes, ^{16}O, ^{17}O, and ^{18}O, with relative abundances of 99.76%, 0.04% and 0.2% respectively. Owing to the greater abundance and the greater mass difference, the $^{18}O/^{16}O$ ratio is normally determined and expressed as $\delta^{18}O$. Two standards can be used to report O isotope compositions: PDB and SMOW (standard mean ocean water), though PDB is normally used when dealing with sedimentary carbonates. The relationship between PDB and SMOW is as follows:

$$\delta^{18}O_{(SMOW)} = 1.03086\ \delta^{18}O_{(PDB)} + 30.86$$

(After Friedman and O'Neil, 1977)

This relationship is based on: the fractionation between CO_2 and water ($\alpha = 1.0412$), the fractionation between CO_2 produced from PDB calcite by 100% phosphoric acid treatment and CO_2 equilibrated with SMOW ($\alpha = 1.00022$), and the fractionation between H_3PO_4-liberated CO_2 and calcite ($\alpha = 1.01025$).

As mentioned earlier it is not possible at present to determine the equilibrium isotope fractionation between dolomite, calcite, and water at low temperatures, and hence extrapolations must be made from high temperature experiments. The relationship between $\delta^{18}O_{carbonate}$, $\delta^{18}O_{water}$, and temperature is fairly well

established (Friedman and O'Neil, 1977), and may be expressed as follows:

$$\ln\alpha_{calcite\text{-}water} = 2.78 \times 10^{6}T^{-2} - 2.89$$

where T is in °K. For dolomite this relationship is imperfectly known.

One problem does arise, which is most pertinent to the dolomites analyzed in the present study, this being that many dolomites have undergone one or more recrystallization events. Land (1980) reports that most ancient dolomites are depleted in ^{18}O with respect to recent examples. Such depleted dolomite must have formed either at elevated temperatures or from fluids depleted in ^{18}O relative to seawater (or both).

Recent studies carried out by Gorzawski et al. (1989) when dealing with stable isotope variations in carbonate cements and rocks, had established that small isotopic changes of O and/or C in sedimentary carbonates are common features which can be used to characterize diagenetic evolution. For instance, a decrease in $\delta^{18}O$ during subsequent diagenetic stages has been reported during progressive diagenesis (Meyers and Lohmann, 1985; Moore, 1985).

Several possibilities exist which can account for diagenetic modifications of the O isotopic composition in carbonate rocks:

a) Variations in temperature conditions.

b) The introduction of isotopically "light" or "heavy" fluids.

c) Progressive changes in porewater composition.

d) A combination in any of the above factors.

1.5 Regional Geology, Evolution of the OML During the Pan African Cycle

1.5.1 The Damara Province

The Damara Province has been subjected to intensive research since 1974, most of which was coordinated under the auspices of the International Geodynamics Project. Significant contributions include those of Martin and Porada (1977), Porada (1979, 1983, 1985), Miller (1979, 1983), Mason (1981), Martin (1965, 1978,

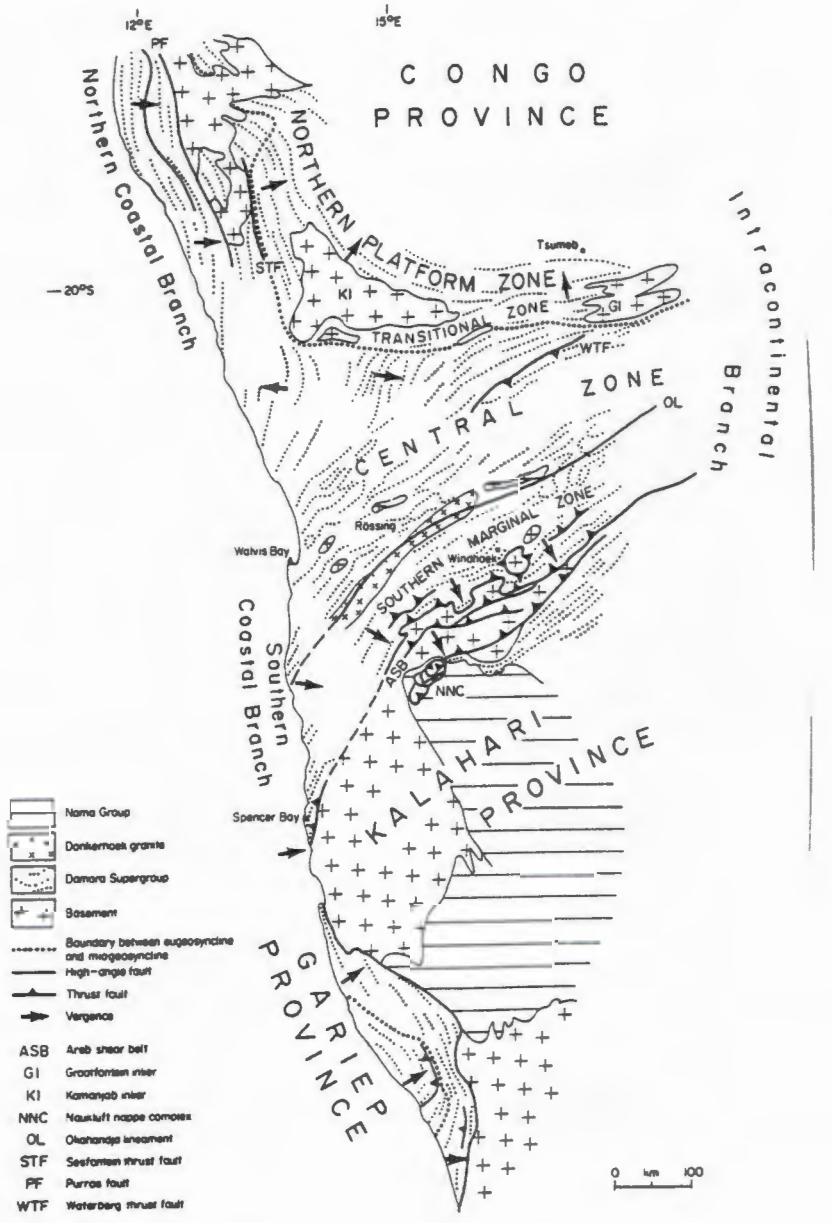

Figure 1.3: Tectonostratigraphic zones of the Damara orogen (after Miller, 1983).

1983a, 1983b), Hartnady (1978), Miller and Hoffmann (1981), and Kröner (1981, 1982).

The intracontinental arm of the Damara orogen, which separates the northern Congo Craton from the southern Kalahari Craton, is divided into several zones (Fig. 1.3), each distinguished on the basis of stratigraphy, structure, grade of metamorphism and aeromagnetic expression (Miller and Hoffmann, 1981; Miller, 1983).

The basal sequence of the Damara is the Nosib Group, a predominantly clastic sequence with minor volcanic rocks and evaporites, which were deposited in five north-east trending grabens (Fig. 1.4).

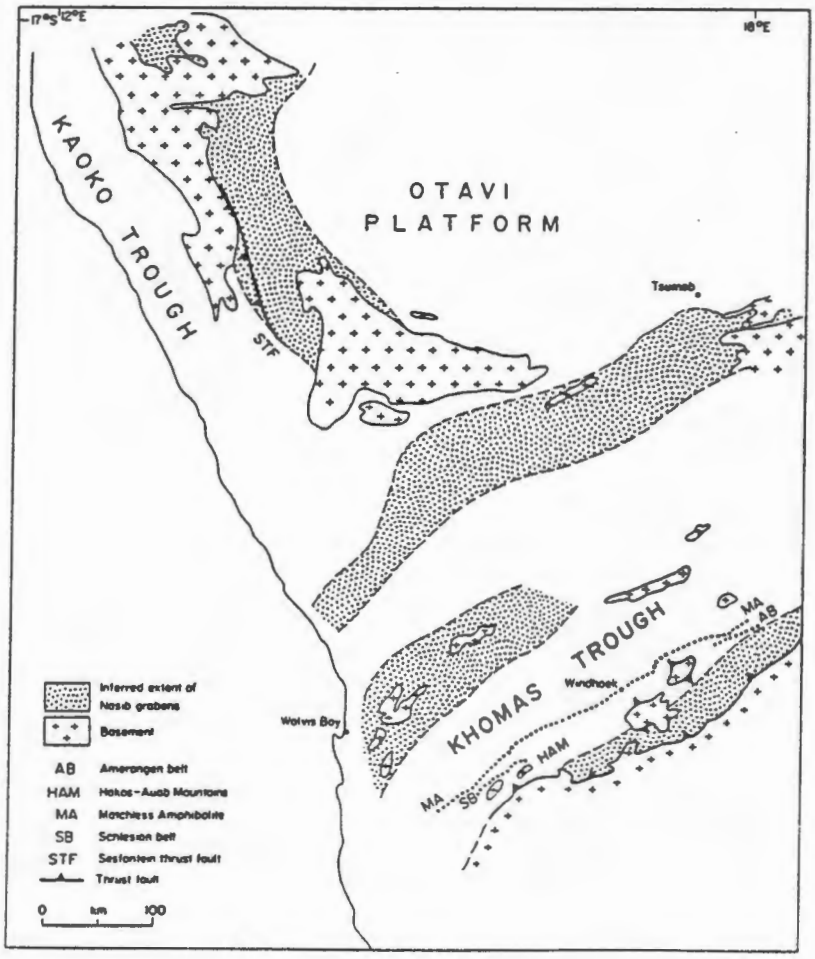

Figure 1.4: Supposed rift systems of the Damara orogen based on facies analysis (after Porada, 1983).

It is postulated (Porada, 1985) that graben development commenced with the Northern Rift approximately 900-800 Ma ago. Porada also argues that rifting was initiated by crustal stretching above a passive mantle, as opposed to a rising mantle plume as was earlier suggested (Porada, 1983).

Following the terrestrial sedimentation in the Nosib grabens, rapid downwarping along the early graben structures resulted in an encroaching sea. Marine transgression proceeded from west to east, commencing with the deposition of a turbiditic sequence (Swakop Group) in the Pan African proto-Atlantic ocean (Miller, 1983). Carbonate sequences at the base of the Swakop Group developed eastwards, as the transgression progressed. The Abenab Subgroup, the lowermost portion of the Otavi Group, developed on the stable Northern Platform along the margins of the early Nosib Northern Rift.

Table 1.2: Geochronological evolution of the Damara orogen (from Kröner, 1982).

455-440 Ma	Uplift and cooling, closure of Rb-Sr isotopic systems
510-455 Ma	(F_4) leading to basement mobilization and formation of dome structures, emplacement of late granite
520-500 Ma	Uplift of central belt, activation of Okahandja Lineament and emplacement of Donkerhoek Granite. Nappe tectonics in southern part of belt
550-540 Ma	Intrusion of post-F_3 granites, peak of metamorphism
580-550 Ma	(F_3) with intrusion of syntectonic Salem-type granite, folding of Molasse in marginal areas
640-560 Ma	Uplift in central belt, deposition of Molasse - Nama Group (south) and Mulden Group (north)
650-620 Ma	(F_2) and strong metamorphism, generation of regional foliation, intrusion of syntectonic granitoids in central part of belt
750±35 Ma	Emplacement of pre-F_2 diorite, (F_1) of unknown regional significance
766±76 Ma	Intrusion of post-Nosib felsic Abbabis dykes
830-760 Ma	"Geosynclinal Phase": deposition of Swakop and Otavi Groups, emplacement of Matchless amphibolite belt at about 775±33 Ma
840±13 Ma	Emplacement of pretectonic Oas syenite, acid volcanism of upper Nosib
1050-900 Ma	"Early rifting phase": Formation of elongate graben zones, deposition of clastic sediments of lower Nosib Group, minor bimodal volcanism

The lower and upper parts of the Swakop and Otavi Groups are separated by the Chuos Formation, an unsorted diamictite assemblage marking a period of widespread crustal disturbance. The origin of this regional marker horizon is still uncertain, though current views vary between a glaciomarine origin to that of a deep water debris flow (Miller, 1983).

The commencement of orogenesis between 650-620 Ma (Kröner, 1982), resulted in deep east-west trending paleo-valleys on the Northern Platform, which were syntectonically filled with intramontane molasse of the Mulden Group. In the eastern portion of the Northern Platform, Mulden sediments have a disconformable relationship with the underlying carbonates. Such a disconformity is more strongly developed towards the west.

A summary of the geochronological evolution of the Damara orogen, as compiled by Kröner (1982), is presented in Table 1.2.

The regional metamorphic grade of the Northern Platform area can be inferred as lower greenschist (T ≈ 300°C), based on the following evidence:

a) Dolomite and quartz remain stable; absence of talc (with the exception of minor talc in quartz veins); absence of tremolite.

b) Illite crystallinity data (Ahrendt et al., 1978).

c) Absence of biotite in the metapelites, but significant presence of chlorite, muscovite, quartz and albite - indicative of a lower greenschist facies.

Similarly, the approximate age of metamorphism lies within a relatively narrow range, and include values of 460 Ma (Ahrendt et al., 1978) and 455 Ma (Clauer & Kröner, 1979), both of which use the K/Ar dating method. A value of 443 ± 67 Ma was calculated by Kroner (1982), based on the Rb/Sr isochron on the Askevold epidosite.

Such ages are younger than the age for the Central and Southern Damaran metamorphism (between 550-540 Ma), and would suggest that

these ages are either cooling ages or represent a younger metamorphic event in the north.

1.5.2 Geology of the OML

The regional geology of the OML was first documented by Söhnge (1957), who collated the results of regional mapping conducted by geologists of the Tsumeb Corporation Limited (TCL) and the South West Africa Company (SWACO). Subsequent studies of the OML were attempted by Grobler (1961), Hedberg (1979), Van der Westhuizen (1984) and Misiewicz (1988), all of which used Söhnge's work as a basis.

Figures 1.5 and 1.6 represent a simplified geological map and cross-section respectively of the OML, which essentially remained unchanged since Söhnge compiled it in 1957.

The OML is the best known portion of the Northern Platform due to its abundant mineral occurrences. The principal rock types exposed are carbonates of the Otavi Group, which were deposited on clastic and metavolcanic sequences of the Nosib Group, in addition to remnants of lower Proterozoic granites and gabbros, which form the basement complex. The molasse sediments of the Mulden Group unconformably overlie the Otavi Group.

Geographically, the OML is a rugged and densely wooded terrain, with higher relief areas dominated by carbonates, which typically exhibit a karst topography. Much of the lower relief flatlands and valleys are masked by a superficial sand and calcrete cover. Basement lithologies are poorly exposed, but are known to be widely occurrent, based on exploration drill hole intersections.

The structural setting of the OML is relatively simple, initiated by the orogenic processes brought about by continent collision, which followed the spreading of the Congo and Kalahari cratons. As discussed in the previous section, the basement topography of the OML was characterized by rift grabens, which formed at the eastern limit of the Northern Rift. The land surface was subsequently folded, at the onset of Damaran orogenesis, to form a series of east-west trending, steeply dipping synclines and anticlines.

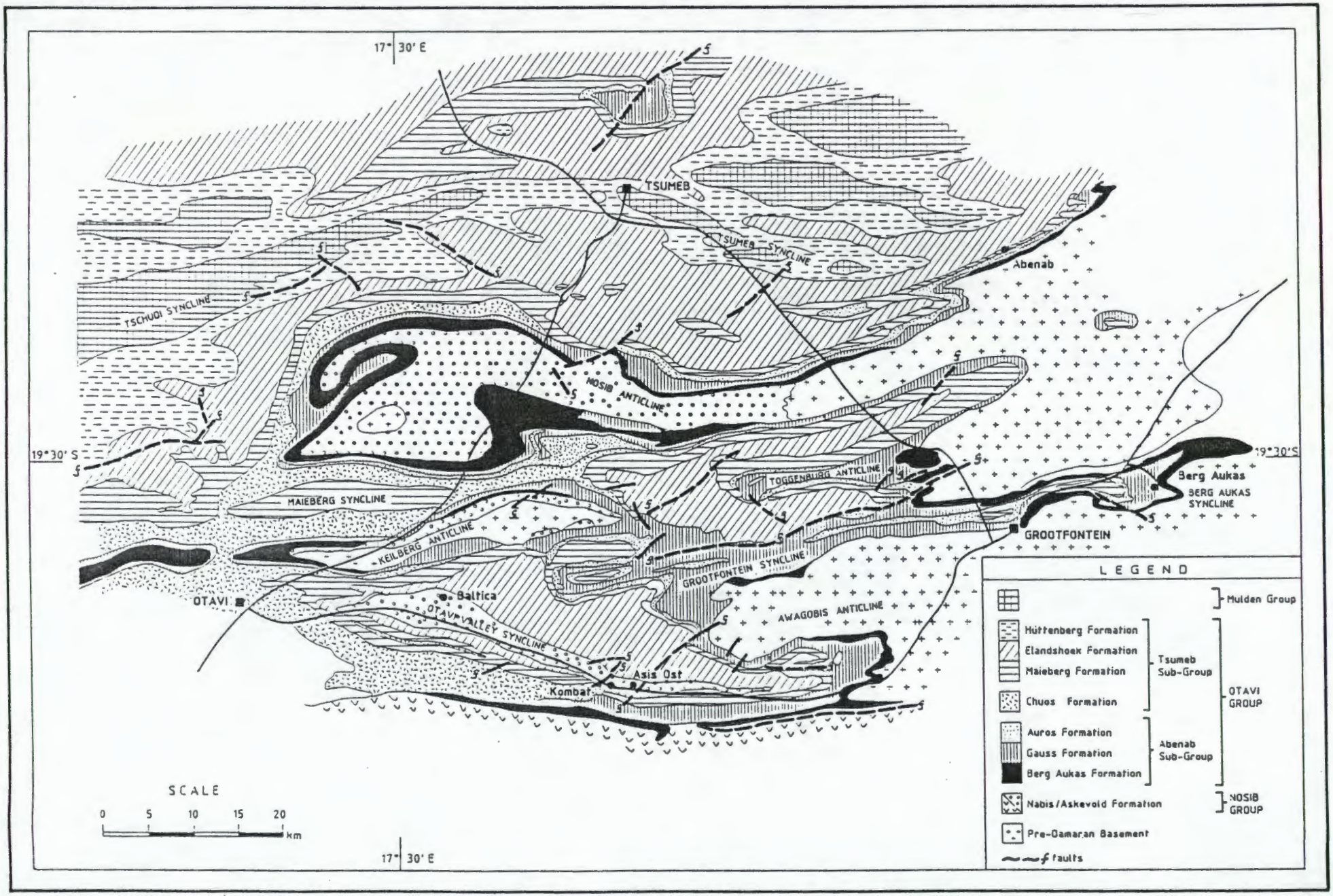

Figure 1.5: Simplified geological map of the OML (modified after Sönge, 1957).

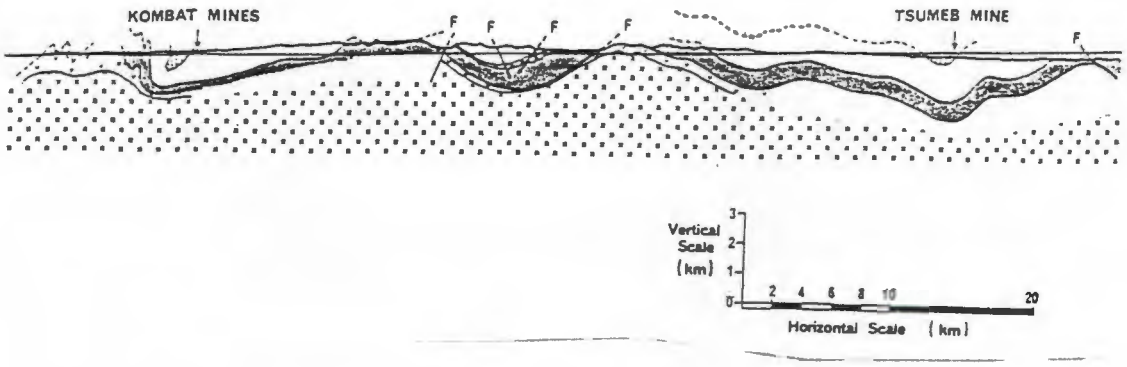

Figure 1.6: Geological cross-section through the OML.

Two phases of folding have been recognized in the OML (Misiewicz, 1988). The first phase of folding (F_1) was the most intense, and was the result of compressional forces from the north and south. This event commenced after the deposition of the Hüttenberg Formation, the uppermost unit of the Tsumeb Subgroup, and prior to and concurrently with the deposition of the Mulden Group. F_1 folding is characterized by tight and in places overturned east-west trending folds.

The second phase of folding (F_2) was initiated by mild east-west compression, resulting in the low-sinuosity re-folding of F_1 synclines and anticlines. The F_2 event was also accompanied by widespread jointing and fracturing, between 650 and 620 Ma.

1.6 Review of Genetic Models for the Ore Deposits

A summation of the genetic models which have been proposed for the ore deposits of the OML is presented by Misiewicz (1988), extracts of which will be described in this section. However, due to the greater economic significance of the Tsumeb and Kombat mines within the OML, these deposits have been subjected to a greater level of investigation, compared to Berg Aukas mine and similar deposits. For this reason, the following models are mainly applicable to Tsumeb-type mineralization, unless otherwise stated.

1.6.1 Magmatic Origin Model

A model based on magmatic processes was developed primarily for the Tsumeb deposit. The concept was reviewed by Lombaard et al. (1986), based on the supposed evidence that the so-called "pseudo-aplite" in the Tsumeb deposit is an igneous rock. The model suggests that the metals were derived from a magmatic source, related to the emplacement of igneous bodies intruded at depth beneath the Otavi Mountains.

The model has generally been rejected, based on the agreement that the "pseudo-aplite" is clearly a feldspathic sandstone, having originated from the Tschudi Formation (Misiewicz, 1988). Furthermore, the hypogene mineralization post-dates the emplacement of the sandstone (Lombaard et al., 1986).

A similar theory was proposed (Söhnge, 1964; Allsopp and Ferguson, 1970), suggesting that the calcitic alteration at Tsumeb might have a carbonatitic origin, since it and the Tsumeb West pipe lie virtually on the Tsumeb West geofracture. This is an east-north-east extension of the Cape Cross-Okarusu lineament, along which a number of alkaline and carbonatitic complexes have been emplaced. Allsopp and Ferguson (1970) tested the theory with Sr isotopes, and found that the $^{87}Sr/^{86}Sr$ ratios do not correlate with those typical of carbonatites.

1.6.2 Basin Dewatering Model

A basin dewatering model was first proposed by Emslie (1980), to account for Kombat and Berg Aukas-type mineralization. This was later modified by Misiewicz (1985), who used the genetic models proposed for the Pine Point deposit in Canada (Kyle, 1981; Anderson and Macqueen, 1983; Garven, 1985) as a basic framework.

The model as applied to the OML incorporates the evolution of hydrothermal brines in a deep geosynclinal trough due to compaction and subsequent diagenesis. The mechanism involves the leaching of metals from the sedimentary pile, and the movement of highly saline metalliferous fluids. The temperature necessary for such a process lies in the range 100 - 250°C, with conduits for fluid migration

being provided by rift-grabens, growth faults, unconformities, and other basement fractures. The mineralization would preferentially be deposited in a carbonate host, in sites produced by solution and collapse during hydrothermal karsting.

Such karstic features may also host a source of S, to provide a chemical means of sulphide precipitation. However, there is uncertainty as to the exact nature of this S source. It has been suggested (Misiewicz, 1988), that the S may have been made available directly from evaporitic sequences within the carbonates. Emslie (1980) estimated that an ore body of one million tons, with a grade of 3 ppm (combined Cu, Pb and Zn), would require a source volume of some 100 km^3.

1.6.3 Mixing Model

The "mixing model", proposed by Allsopp et al. (1981), is a variation of the dewatering model, as it was first perceived by Emslie (1980). The model was designed to explain the anomalous differences in Pb-isotope data, which exists between the various types of ore bodies found in the OML. It is postulated that the Pb leached from two different sources, thus generating ores of different Pb-isotopic character. As the hydrothermal fluids migrate, they will adopt different isotopic signatures, depending on the rock types through which these fluids percolate.

1.6.4 Berg Aukas Model

The current status as to the genetic model designed to account for the Berg Aukas Zn-Pb-V deposit, is reflected in the model described by Misiewicz (1988). The sequence of events leading to the formation of the Berg Aukas deposit commenced with the deposition of Nosib clastics, and the subsequent deposition of carbonates in a localized basin. A nearby basement granite dome in addition to a regional fracture pattern had influenced the pattern of sedimentation, by generating a series of unconformities beneath and within the carbonates.

The Damaran orogeny was responsible for providing structurally induced conduits, which facilitated the movement of hydrothermal fluids originating from basin dewatering of the Swakop Trough (Misiewicz, 1988). A basal unconformity in the vicinity of Berg Aukas acted as an aquiclude surface, having guided the inferred brines toward the overlying porous and permeable carbonates. Permeability barriers within the carbonates, in the form of carbonate mudstones, may then have initiated karsting and ore deposition, assuming an adequate source of S to have been present.

Subsequent oxidation by circulating meteoric waters concentrated the ore body, and deposited vanadium which was transported as calcium metavanadate complexes. The V was derived either from the weathered components of the gabbros in the underlying basement complex, or from sediments which were derived from the basement.

2. GEOLOGICAL AND PETROGRAPHIC INVESTIGATIONS IN THE VICINITY OF THE BERG AUKAS MINE

2.1 Introduction - Field Work and Sampling

Mapping and sampling of the study area were conducted during 1989-1991, using an exploration grid which had initially been established for various soil geochemical and geophysical surveys. The north-south trending lines were cut perpendicular to an east-west base line, with a spacing which range from 40 m (in close proximity to the mine) to 120 m. Appendix I is a geological map of the study area, on a scale of 1:10 000.

Representative samples were selected from boreholes, in addition to all the major outcrops at obvious changes in lithology. Sample localities are indicated in Figure 2.2, which represents a geological interpretation of the mapping data. Due to inferred structural complications and calcrete covered intervals within the study area, no reliable correlation between outcrops or features could be accomplished. Additional samples were taken from drill core which had been drilled subsequent to the closure of the mine. Regrettably, the core of some 150 holes which were drilled whilst the mine was functioning had been discarded just prior to mine closure.

The different lithotypes distinguished are listed in Table 2.1. Due to the extent of neomorphic alteration and extensive calcrete cover over a large portion of the study area, lateral relations between lithotypes are difficult to determine. However, an attempt was made to characterize a particular lithotype on the basis of colour and depositionally derived features (where these have been preserved). All of the rocks at Berg Aukas have been diagenetically altered to varying degrees. The least altered samples retain a fine-grained micritic fabric which occasionally contains reasonably well-preserved allochems. Sedimentary laminations have been preserved in some of the finer grained units, whereas the coarser grained units appear massive. The more altered samples within any lithotype are composed of a hypidiotopic to xenotopic dolomite mosaic, that may contain "ghosts" of allochems or shows no retention of any primary sedimentary features.

Table 2.1: Lithotypes and associated depositional environments of Berg Aukas carbonates.

Code	Lithotype	Depositional Environment
A	Finely laminated dolomite	Deep shelf carbonates
B	Dark grey boundstone	Toe-of-slope bioherms and bioclastic detritus
C	Dark grey rhythmite	Slope rhythmites
D	Light grey dolomicrite/ dolo-arenite	Carbonate sand shoals (platform margin)
E	Laminated mudstone	Tidal mud flats
F	Light grey boundstones/ dolo-arenite & oolite	Organic reef with sands on platform edge
G	Pale grey dolomicrite	Open platform
H	Dark grey dolomicrite with conglomerate	Lagoonal muds with channel conglomerates
I	Laminated limestones	Basin and slope carbonates

2.2 Surface Geology

The general geology of the Berg Aukas area has previously been described in some detail (Söhnge, 1957; Weilers, 1959; Schreuder, 1969; Gavine, 1979; Misiewicz, 1987). However, past geological descriptions failed to distinguish between primary sedimentary features and the overprinted alteration features. This study attempts to separate these two attributes, though the degree of neomorphic alteration of the initial carbonate can be so intense, that it has been necessary to infer the original nature of the sediment, based on the nature of both overlying and underlying units. It will become apparent, in the subsequent sections, that significant differences exist between both the stratigraphic setting and structural interpretations presented by previous workers, compared to what is to be presented in this study.

A geological plan of the study area on a scale of 1:10 000 is appended (Appendix I), and constitutes numerous lithotypes as mentioned earlier. No inference as to the stratigraphic setting of the different lithotypes has been made on the plan. Similarly,

only those structural features which can be seen in the field have been included on the plan. Appendix II represents a series of cross-sections as based on the surface geology. Once again, no inference has been made as to any major structures present, and furthermore, owing to the extensive calcrete and soil cover in places, lithological contacts can only be estimated.

Dominant rock types include dolomicrites, laminated dolostones, dolomitic boundstones/cryptalgal laminates and limestones (Table 2.1). As opposed to the limestones, which are generally brownish in colour, the dolomites vary in colour from a dark grey/black to a very pale grey. The majority of the carbonates at Berg Aukas appear massive, with the exception of the occasional laminated/rhythmitic units and those boundstone units whose stromatolitic components are still preserved.

2.2.1 Lithostratigraphy

The carbonate rocks of the Berg Aukas area form the base of the Abenab Subgroup, the lowermost stratigraphic unit of the Otavi Group. These platform carbonates rest unconformably on rift-fill clastics and metasediments of the Nosib Group to the north of the study area (Hedberg, 1979; Misiewicz, 1988), and abut against a major mafic intrusive, known locally as the Grootfontein Mafic Body (GMB), which sub-outcrops to the south-east.

Significant differences were noted in this study, as regards to the stratigraphic setting of the so called Berg Aukas and Grootfontein "Synclines", as described by Misiewicz (1988). In essence, both these synclinal features are not synclines. For the case of both the larger "Grootfontein Syncline" and the smaller "Berg Aukas Syncline", there are extreme differences in the lithological composition of the opposing limbs which constitute each of the individual "synclines". This can be observed in Appendix II, where section A-A' is drawn across the northern part of the "Grootfontein Syncline"; section B-B' transects the "Berg Aukas Syncline"; and sections C-C' and D-D' both transect the "Grootfontein Syncline" further to the south west.

Such differences in lithology on opposing limbs of both "synclines"

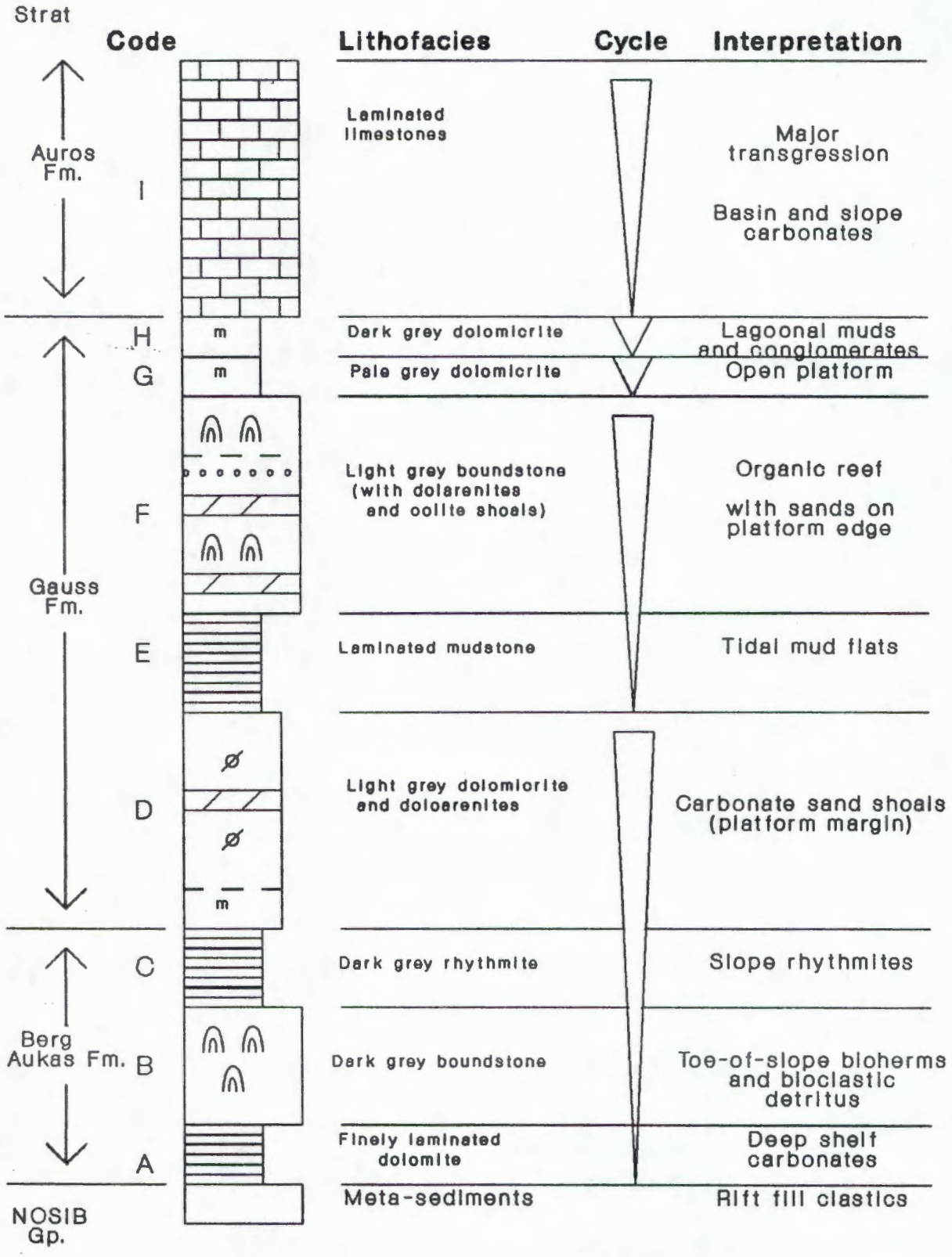

Figure 2.1: Genetic stratigraphy of the Berg Aukas area (not drawn to scale).

is, according to this study, the result of major structural

movement, as opposed to lateral facies changes as proposed by Misiewicz (1988).

An idealized stratigraphic column as proposed for the Berg Aukas area is presented in Figure 2.1, whilst a comparison of the lithostratigraphic units as proposed by Misiewicz (1988) is presented in Table 2.2.

Table 2.2: Relationship of Abenab Subgroup formations to previously described units (lg = light grey; dg = dark grey; dol = dolomite; l/stn = limestone; b/stn = boundstone).

This Study			Misiewicz (1988)		
Strat.	Code	Description	Description	Code	Strat.
Auros Fm.	I	laminated l/stn	brown l/stn	(OAa3)	Auros Fm.
Gauss Fm.	H	dg dolomicrite with conglomerate	?		
	G	lg dolomicrite	massive lg dol	(OAa2)	
	F	lg b/stn /dolo-arenite & oolite	?		Gauss Fm.
	E	laminated mudstone	?		
	D	lg dolomicrite/ dolo-arenite	lg colloform dol	(OAg1c)	
			recrystallized lg dol	(OAg1b)	
			massive lg dol	(OAg1a)	
Berg Aukas Fm.	C	dg rhythmite	laminated dg dol	(OAb4)	Berg Aukas Fm.
	B	dg boundstone	stromatolitic lg dol	(OAb3)	
	A	laminated mudstone	laminated lg dol	(OAb2)	
N O S I B G R O U P M E T A S E D I M E N T S					

It should be noted that the lithostratigraphic units used by Misiewicz (1988) were adopted from the nomenclature used by mining geologists at Berg Aukas, during the period when the mine was operational. The stratigraphic setting so described may well have been applicable for the comparatively small confines of underground

development, but difficulties soon arise when applying this stratigraphic concept on a more regional scale. Furthermore, it would appear that little regard was taken in delineating pre-, syn- and post-depositional structures.

For instance, terms such as "laminated dark grey dolomite" (OAb4) are readily associated with "recrystallized light grey dolomite" (OAg1b) and "light grey colloform dolomite" (OAg1c). In this case syn-depositional descriptions are used in the same context as post-depositional descriptions. It is regrettable that a broad (regional) picture of the sedimentary domains of the carbonate sequence is lacking.

During this study an attempt has been made at delineating lithozones, based on defining lithofacies associations, lithofacies cycles and increments of sedimentation within the sequence as such, and within specific lithozones. Beukes (1989) described how the application of the basic principles of genetic stratigraphy, can be used to distinguish between "sedimentary" and "tectonic" stratigraphic contacts, especially with regards the recognition of low-angle strike-slip and/or bedding plane faults. Such principles have been applied in this study.

The stratigraphic column proposed in this study is based purely on the attributes described earlier, and little inference has been given to the altered/recrystallized appearance of the rock. A geological interpretation of the study area, incorporating the stratigraphic zones presented in this study appears in Figure 2.2, whilst Figure 2.3 represents a series of cross-sections based on the inferred geological setting.

2.2.2 Structure

In describing the structural setting of Berg Aukas, it is important to realize that there is very little surface expression as to the occurrence of any major structural features. Apart from extensive surficial calcrete development, the extent of neomorphic alteration may well have masked any earlier structural features.

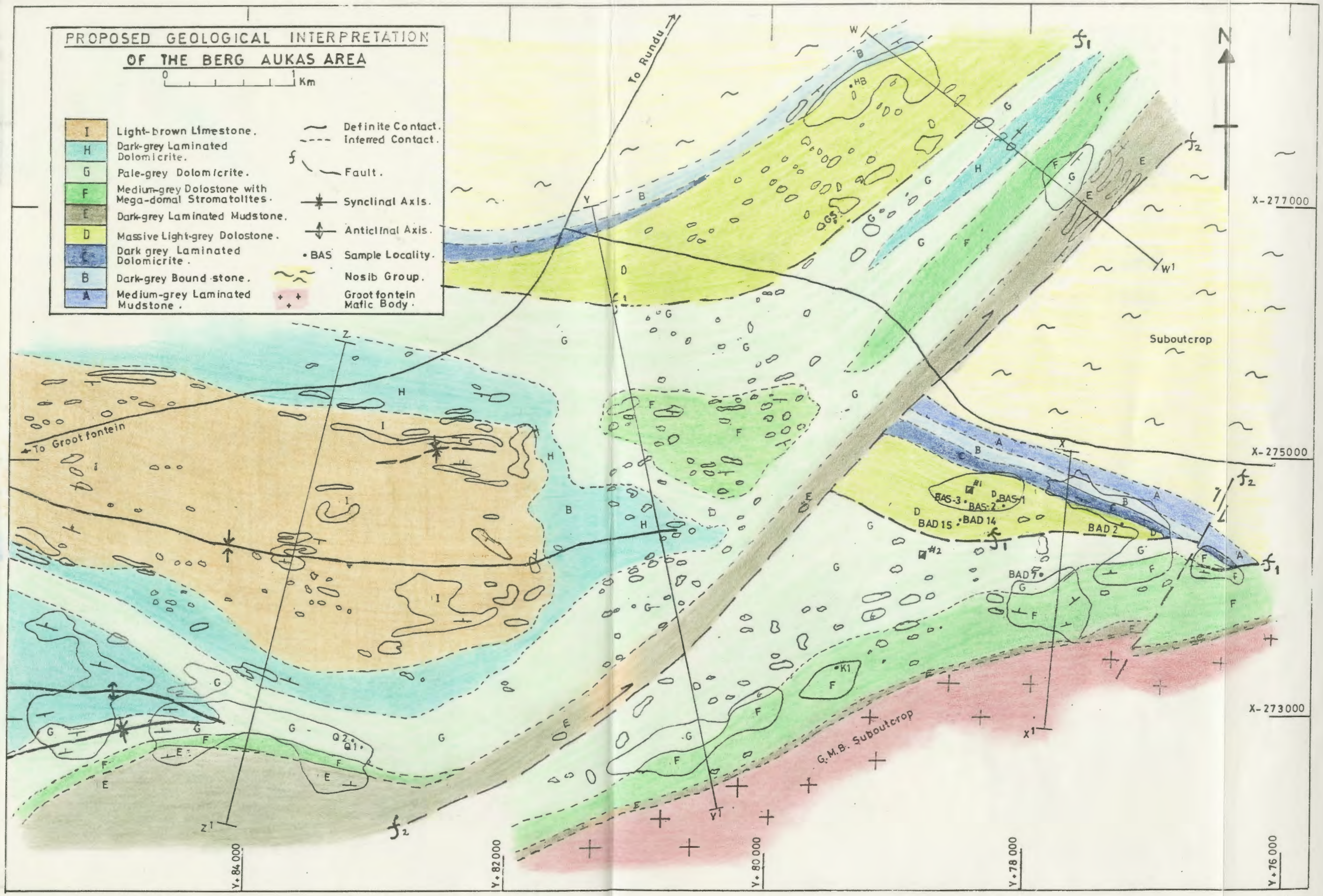

Figure 2.2: Geological interpretation of Berg Aukas.

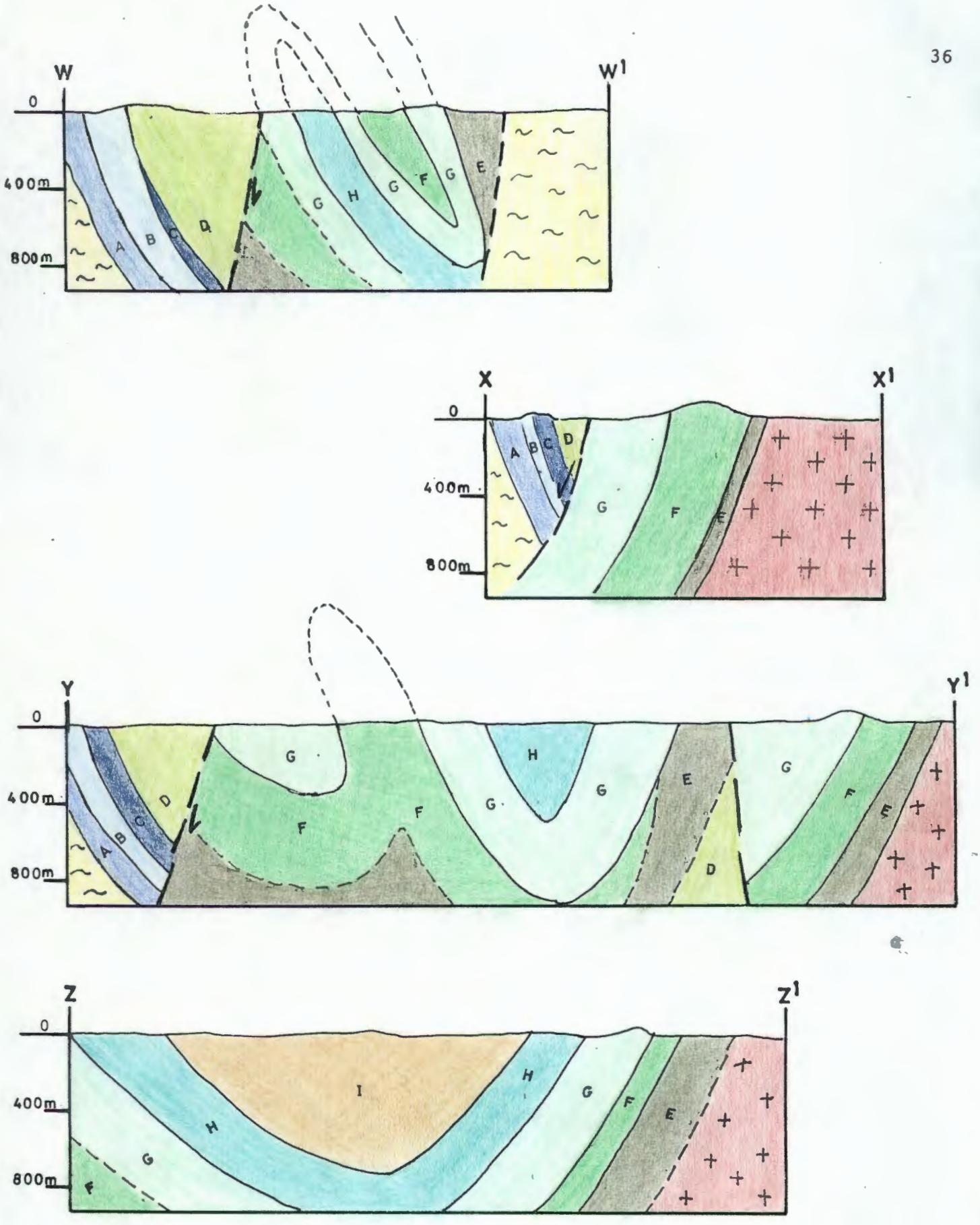

Figure 2.3: A series of cross-sections based on inferred surface/structural geology.

To account for the geological interpretations presented in Figures 2.2 and 2.3, it is envisaged that there was an early phase of "extensional tectonics", followed by a later period of "compressive tectonics".

Extension in the basement rocks resulted in the development of regional grabens, followed by the development of syn-tectonic basins, and subsequent subsidence. Basement-controlled graben faults then propagated upwards through the overlying sediments. Such a scenario is represented in Figure 2.4 as taken from Roering (1989), and represents a cartoon of a carbonate coastal/shelf half-graben, and the various sedimentary facies associated with it.

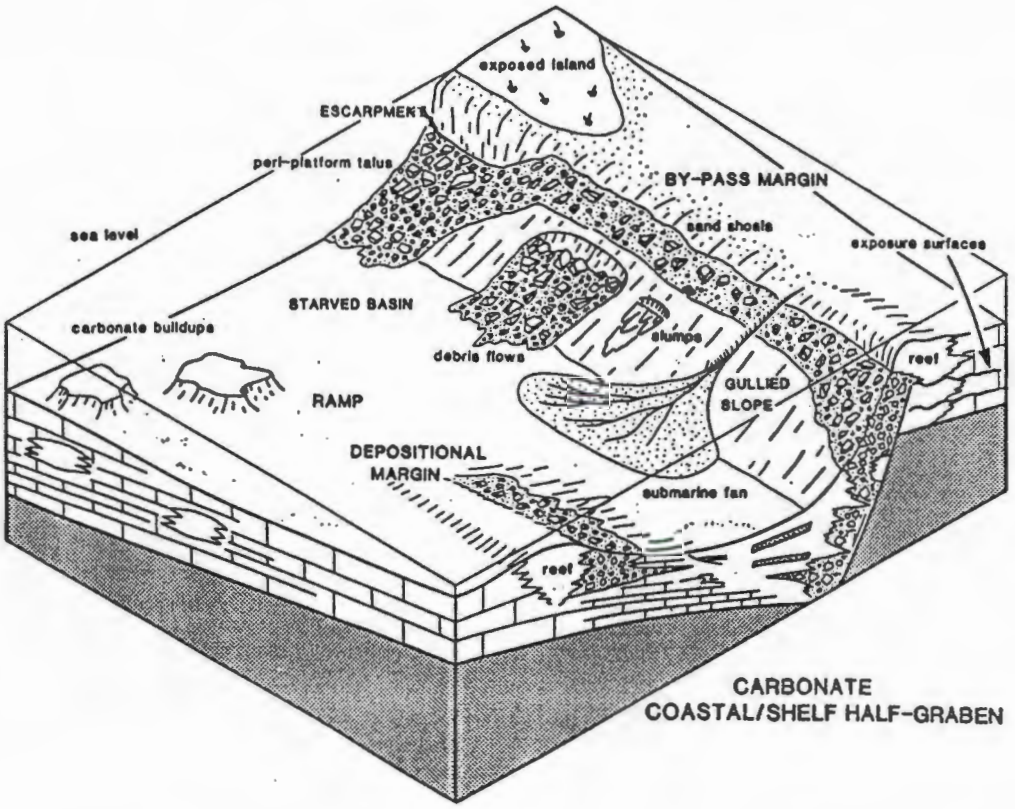

Figure 2.4: Carbonate coastal/shelf half-graben showing the associated carbonate facies (after Roering, 1989).

Both the Nosib and Otavi Groups would have been deposited on the northern flank of a graben over basement extension faults (normal faults), termed here as half-grabens, as illustrated in Figure 2.5.

Evidence for such syn-tectonic sedimentation in the Berg Aukas area include soft-sediment slump-structures of various orientations within the lowermost boundstone unit, on the northern limb of the so called Berg Aukas "Syncline". As shown in Figure 2.2, the half grabens are separated by cross-faults, which strike oblique to the main graben edge.

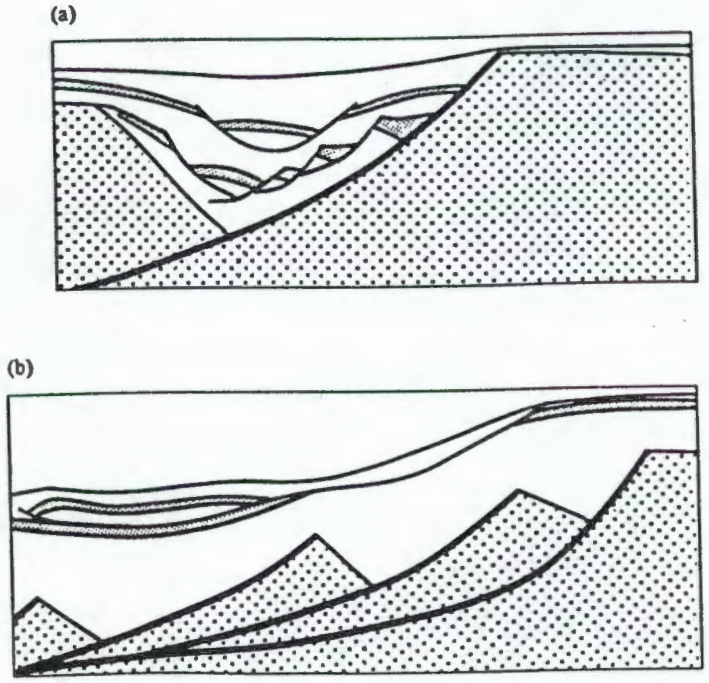

Figure 2.5: Structures developed above basement extension faults. (a) Distributed extension within sedimentary wedge coupled to basement faults. Tops of basement blocks are eroded. (b) Gravity slide on starved basin margin above extended basement - note repetition of section.

During a later period of compressive tectonics, older normal faults were reactivated as reverse faults. This type of inversion tectonics is illustrated in Figure 2.6. and a good presentation as to the geometrical characteristics of inversion, is presented by Hayward and Graham (1989). The shortening due to compression is largely taken up by reverse movement along the faults, with only limited shortening being taken up by buckling.

With continued compression, thrusting is developed along new shallow-angle-zones of movement as shown in Figure 2.7.

Such a structural scenario for Berg Aukas differs greatly from the model proposed by Misiewicz (1988), as illustrated in Figure 2.8,

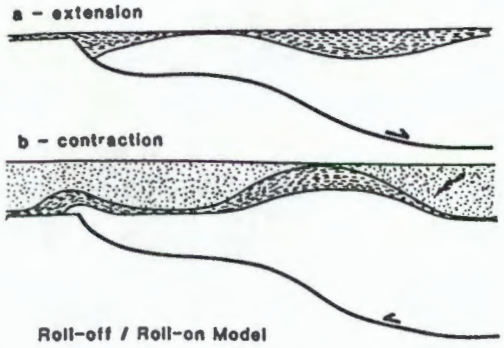

Figure 2.6: Development of hangingwall basins during extension (a) and compression (b) on a stepped fault system during regional subsidence.

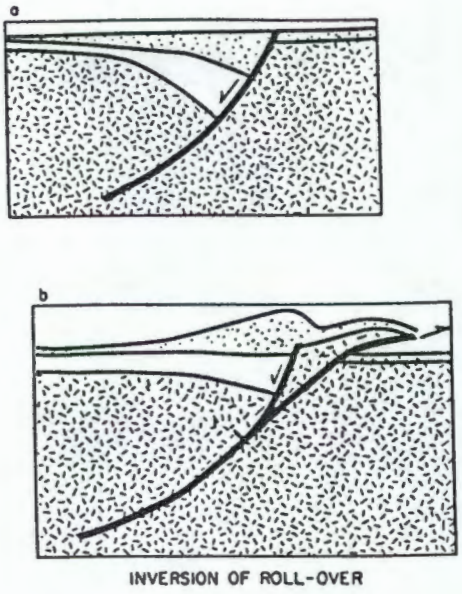

Figure 2.7: Collapse of roll-over with the development of back thrusts and a shallower compressional ramp breaking through under the extensional block.

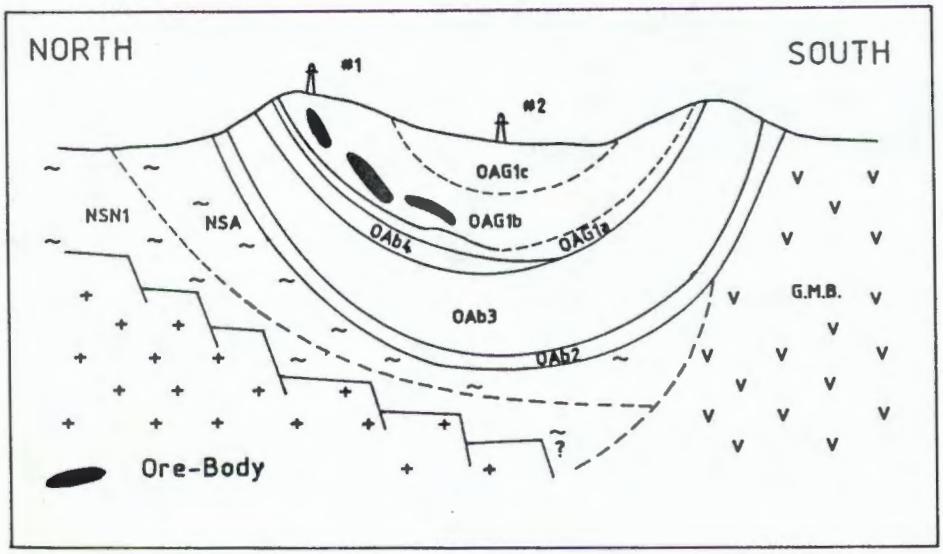

Figure 2.8a: The tectono-stratigraphic setting of the Berg Aukas "syncline", after Misiewicz (1988).

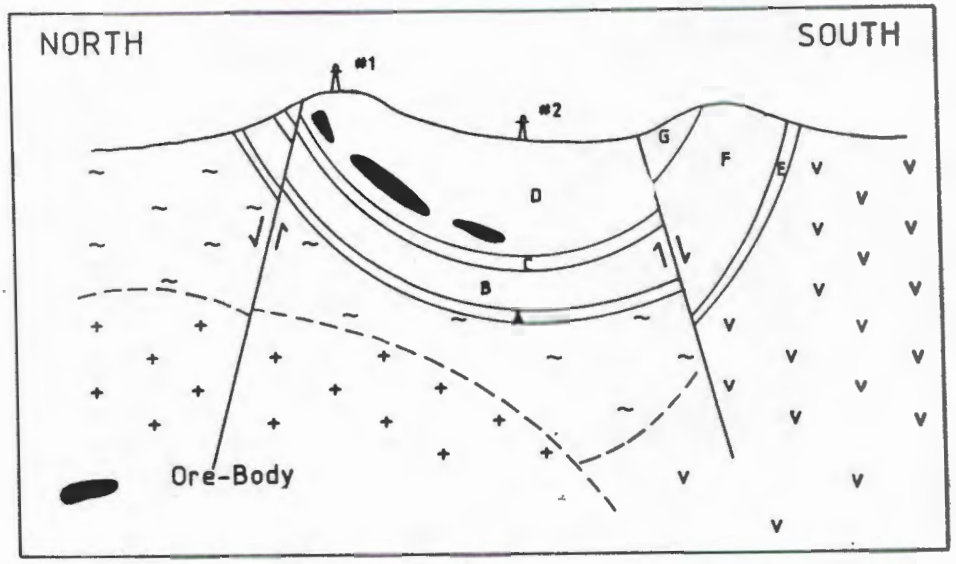

Figure 2.8b: The tectono-stratigraphic setting of the Berg Aukas syncline as proposed in this study.

which compares a section across the Berg Aukas "Syncline" as proposed by Misiewicz (Fig. 2.8a) with that proposed in this study (Fig. 2.8b).

2.2.3 Alteration

It has been emphasized in previous sections, that precise identification of Berg Aukas carbonates for the purpose of environmental interpretation is difficult, due to their susceptibility to diagenetic alteration. Prevailing neomorphic crystallization, cementation, and mineralogical replacement of the original carbonate sediment, may result in a mat of dense crystal fabric.

An attempt was made to qualify, and to a lesser extent quantify, the degree of recrystallization or neomorphic alteration on a megascopic scale. Parameters would include the visible extent of alteration, in terms of replacement dolospar which may occur in fractures and vugs, in addition to the grain size of individual carbonate crystals. The presence of silicified fracture- and vug-

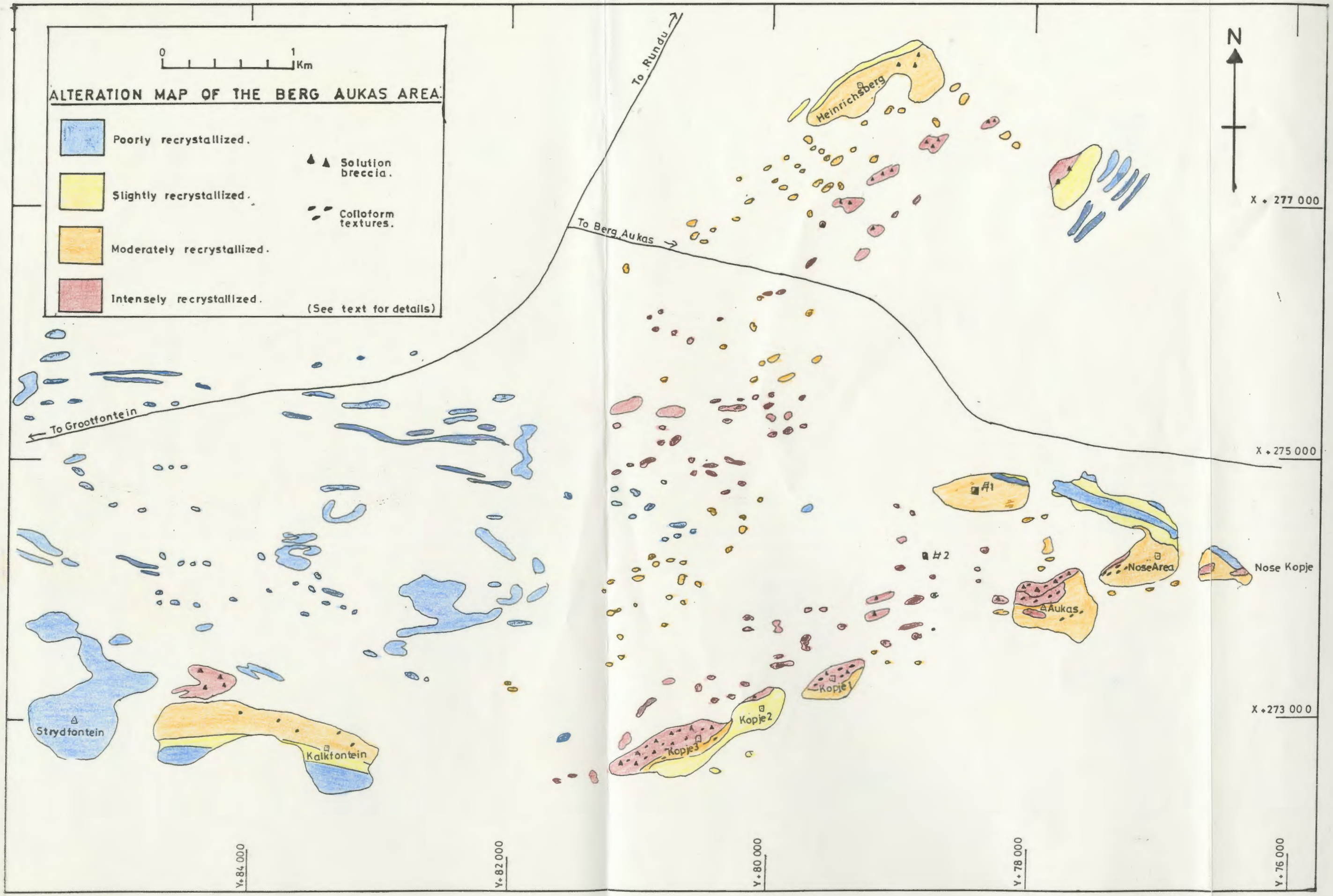

Figure 2.9: Alteration map of the Berg Aukas area.

filled material, was also used as a measure of the degree of alteration.

For the purpose of this study, the following alteration groups were derived:

i) **Poorly developed neomorphic alteration:** The rock may have a minor component of finely crystalline microspar, but appears unaltered. Primary sedimentary laminations may well be preserved.

ii) **Slightly neomorphosed, finely crystalline rock:** The rock consists almost exclusively of fine- to medium-crystalline microspar. Colloform textures and coarse dolospar inclusions are rare.

iii) **Moderately recrystallized/neomorphosed rock:** The rock is medium- to coarsely-crystalline, with minor development of colloform textures and replacement dolospar. Selective silicification of cryptalgal and stromatolitic laminations are common within the boundstone units.

iv) **Intensely recrystallized/neomorphosed rock:** The rock appears coarsely crystalline, with a major component of coarse dolospar. Colloform textures are abundant, and the degree of silicification is higher than in the previous types.

Figure 2.9 is a reduced sketch of the Berg Aukas area and reflects the state of rock alteration, based on the aforementioned criteria. There would appear to be a close association between the extent of recrystallization and the inferred lithofacies. This may in part reflect the porosity and related grain size of the initial carbonate. For instance, the laminated mudstones appear to be poorly recrystallized, whereas the more porous stromatolitic horizons appear to be moderately to intensely recrystallized.

The extent of recrystallization may also reflect the degree of secondary porosity, derived either by the dissolution of the original carbonate, or by tectonic processes. Once again a degree of caution is required to distinguish "sedimentary" from "tectonic" stratigraphic contacts.

2.2.4 Types of Brecciation

Three broad types of brecciation have been observed within the Berg Aukas area, and can be described as follows:

i) **Karst-fill/collapse breccia:** This type comprises of dolomitic clasts of varying size, supported by a well consolidated matrix of either dolomitic mud or a coarser carbonate sand (Plates 2.1a and b). This is considered to be the result of primary karsting, as opposed to secondary karsting which is characterized by the occurrence of an assortment of poorly consolidated breccia blocks cemented by predominantly calcite and descloizite (Gavine, 1979).

ii) **Tectonic breccia:** As illustrated in Plate 2.1c, this breccia type is more the result of tectonic movement, as opposed to chemical dissolution and collapse as in the karst associated breccia types. It is generally observed that the physical disturbance of the rock post-dates the formation of the primary recrystallization event. The porosity generated by brecciation was subsequently occluded by a medium- to coarsely-crystalline, white sparry dolomite.

iii) **Solution breccia:** This describes a breccia type which is believed to have formed by the chemical dissolution of the initial dolomite. The matrix consists of a secondary carbonate which may display varying degrees of recrystallization. In the example presented here (Plate 2.1d), the initial lighter coloured dolomicrite has undergone dissolution, to be replaced by a coarser and darker-coloured recrystallized dolomite. Secondary porosity has subsequently been occluded by a coarser, milky white dolospar. It is possible that the sites for chemical dissolution may have been initiated by fractures. Such a breccia type may be similar to the replacement breccia described by Gavine (1979). Furthermore, a solution breccia will differ from a tectonic breccia, in that a solution breccia will not show any obvious signs of movement of clasts or other rock fragments.

a. b. c.

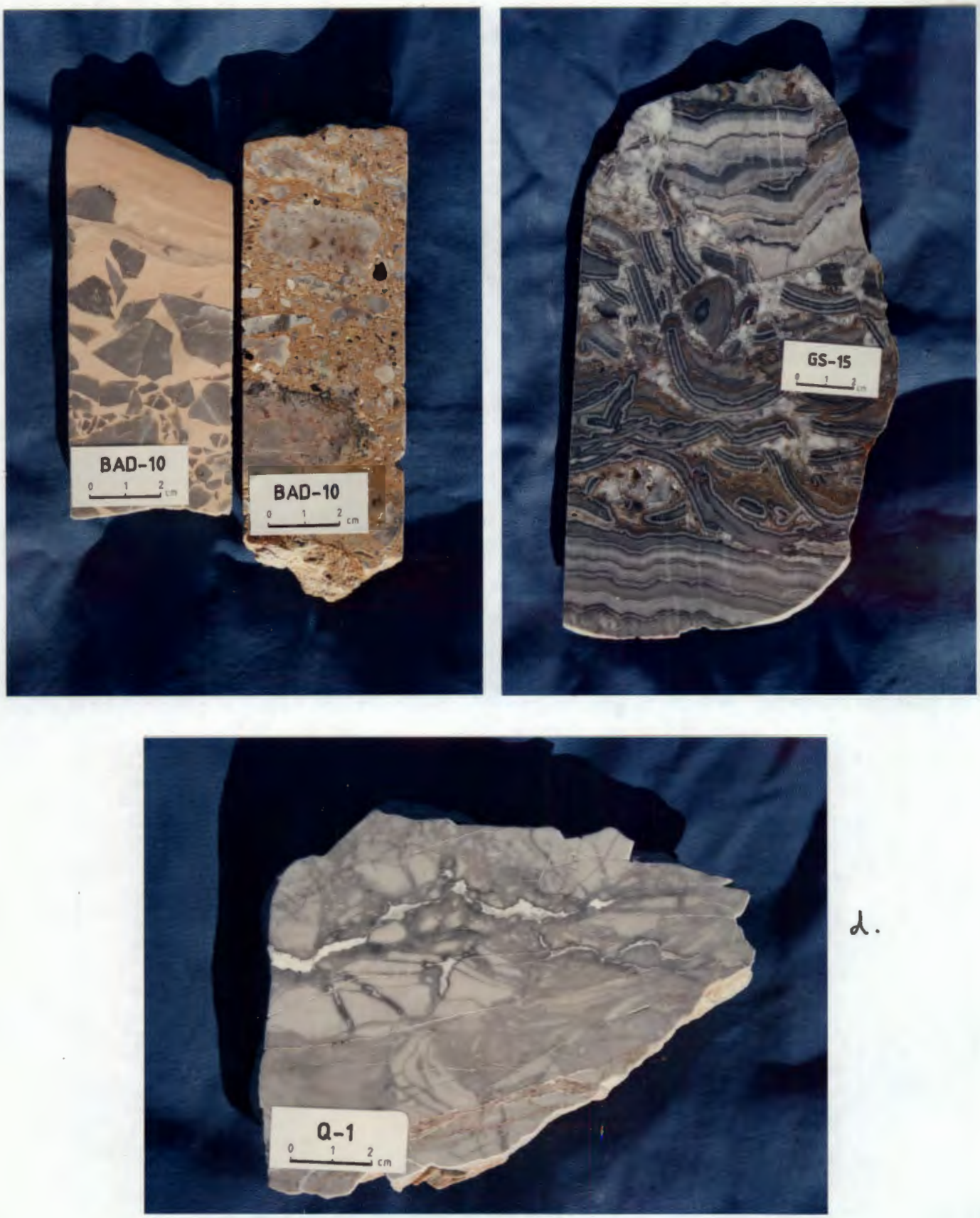

d.

Plate 2.1: Types of brecciation as found at Berg Aukas:- Karst-fill/collapse (a and b); Tectono-solution (c) and solution type (d).

2.3 Types of Ore Bodies

According to mine records, there are 3 broad types of ore body that can be found at Berg Aukas. These are the Northern Ore Horizon (NOH), the Central Ore Body (COB), and the Hanging Wall ore body (HW). Figures 2.10 and 2.11 represent a composite underground plan of the Berg Aukas mine, and a simplified section through the deposit, respectively. A brief description of each type follows.

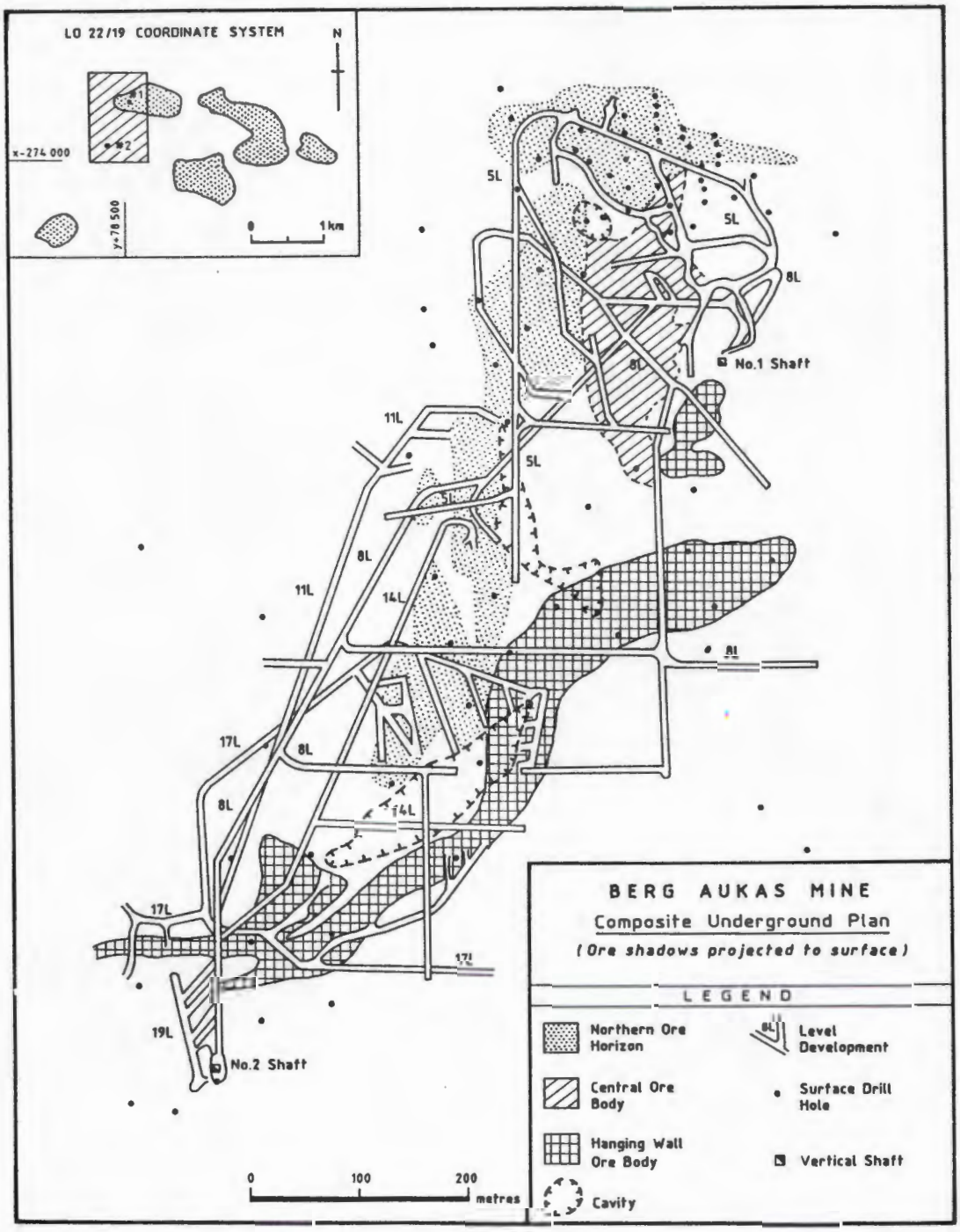

Figure 2.10: Composite underground plan of the Berg Aukas deposit.

2.3.1 The Northern Ore Horizon (NOH)

The NOH comprises 3 lenses of stratabound, largely oxidized sulphides, lying on the contact between the Massive Grey Dolostone and the Light Grey (recrystallized) Dolostone (Misiewicz, 1988). The mineralization of this ore body strikes east-west and dips steeply to the south, in conformity with the local bedding.

The mineralized lenses have been subjected to considerable oxidation and brecciation. According to Weilers (1959), a typical lens would consist of a massive sulphide at the base, comprising coarse grained sphalerite and galena in ratios of approximately

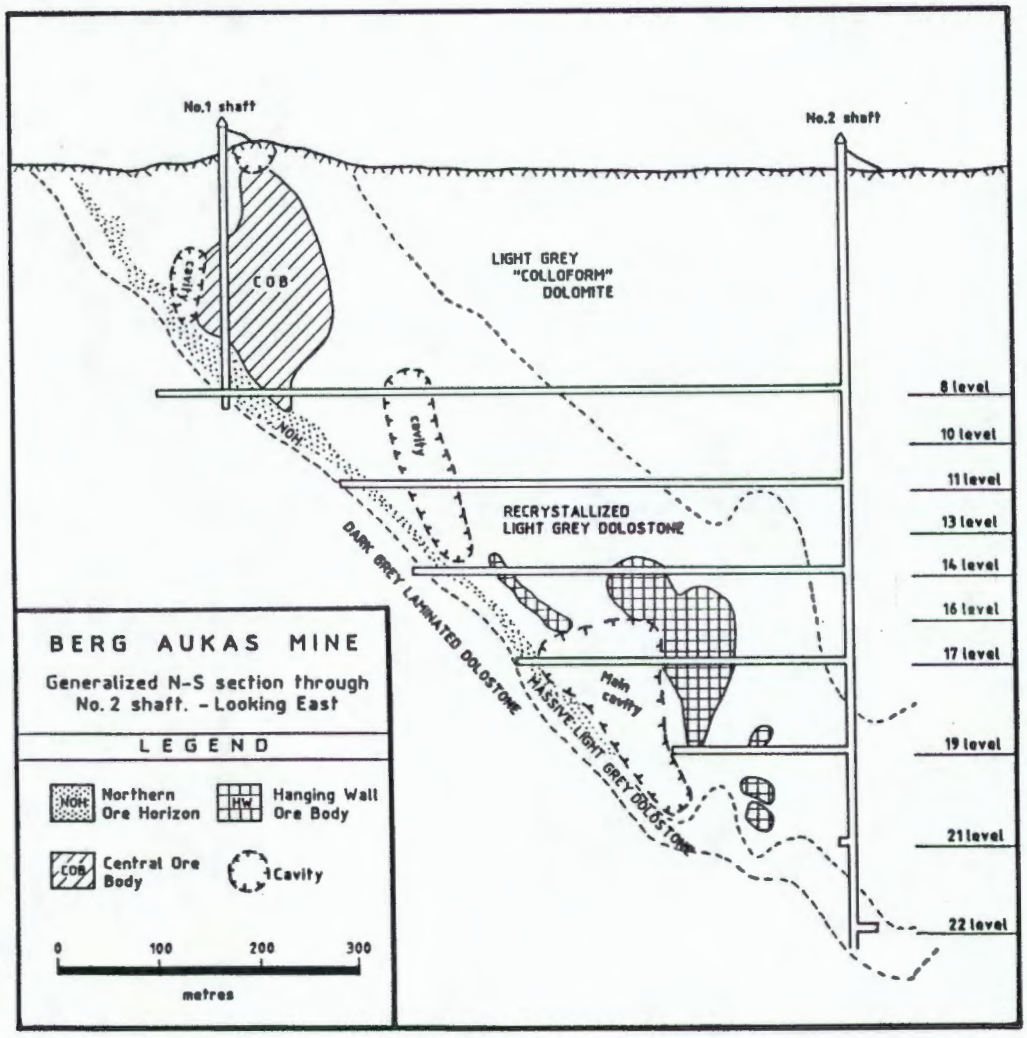

Figure 2.11: Simplified north-south section (looking east) through the Berg Aukas deposit.

3.4:1. The upper portion of the sulphide body is usually oxidized into predominantly willemite, and subordinately smithsonite and cerussite. Primary and oxidized sulphides are capped by a dolomitic breccia enriched in descloizite.

Such ore lenses are in sharp contact with the host dolostone, and usually incorporate a system of cavities in close proximity to the ore lens. Caliche sand and mud enriched in descloizite have been found to occlude these cavities.

2.3.2 The Central Ore Body (COB)

As documented by Misiewicz (1988), the COB is a term used for a discordant brecciated pipe-like body which extended vertically, from the Massive Grey Dolostone contact into the hanging wall. Though similar to the Hanging Wall ore bodies, the COB is distinguished by a higher grade of ore.

The COB was exposed on surface as a series of mineralized mud-filled fractures, but was not greater than 40 x 10 m in extent. Below surface it developed into an elliptical body, due to the concentration of a complex network of steeply dipping north-south fractures (Schreuder, 1969).

The ore was extensively oxidized and enriched in vanadiferous muds and breccia. The breccia consisted of clasts of barren dolostone, supported by a matrix consisting of partially oxidized sphalerite and galena intermixed with vanadiferous caliche. According to mine records, cavities found in close proximity to the COB, were frequently lined with massive willemite and descloizite.

2.3.3 The Hanging Wall Ore Body (HWOB)

The HWOB collectively includes all those north-south trending lenses of steeply dipping ore-filled fractures, which were developed in the Light Grey (recrystallized) Dolostones, stratigraphically above the NOH. Unlike the NOH body, the HW ore is near vertical in orientation, and does not appear to have any stratigraphic control as such. Though this type of mineralization

is of similar grade to that of the NOH, it's development was more erratic. Such an attribute made this type of ore body less favourable for efficient mining.

2.4 Types of Mineralization

2.4.1 Hypogene Mineralization

The mineralogy of the hypogene ores as found in the Berg Aukas deposit, have been described in detail by Markham (1958a) and Emslie (1979). In essence, the hypogene mineralogy is dominated by primary sulphides, consisting of sphalerite and galena, with lesser amounts of pyrite.

A reflected light study of polished briquettes was carried out by Misiewicz (1988), who compiled the following table of hypogene mineralogy (Table 2.3):

Table 2.3: The hypogene mineralogy of Berg Aukas (* denotes an accessory mineral).

Sphalerite	ZnS	
Galena	PbS	
Pyrite	FeS_2	*
Tennantite	$Cu_{12}As_4S_{13}$	*
Jordanite	$Pb_{14}As_7S_{24}$	*
Enargite	Cu_3FeS_2	*
Chalcopyrite	$CuFeS_2$	*
Renierite	$Zn_3(AsO_3)_2$	*
Dolomite	$CaMg(CO_3)_2$	
Calcite	$CaCO_3$	
Quartz	SiO_2	

2.4.2 Supergene Mineralization

The Berg Aukas deposit has been subjected to extensive supergene enrichment, with the supergene ores contributing substantially to the total reserve (Misiewicz, 1988). The mineralogy is varied and has been described in two unpublished reports: by Markham (1958b)

and von Rahden (1963). The supergene minerals found at Berg Aukas are summarized in Table 2.4.

Of all the supergene minerals, willemite is the most important and most widely distributed (Markham, 1958b). It occurs in all parts of the mine, and it has been estimated (Misiewicz, 1988) that up to

Table 2.4: The supergene mineralogy of Berg Aukas.

Galena	PbS
Chalcocite	Cu_2S
Covellite	CuS
Greenockite	CdS
Willemite	Zn_2SiO_4
Smithsonite	$ZnCO_3$
Cerussite	$PbCO_3$
Calcite	$CaCO_3$
Dolomite	$CaMg(CO_3)_2$
Aragonite	$CaCO_3$
Quartz	SiO_2
Goethite	$FeO(OH)$
Hematite	Fe_2O_3
Descloizite	$PbZn(VO_4)OH$
Malachite	$Cu_2(CO_3)(OH)_2$

40% of the total zinc resource occurs in this form.

An equally important supergene ore mineral, but not as extensively developed as willemite, is smithsonite. Markham (1958b) notes that it is more common in the upper portions of the COB, and is an alteration product formed by the replacement of sphalerite.

Cerussite is not a well developed phase, accounting for less than 1% of the ore minerals. It forms by replacement of galena and is often found within the supergene ores.

Descloizite occurs throughout the supergene fraction, and Berg Aukas has been reported as being the world's leading accumulation of this mineral (Misiewicz, 1988). It is often found as vug and fracture fill associated with karst-fill/collapse breccias.

2.5 Petrographical Studies

For the petrographical investigation of the Berg Aukas area more than 60 thin sections (of which 26 are polished thin sections) have been examined. Most of the thin sections were prepared at the mineralogical laboratory of Tsumeb Corporation Limited (TCL) in Tsumeb, whilst the remaining thin sections and all of the polished thin sections were prepared at the Department of Geology and Mineralogy, University of Cape Town. Most of the sections prepared by TCL were routinely stained with alizarin to distinguish calcite from dolomite.

Four broad dolomite texture groups were observed in the Berg Aukas rocks. The crystal fabrics are informally designated fabrics A-D for this discussion. The fabrics described below are found in varying amounts within all of the lithotypes listed in Table 2.1. Most samples contain more than one of the fabrics described. In general, fine-grained fabrics become less common and coarse-grained fabrics become more common as samples become more recrystallized.

A summation of the dolomite types are listed in Table 2.5, which is followed by a more detailed account of each type.

Table 2.5: Characteristics of dolomite types.

Dolomite Type		Fabric Components
A	Micritic:	- diffuse, micron sized crystals
B	Mosaic:	- fine to coarsely crystalline dolomite, anhedral to subhedral crystals
C	White sparry:	- coarse white dolomite spar
D	Colloform:	- coarse, clear "bladed" scalenohedral dolomite

i) **Type A - Micritic dolomite:** Consists of diffuse micron-sized, clear, subhedral crystals scattered throughout matrices of otherwise unaltered or partially altered dolomitic mudstone (Plate

2.2a). Laminations are common and may be due either to differences in crystal size or to layers of dark, amorphous material. In hand specimen micritic dolomite is more commonly light grey to creamy in colour, though a dark grey/black equivalent has been observed at Berg Aukas.

ii) **Type B - Mosaic dolomite:** A broadly defined category which includes a variety of textures and crystal forms. It incorporates most homogeneous and inhomogeneous areas and patches of crystalline dolomite. Though a broad group, it may be sub-divided into 3 sub-groups, on the basis of crystal size as follows:

B_1 - **Fine crystalline dolomite.** Consists of anhedral to subhedral crystals less than 0.1 mm (usually <0.05 mm) in size, that are tightly intergrown, causing a low porosity (Plate 2.2b).

B_2 - **Medium crystalline dolomite.** Consists of anhedral to subhedral crystals which are 0.1 to 0.5 mm in size and are tightly intergrown. With the exception of the larger crystal size, medium crystalline dolomite resembles fine crystalline dolomite in appearance (Plate 2.2c).

B_3 - **Coarse crystalline dolomite.** Consists of crystals ranging from 0.5 to greater than 1 mm (Plate 2.2d). Straight crystal boundaries are more common in this dolomite type, and tend to be anhedral to subhedral in shape, resembling the xenotopic fabric described by Gregg and Sibley (1984).

Mosaic dolomite is typically light grey in colour, though medium to dark grey varieties have been observed in the field.

iii) **Type C - White sparry dolomite:** A medium crystalline to very coarse (up to several millimeters) dolomite spar (Plate 2.2e). Such dolomite may occur with mosaic (Type B) dolomite or as a fracture/void fill, and displays distinct growth zonation with a coarsening of crystals towards the center of the space which this dolomite occludes. Where voids have been preserved associated with this dolomite, the spar crystals are euhedral facing inward toward the void, indicating growth into open space. Contacts between white sparry dolomite and mosaic dolomite may be sharp (<1 mm) in the case of a fracture fill, or may be gradational over

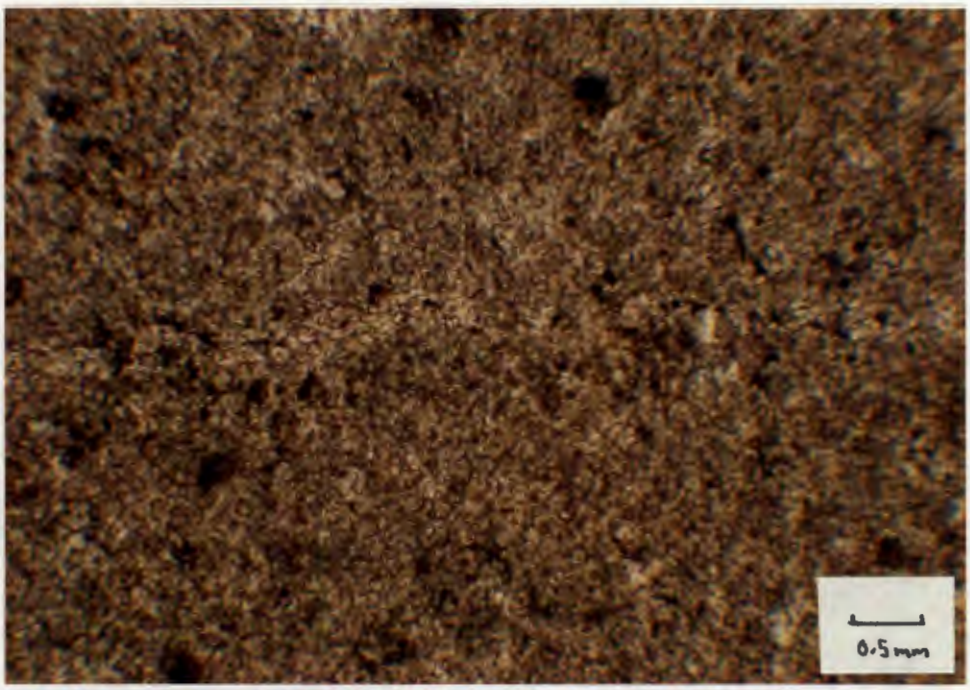

Plate 2.2a:
(BA 74; PPL)
Micritic dol.

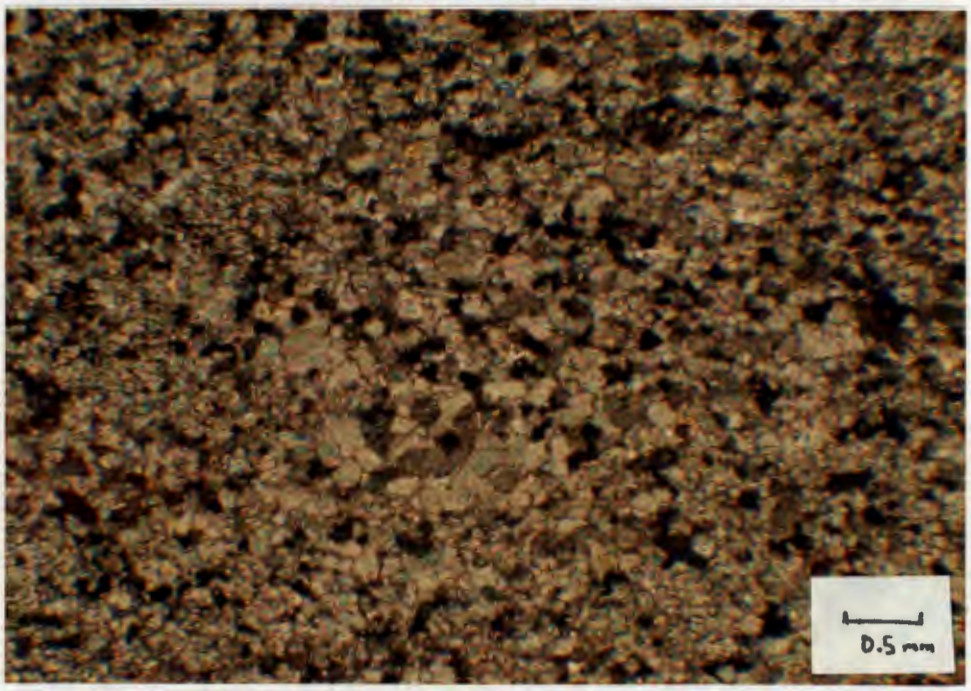

Plate 2.2b:
(BAD 2/1a; XP)
Mosaic dol. - fine.

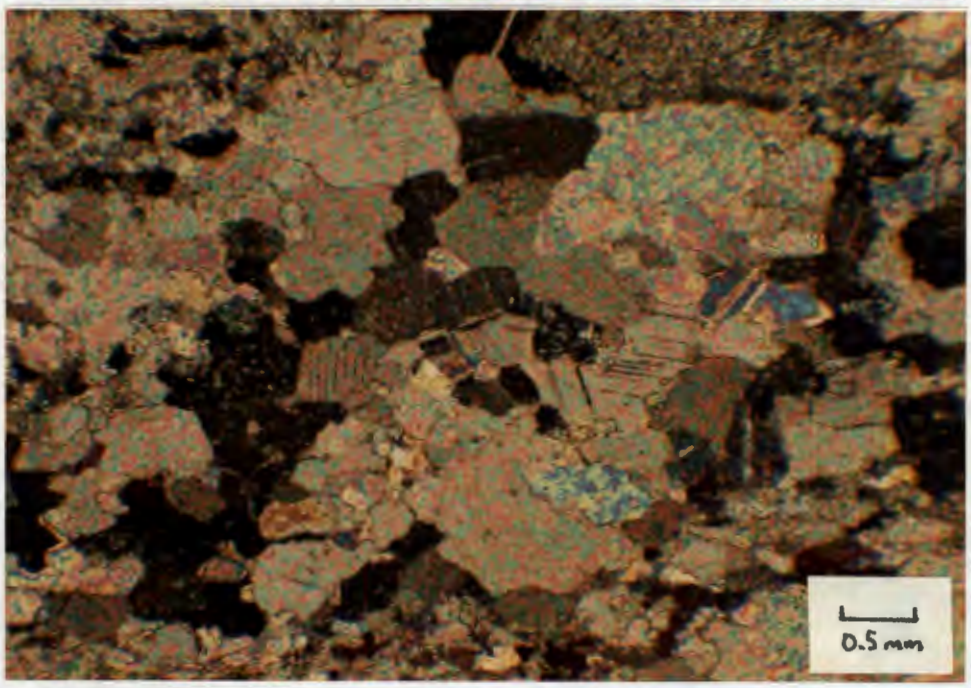

Plate 2.2c:
(GS-1; XP)
Mosaic dol. - medium.

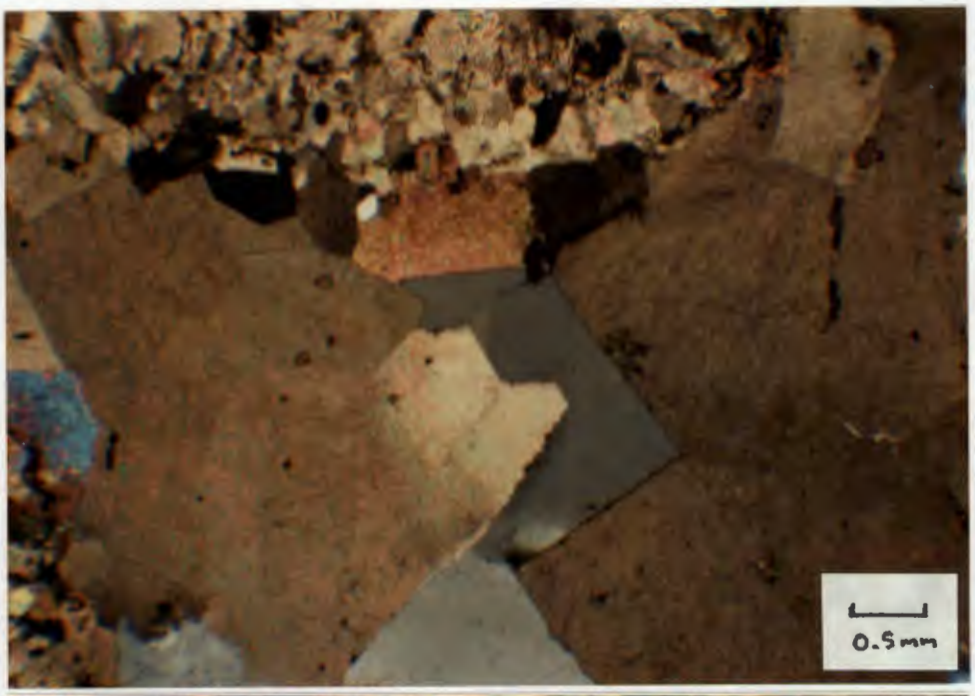

Plate 2.2d: (GS-15; XP) Mosaic dol. - coarse.

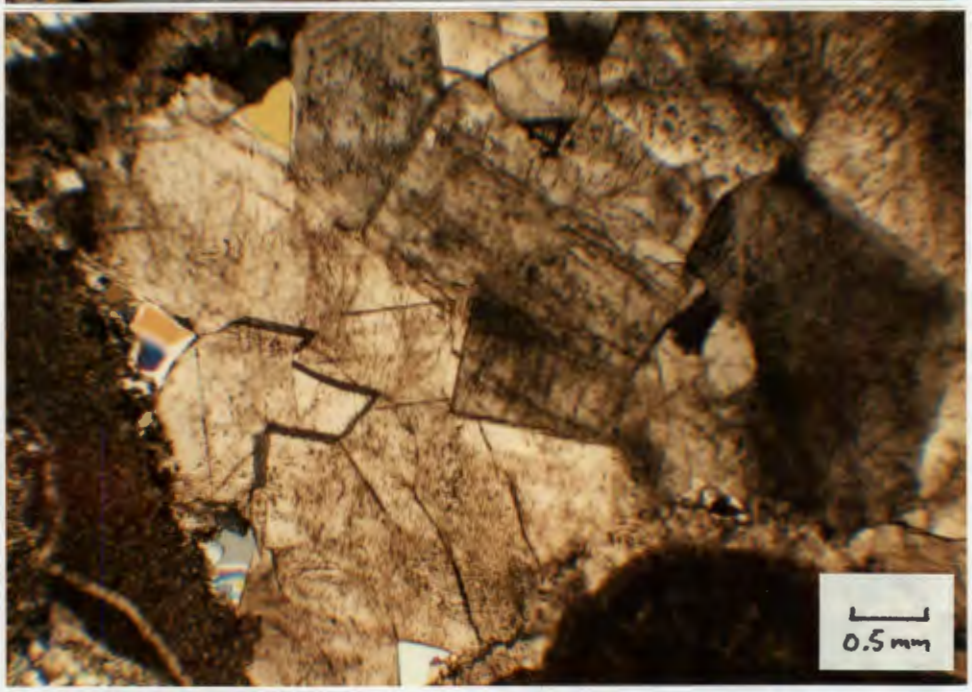

Plate 2.2e: (BAD 8/8; XP) White sparry dolomite.

Plate 2.2f: (GS-7; XP) Colloform dolomite.

several millimeters, with the gradational boundary characterized by crystal overgrowths.

iv) **Type D - Colloform dolomite:** Consists of medium to very coarse (up to centimeter-sized) anhedral to euhedral, white to pink crystals with a distinct "bladed" shape. The term "colloform" is used here in a textural sense as described by Roedder (1968), and includes radial structures consisting of fibrous/bladed, acicular, or columnar crystals which develop approximately perpendicular to fracture walls or void linings (Plate 2.2f). Crystal grains which constitute this dolomite type often exhibit undulose extinction when viewed under crossed polars in thin section. Such features as undulose extinction are closely related to the features of "saddle" dolomite as reported by Radke and Mathis (1980), whilst the overall description of this dolomite type closely reflects that of "Baroque" dolomite (Mattes and Mountjoy, 1980; Horton and De Veto, 1990; Horton and Geissman, 1990).

As a result of the variation in terms of size and shape of these "colloform" textures, and their widespread occurrence throughout the dolostones of the OML, a special section has been set aside in Chapter 5 in an attempt to describe the evolution and formation of these features.

2.6 Host Rock Mineralogy

The mineralogy of the host carbonate was established by means of X-ray diffractometry (XRD), and by limited electron microprobe data. XRD analyses were performed on finely ground air dried rock powder of all the fabric types which were sampled for the isotope study, as discussed in the previous section.

XRD data were obtained using a Philips semi-automated X-ray diffractometer equipped with a graphite monochromator and CuKα radiation, generated at 40 kV and 30 mA. Whole rock, random powder patterns were scanned from 20° to 53° using the step-scan mode, with the data being captured on magnetic disc using a micro computer. For a more detailed account of the machine parameters the reader is referred to Appendix IV.

The following three tasks were performed:

a) Determination of the presence of calcite and quartz in the predominantly dolomite rich samples;

b) determination of the degree of non-stoichiometry by observing the shift of the dolomite 104 peak, based on the method of Lumsden (1980);

c) determination of the degree of dolomite crystallinity by comparing the ratios of the dolomite 104 and dolomite 110 peaks, using the method of Lumsden & Chimahusky (1988).

For the semi-quantitative evaluation of each of the samples, heights of selected peaks were measured and their sum equated to 100%, the results presented here being peak height proportions, as opposed to corrected modal proportions. Identification was based on the 104 reflections for both dolomite and calcite, whilst the 101 reflection was used for quartz. A summation of this data is presented in Table 2.6.

Dolomite is clearly the most dominant mineral type present in most of the rock samples studied, with the exception of occasional siliceous veinlet or void fill (Q2-1c). However, some calcite contamination is present in some of the samples, though the mineral seldom exceeds 5% in mode. Special attention will be given to these samples in the following chapter, when discussing O and C isotope geochemistry.

Examples of diffractograms which illustrate the common tri-mineral assemblages (dolomite-calcite-quartz) appear in Figures 2.12 (a to e). The following groups are evident: dolomite only (Fig. 2.12a); dolomite and minor calcite (Fig. 2.12b); dolomite and quartz (Fig. 2.12c); dolomite with minor quartz and calcite (Fig. 2.12d); and lastly quartz with minor dolomite (Fig. 2.12e).

The second task attempted using the XRD method was that of determining the degree of non-stoichiometry of the host dolomite, by means of observing the shift of the dolomite 104 reflection with respect to an internal standard reflection. The method used is that of Lumsden (1980), who defines non-stoichiometry as the degree

to which the original depositional fabric has been altered by the growth of dolomite crystals, i.e. to measure the departure from the ideal stoichiometric composition $Ca_{0.5}Mg_{0.5}CO_3$.

Table 2.6: Semi-quantitative evaluation of Berg Aukas samples determined by XRD.

Sample No.	Fabric Type	Peak Intensity c/s Qtz (101)	Cal (104)	Dol (104)	Qtz %	Cal %	Dol %
BAD 14/3	A	571	462	12093	4	4	92
BAD 7/1a	A	-	-	21042	-	-	100
Q1-4a	A	712	-	30922	2	-	98
K1-1a	A	-	-	20490	-	-	100
K1-2a	A	613	-	17757	3	-	97
K1-3a	A	-	-	29389	-	-	100
BAD 14/2	A	316	-	22006	1	-	99
BAD 15/13a	A	-	-	20988	-	-	100
BAD 2/1a	B	1698	-	42024	4	-	96
Q2-1a	B	1731	-	25366	6	-	94
Q2-1b	B	-	-	19444	-	-	100
K1-1e	B	-	1579	81774	-	2	98
BAD 15/12	B						
BAD 15/13b	B	1840	-	43392	4	-	96
BAS-1a	B	497	-	24737	2	-	98
BAS-1b	B	1423	-	30802	4	-	96
BAS-2a	B	1588	-	27859	5	-	95
BAS-2b	B	4892	-	45236	10	-	90
BAS-3a	B	2175	-	36288	6	-	94
BAS-3b	B	2941	-	43733	6	-	94
HB-1a	B	3685	-	22194	14	-	86
HB-1b	B	-	-	56763	-	-	100
HB-2	B	-	-	30831	-	-	100
BAD 2/8	B	-	-	36530	-	-	100
BAD 2/3	B	10788	-	14523	43	-	57
BAD 2/2	B	38251	-	8618	82	-	18
BAD 2/7a	B	5434	-	29711	15	-	85
BAD 2/1b	C	7009	-	126056	5	-	95
BAD 2/7b	C	-	-	126409	-	-	100
BAD 7/4b	C	16221	-	82467	16	-	84
Q1-4c	C	7737	-	46951	14	-	86
Q1-10	C						
Q2-1c	C	45108		465	99	-	1
K1-1c	C	-	3485	68581	-	5	95
K1-2c	C	1740	-	89745	2	-	98
BAD 15/13c	C	-	-	65282	-	-	100
BAD 7/3	C	37942	-	2713	93	-	7
BAD 7/1c	D	-	-	61655	-	-	100
BAD 7/4a	D	-	-	80886	-	-	100
BAD 7/2a	D	-	-	77603	-	-	100
Q1-4b	D	-	-	84697	-	-	100
K1-1b	D	-	537	39333	-	1	99
K1-1d	D	-	1390	48093	-	3	97
K1-2b	D	2281	215	37392	6	1	93
K1-3b	D	552	-	53701	1	-	99
K1-3c	D	-	-	91748	-	-	100

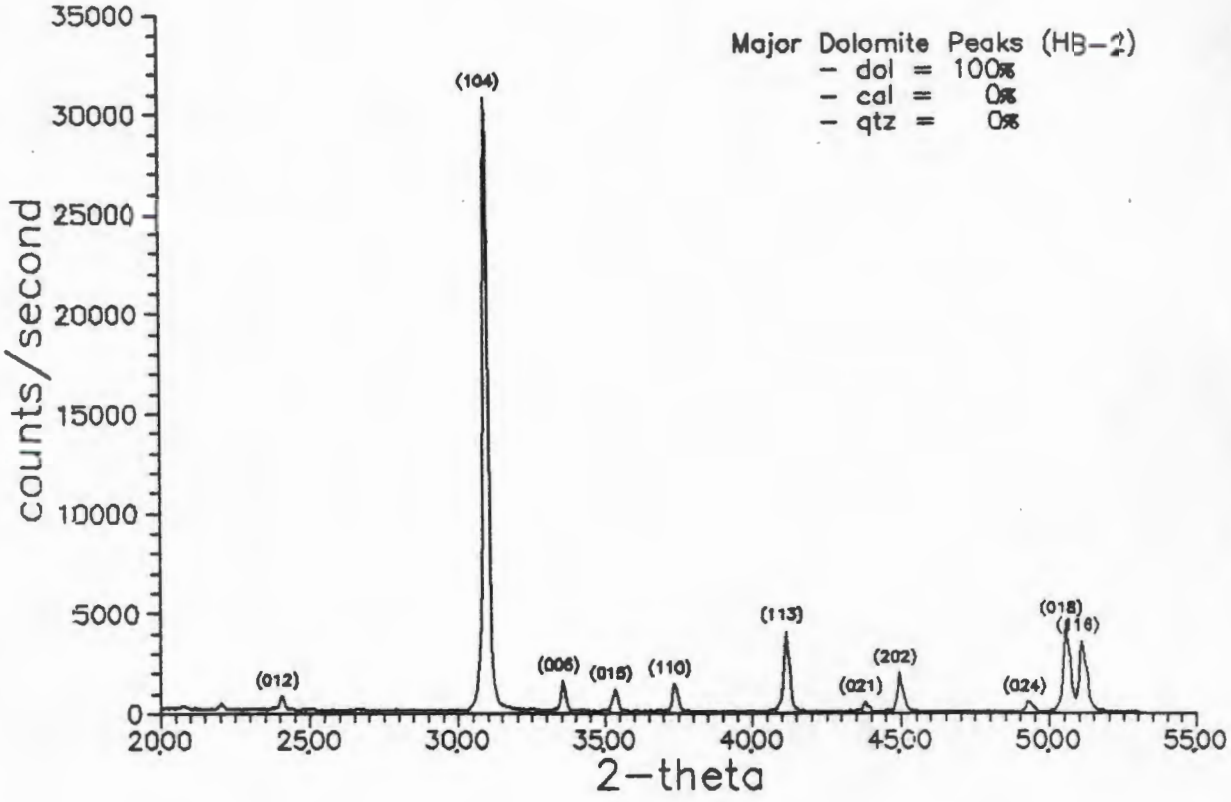

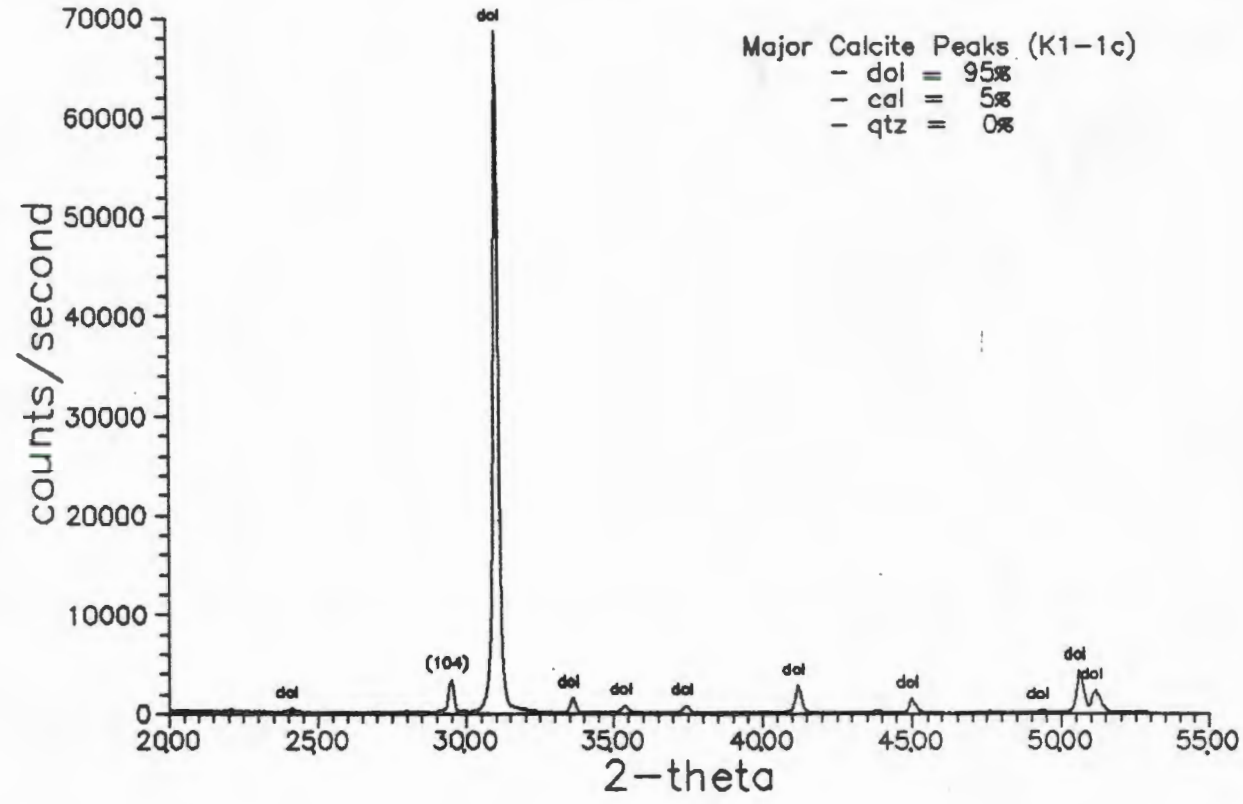

Figures 2.12a,b: Examples of X-ray diffractograms illustrating the groups, (a) dolomite only; (b) dolomite and minor calcite.

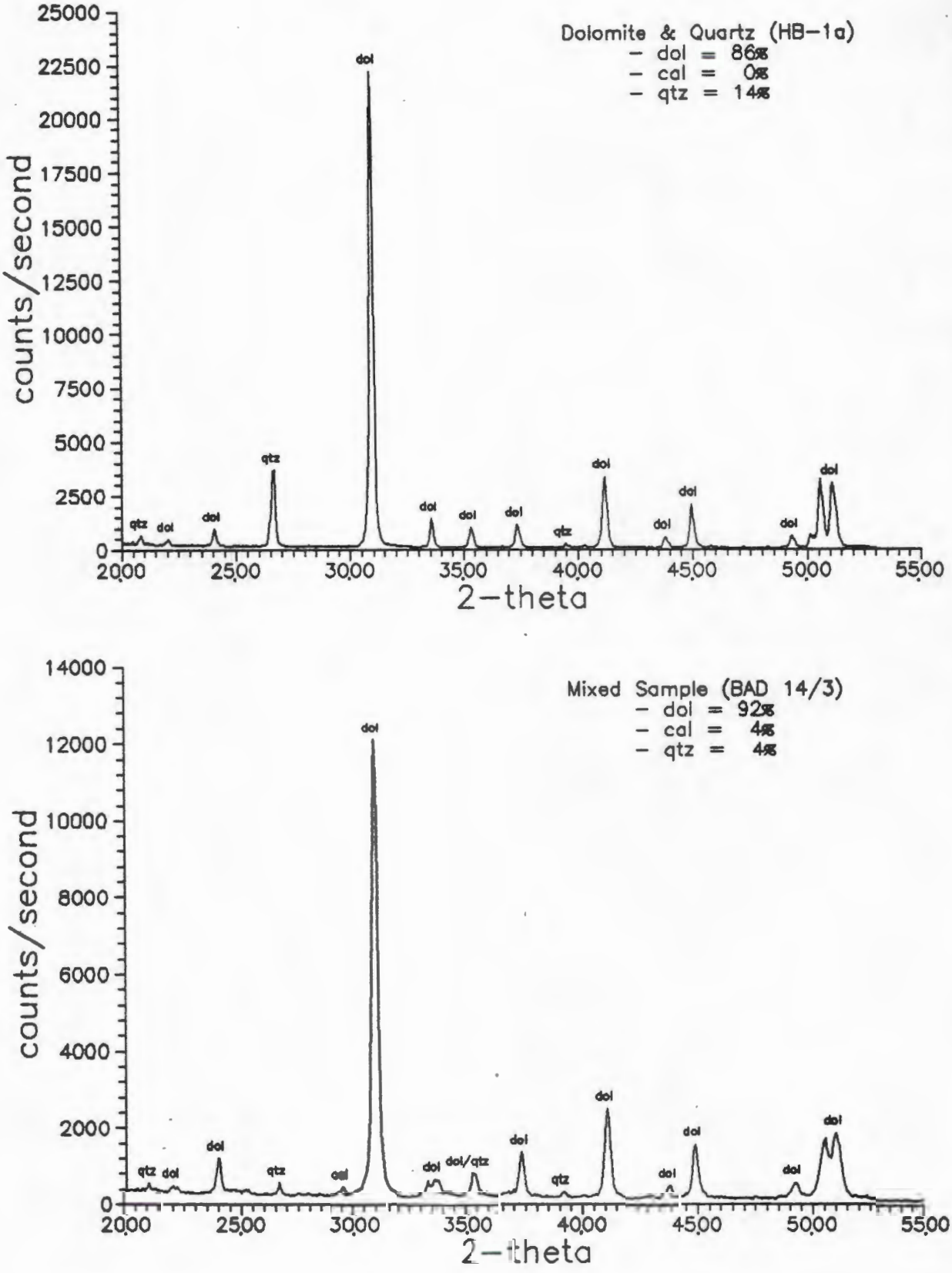

Figures 2.12c,d: Examples of X-ray diffractograms illustrating the groups, (c) dolomite and quartz; (d) dolomite with minor calcite and quartz.

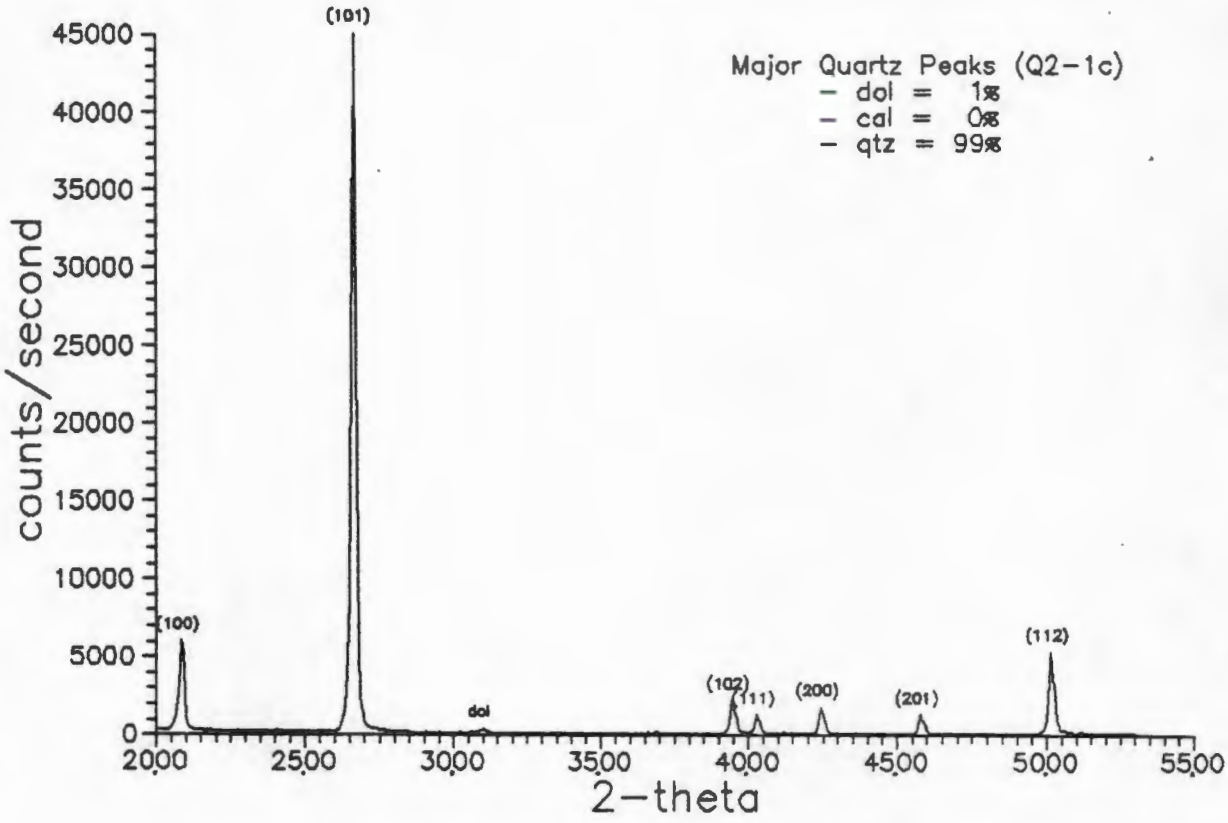

Figure 2.12e: Example of an X-ray diffractogram illustrating a predominantly quartz rich group.

Lumsden succeeded in determining the relationship between the Ca content and the d-spacing of the dolomite 104 reflection.

Table 2.7: Mole % of $CaCO_3$ in Berg Aukas samples as determined by XRD.

Sample No	$dol_{(104)}$ 2θ	$hal_{(200)}$ 2θ	$dol_{(104)}$ Corr. A	N_{CaCO_3} mole %
BAD 2/1a	30.94	31.68	2.886	50.0
BAD 2/1b	30.90	31.62		
BAD 2/2	30.90	31.62		
BAD 2/3	30.94	31.66		
BAD 2/7b	30.90	31.66	2.888	50.6
BAD 2/8	30.86	31.60	2.886	50.0
BAD 7/1a	30.92	31.66	2.886	50.0
BAD 7/1c	30.90	31.64	2.886	50.0
BAD 7/2a	30.92	31.66	2.886	50.0
BAD 7/3	30.90	31.66	2.888	50.6
BAD 7/4a	30.94	31.66		

The subtle shift in the position of the 104 reflection can be accurately measured when compared to the nearby 200 reflection of halite, which is used as an internal standard.

Table 2.8: Dolomite crystallinity of selected Berg Aukas samples based on XRD peak intensity ratios.

Sample No.	Fabric Type	Peak Intensity c/s Dol (015)	Dol (110)	$I_{(015)}/I_{(110)}$
BAD 14/3	A	703	1360	0.52
BAD 7/1a	A	1224	2073	0.59
Q1-4a	A	1485	2060	0.72
K1-1a	A	1043	1757	0.59
K1-2a	A	1034	1353	0.76
K1-3a	A	1403	1921	0.73
BAD 14/2	A	1010	1174	0.86
BAD 15/13a	A	1062	1303	0.81
BAD 2/1a	B	1303	1669	0.78
Q2-1a	B	1002	1092	0.92
Q2-1b	B	1185	1416	0.84
K1-1e	B	853	1019	0.84
BAD 15/13b	B	1158	1194	0.97
BAS-1a	B	1213	1283	0.94
BAS-1b	B	1140	1470	0.77
BAS-2a	B	958	1336	0.72
BAS-2b	B	934	1048	0.89
BAS-3a	B	1239	1325	0.93
BAS-3b	B	989	1179	0.84
HB-1a	B	1020	1153	0.88
HB-1b	B	1183	1058	1.12
HB-2	B	1185	1451	0.82
BAD 2/8	B	1446	1498	0.96
BAD 2/3	B	1026	1091	0.94
BAD 2/2	B	392	479	0.82
BAD 2/7a	B	1334	1277	1.04
BAD 2/1b	C	1484	1165	1.27
BAD 2/7b	C	753	913	0.82
BAD 7/4b	C	898	705	1.27
Q1-4c	C	1127	1572	0.72
K1-1c	C	902	885	1.02
K1-2c	C	1144	1179	0.97
BAD 15/13c	C	1126	999	1.13
BAD 7/3	C	357	400	0.89
BAD 7/1c	D	1400	1432	0.98
BAD 7/4a	D	1208	1082	1.12
BAD 7/2a	D	1249	1130	1.10
Q1-4b	D	1446	1427	1.01
K1-1b	D	1148	1056	1.09
K1-1d	D	919	925	0.99
K1-2b	D	865	939	0.92
K1-3b	D	1349	1303	1.03
K1-3c	D	1342	1245	1.07

The linear relationship between the dolomite 104 peak position and abundance of $CaCO_3$ in dolomite is as follows:

$$N_{CaCO_3} = (333.33 * d) - 911.99 \qquad \text{(after Lumsden, 1980)}$$

where: N_{CaCO_3} = mole % $CaCO_3$ in dolomite

d = observed $d_{(104)}$ in Å

A representative selection of fabric types was chosen for this method, the results appearing in Table 2.7. Inspection of the data suggests that all the dolomite fabrics present are near perfectly stoichiometric, with an equal distribution of Ca and Mg ions within the crystal lattice.

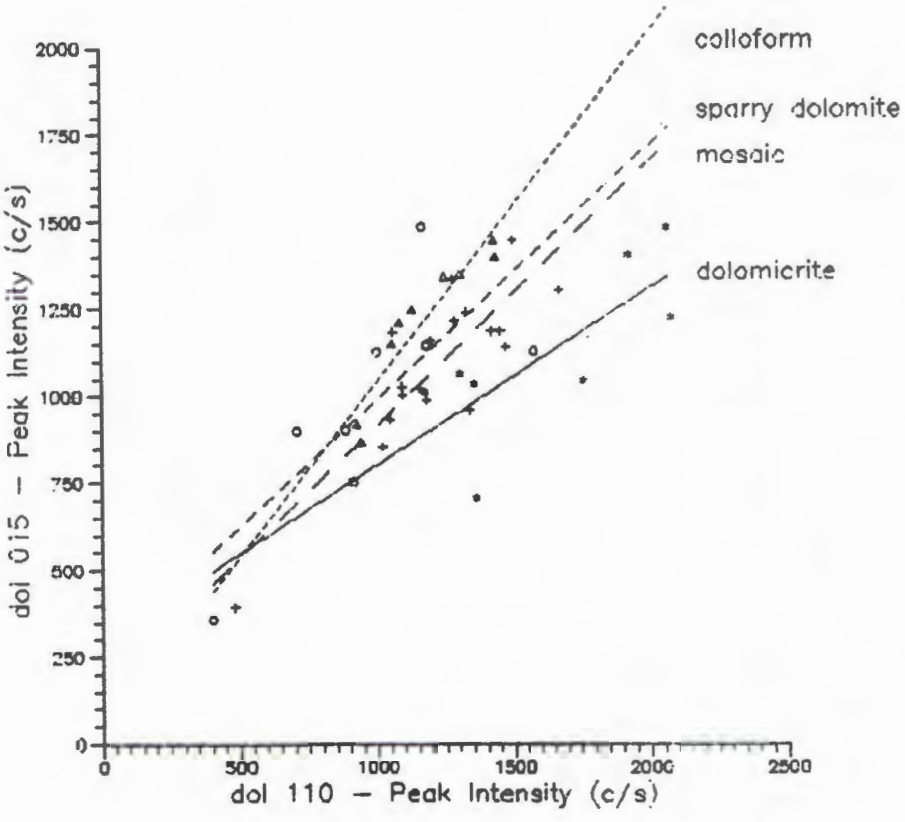

Figure 2.13: A plot of peak intensities for the dolomite 110 versus the dolomite 015 peaks.

The third task attempted by XRD was to determine the degree of crystallinity, following the method of Lumsden & Chimahusky (1988). The technique involves comparing the peak intensities of the dolomite 015 and 110 reflections. The results of this exercise are listed in Table 2.8, which also includes the fabric type as defined by petrographic observation. A simple graphical plot of peak intensities for the dolomite 015 and 110 peaks, is presented in Figure 2.13.

The gradient of the best fit lines depicted in Figure 2.13 represents the ratio of the size of the [015]/[110] peaks. The mean values for each of the different dolomite types is listed in Table 2.9.

Table 2.9: Mean values of $I_{(015)}/I_{(110)}$ peaks for different dolomite types.

dolomite type	$I_{(015)}/I_{(110)}$
A. micritic	0.69 (± 0.11)
B. mosaic	0.89 (± 0.09)
C. white sparry	1.01 (± 0.20)
D. colloform	1.03 (± 0.06)

It would appear from the above data that a correlation exists between the degree of dolomite crystallinity, as deduced petrographically, and the ratio of the size of the 015/110 dolomite peaks. A marked difference in crystallinity exists between the micritic dolomite and the white sparry dolomite, whilst that of both the mosaic dolomite and the colloform textured dolomite has a similar crystallinity signature, as deduced by means of XRD. Hence, this technique would supplement petrographic observations pertaining to the degree of coarseness or crystallinity of a sample, though an increase in the crystallinity index ($I_{(015)}/I_{(110)}$) does not necessarily follow the diagenetic sequence of formation, of the different dolomite types.

No relationship exists between nonstoichiometry and either crystal size or the amount of dolomite in a sample. However, it is possible, to some extent, to deduce the relative degree of dolomite

crystallinity by means of XRD, and furthermore to possibly use this technique as a rough measure as to the degree of recrystallization.

2.7 Cathodoluminescence

Selected polished thin sections of dolomite samples in the Berg Aukas and Odin areas were examined with cathodoluminescence. This method is based on the effect that every mineral which gets an electronic irradiation emits one or two characteristic colours of luminescence (CL). The electronic irradiation is emitted from a cathode with a high-tension between 10 - 20 kV, and the non-thermal electron beams are led directly onto the sample.

For the purpose of this study, a Technosyn Model 8200 Mk II at the Electron Microscope Unit of the University of Cape Town was used. Photomicrographs were taken on a Wild M400 optical system, using KODAK ESS ektochrome rated at 1600 ASA.

In carbonates, the resulting colours may depend on the following (Gorzawski, 1989):

i) Variations in the crystal structure or the distance between the atoms.

ii) The chemical composition of the mineral, which largely depends on the chemical composition of the fluid from which the carbonate has crystallized.

iii) The diagenetic evolution of the rock.

In the present study the colours observed in CL are listed in Table 2.10.

Table 2.10: The different colours observed in CL associated with various mineral types.

MINERAL	CL
dolomite	red - red (-orange) - yellow
galena	black
quartz	dark red/brown

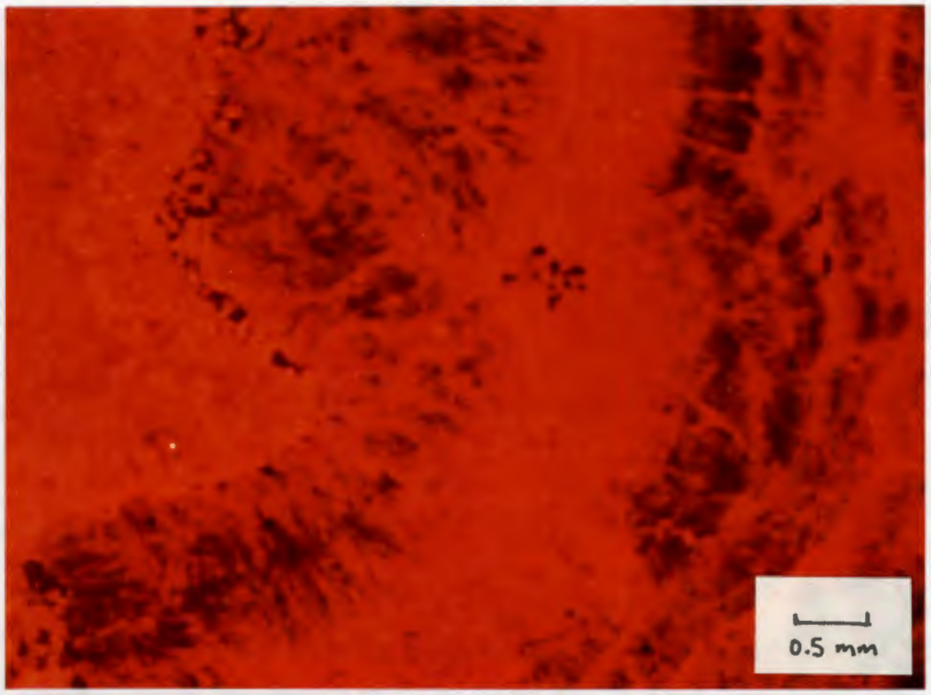

Plate 2.3a:
(K1-2; CL)
Micritic/coll-
form contact.

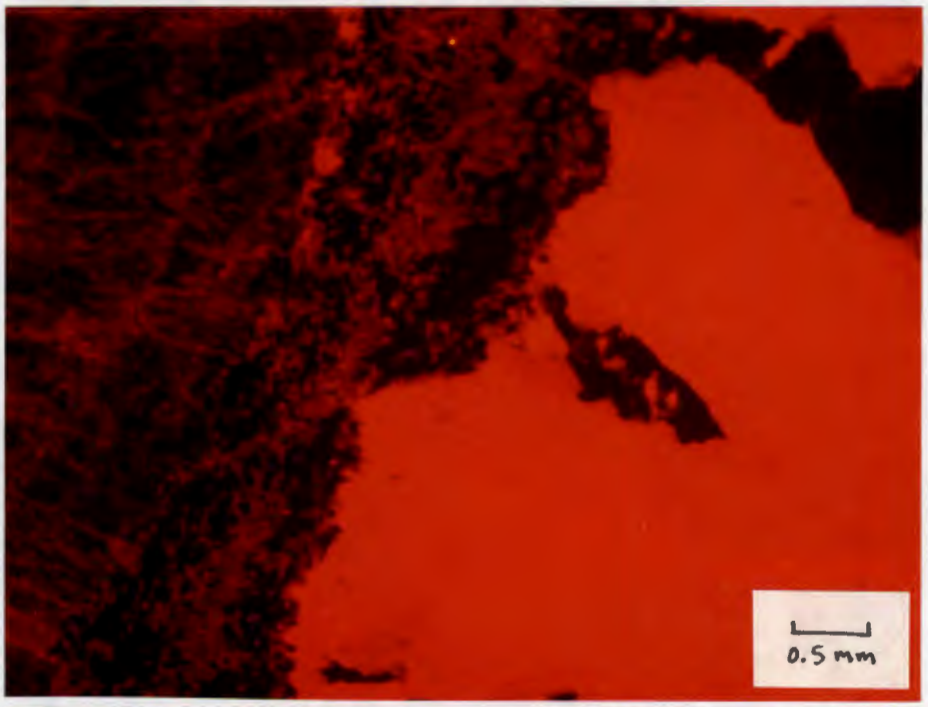

Plate 2.3b:
(K1-2; CL)
Coarse spar/
colloform
contact.

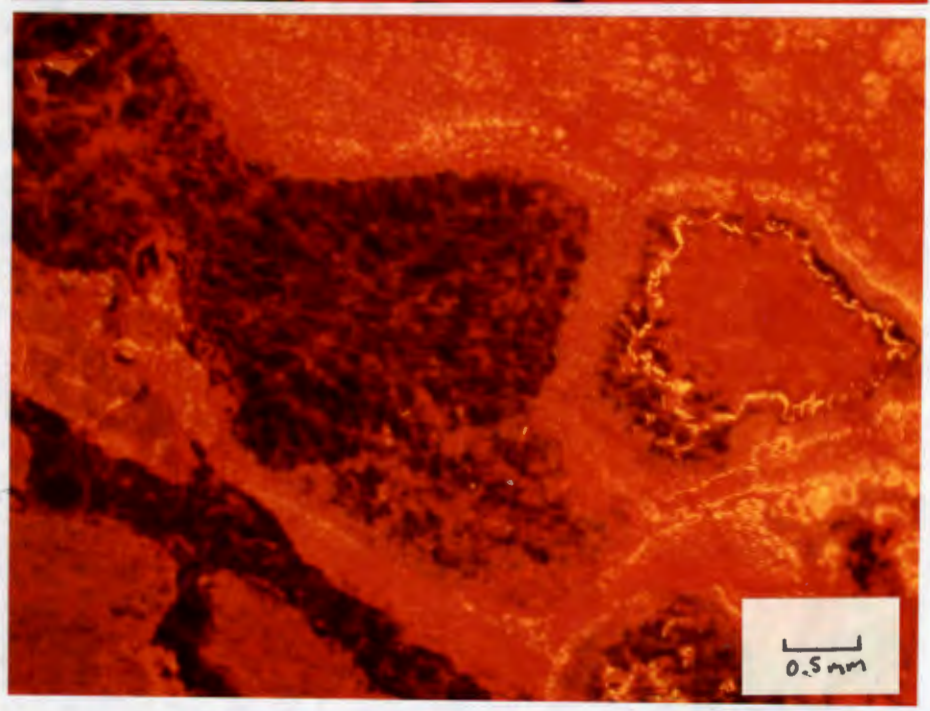

Plate 2.3c:
(Q2-1a; CL)
Spar, micrite
& quartz.

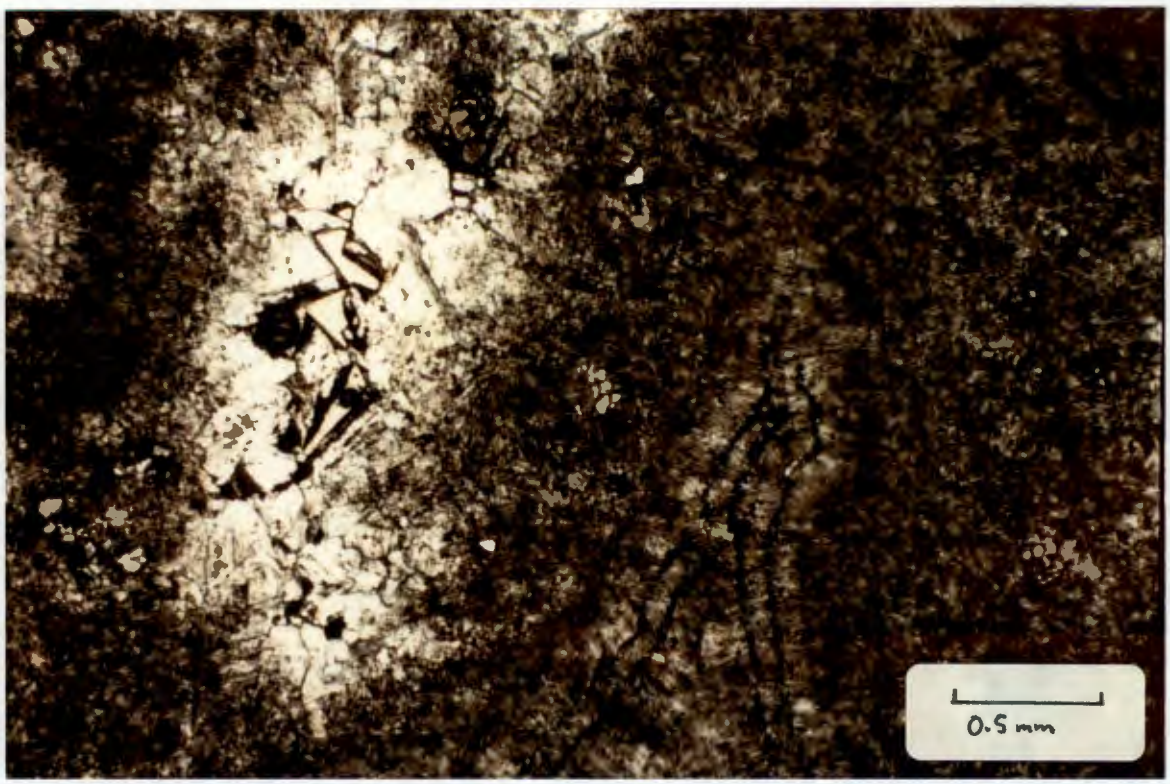

Plate 2.3d: Relationship between coarse white spar and colloform dolomite, as seen in PPL (Sample OS-2).

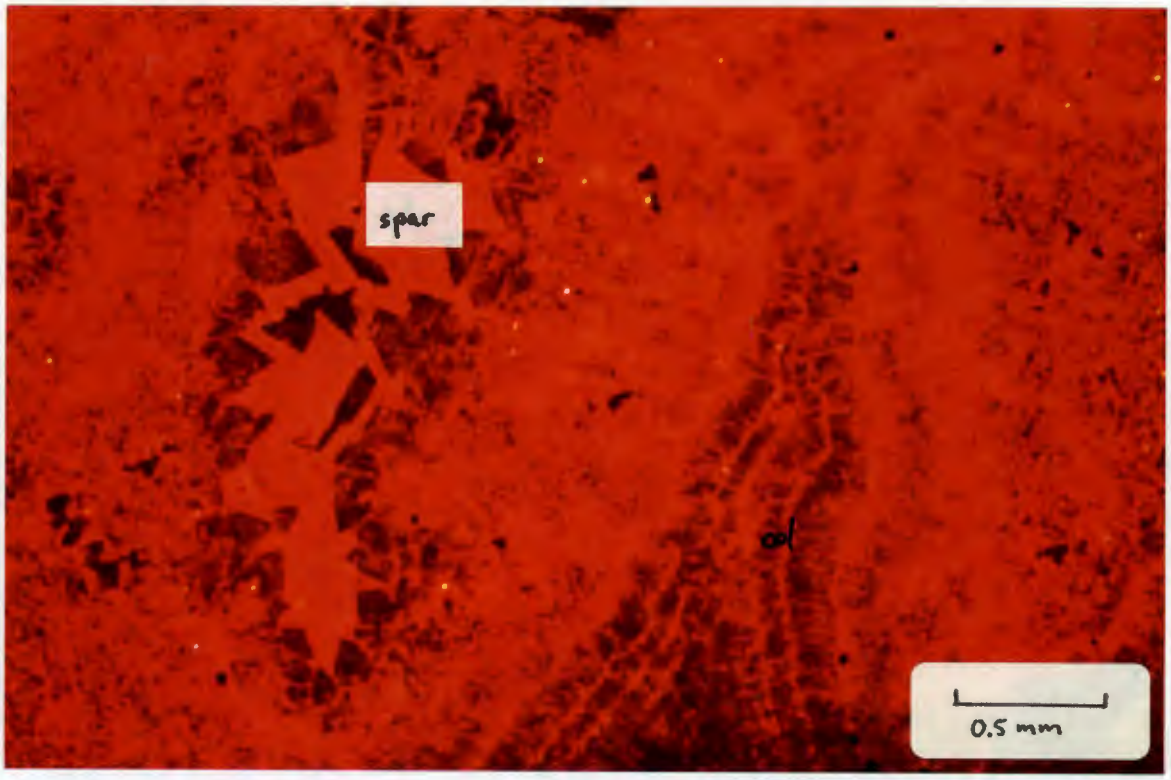

Plate 2.3e: Same section as above, as seen in CL.

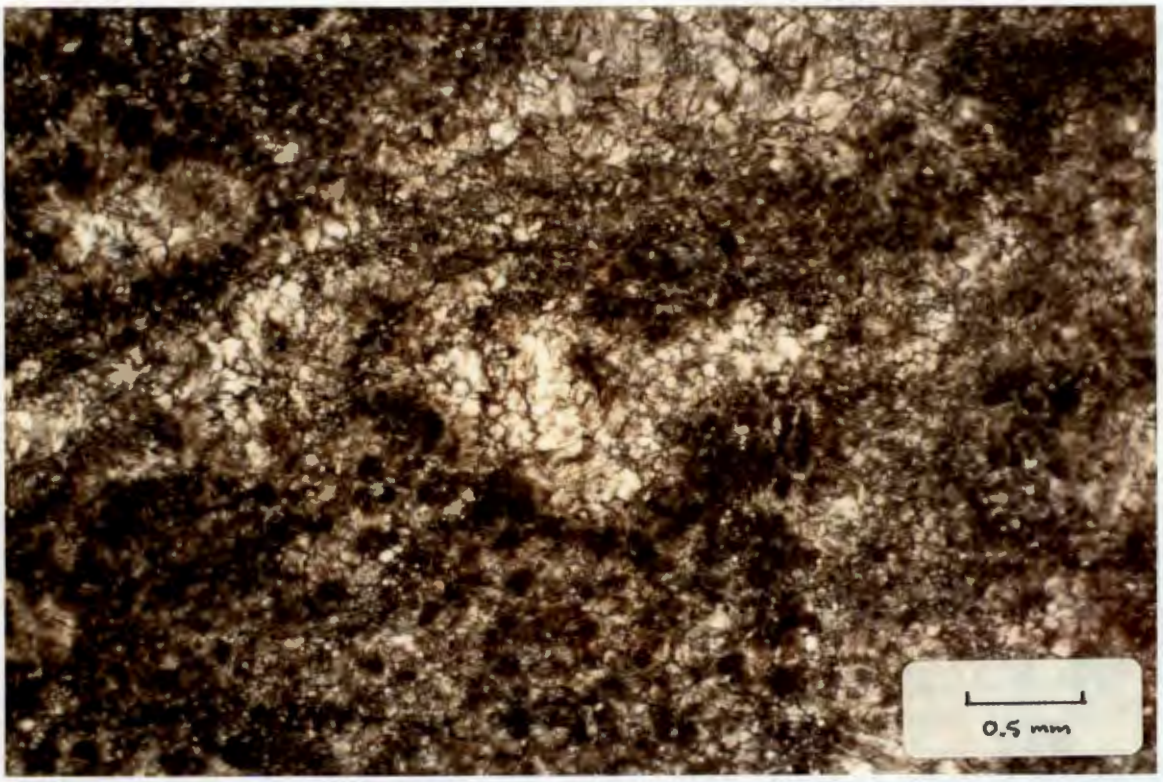

Plate 2.3f: Relationship between mosaic dolomite and quartz, as seen in PPL (Sample Q1-10).

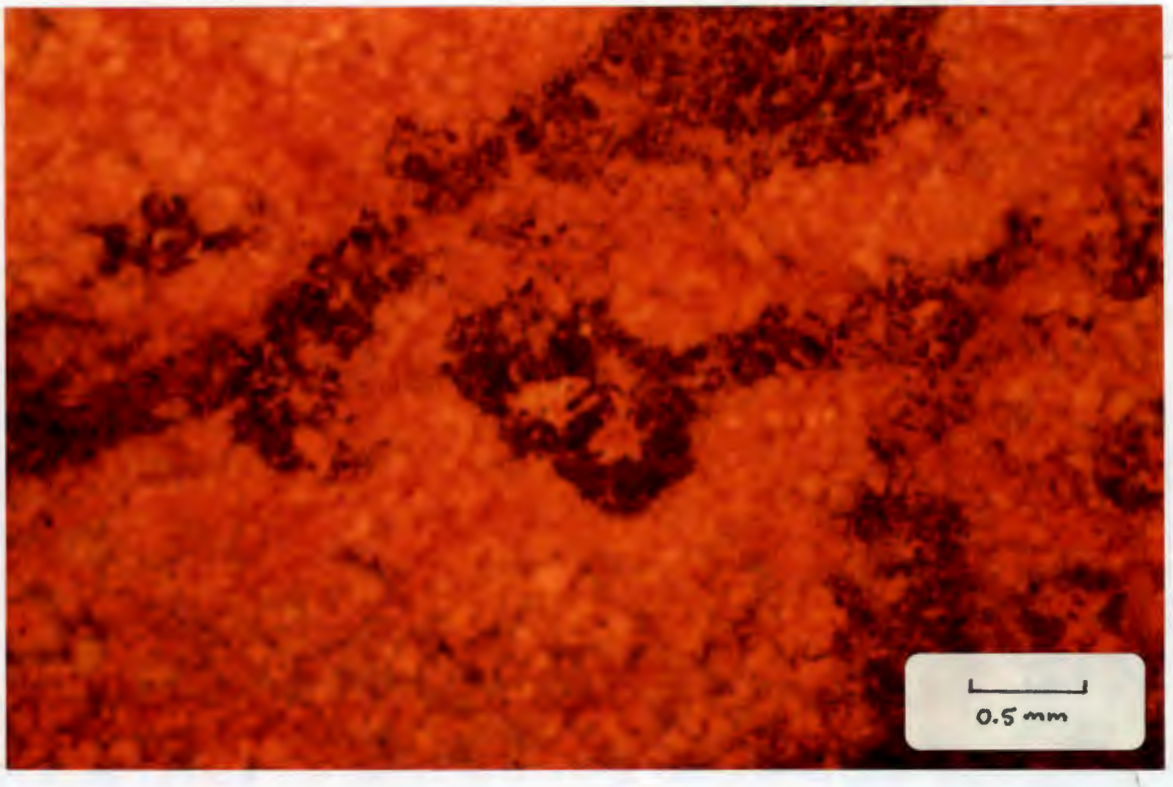

Plate 2.3g: Same section as above, as seen in CL.

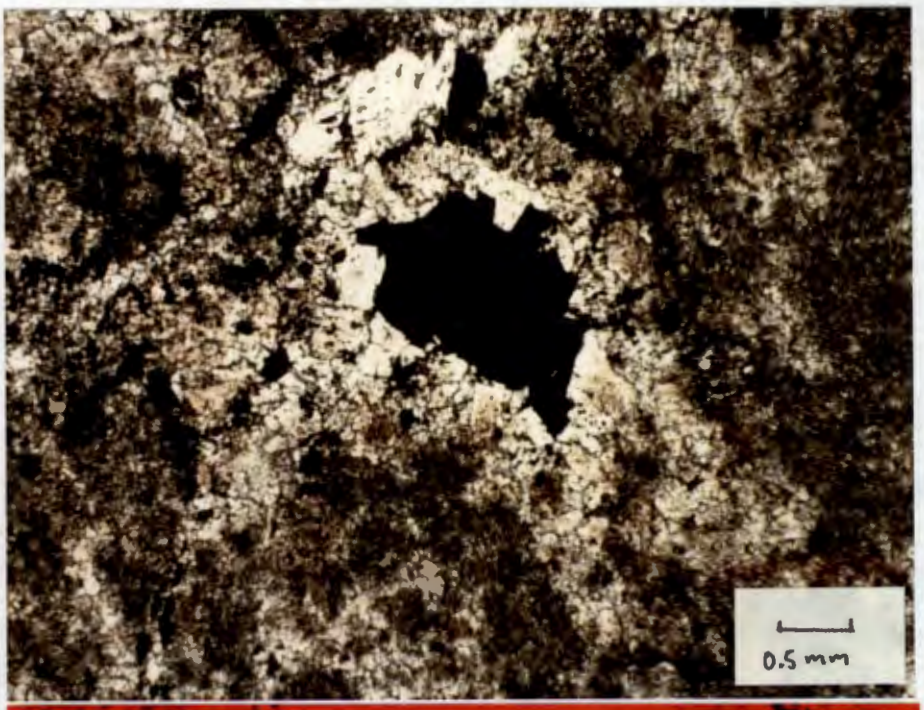

Plate 2.3h: (OS-2; PPL) galena & different dol. types.

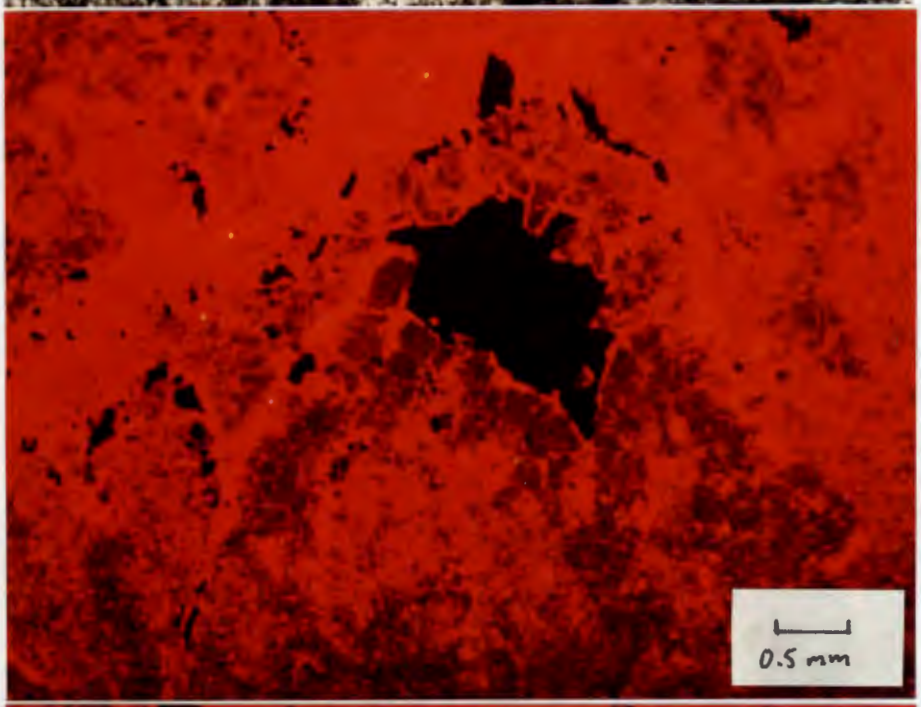

Plate 2.3i: (OS-2; CL) As above

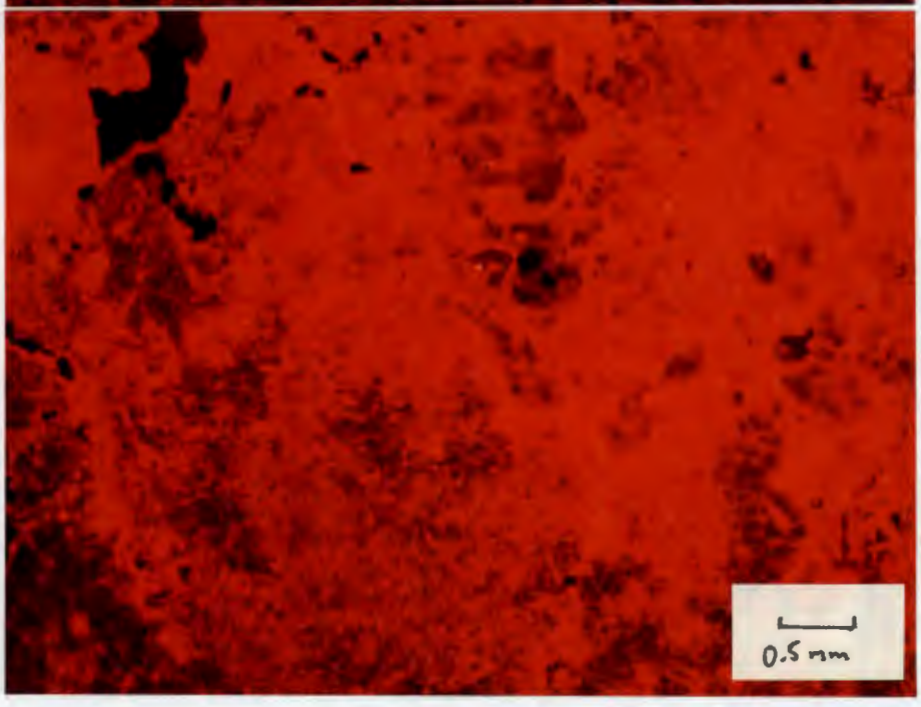

Plate 2.3j: (OS-2; CL) Similar to above.

The cathodoluminescence results succeed in distinguishing between the different dolomite types, and furthermore to establish a chronological order of dolomite crystallization. The differences in the different dolomite types, as seen at Berg Aukas, can be described as follows:

i) **Type A - Micritic dolomite:** This finely crystalline dolomite is characterized by a a reddish-orange colour when viewed in CL, as illustrated in Plates 2.3a,c. It would appear that this dolomite constitutes the major portion of all the dolomite types.

ii) **Type B - Mosaic dolomite:** Though varying in crystallinity from fine to reasonably coarse, the characteristic colours of this dolomite type as seen in CL, appear to be a mottle of brighter reds and oranges. This is evident in Plates 2.3g,i,j. It would seem likely that mosaic dolomite is a comparatively later formed dolomite, as it tends to occlude fractures and may be closely related to sulphide mineralization.

iii) **Type C - White sparry dolomite:** This dolomite phase has a distinct bright orange/yellow colour, and would appear to occlude further secondary porosity. This dolomite type has also been seen to host sulphide mineralization and silicification phenomena, though the dominant silicification would postdate this dolomite stage. The exact relationship between this dolomite type and the mosaic dolomite, could not be clearly resolved using CL microscopy.

iv) **Type D - Colloform dolomite:** This dolomite type is characterized by alternating bands of lighter and darker reds, as seen in Plates 2.2a,b,e. This dolomite type is strongly recrystallized which builds up complex diagenetic textures and structures. Such colloform features are often associated with the micritic dolomite, and may actually have formed as a result of the dissolution of the initial dolomite.

There is no doubt that cathodoluminescence is a remarkably useful technique to use, especially in distinguishing between the different dolomite types, far more so than relying purely on differences in grain size.

3. ISOTOPE - GEOCHEMICAL STUDIES (Sr, C, O)

3.1 Introduction and Sample Description

As described in the previous chapter, petrographical studies of the Berg Aukas dolostones display several phases of recrystallization, dissolution, and reprecipitation processes. It is anticipated that the isotope-geochemical investigations on the different mineral generations, or which has loosely been referred in this thesis as "fabric types", should contribute to the identification of the fluids from which the various recrystallization processes had taken place. Furthermore, particular care will be taken for those mineral generations which are directly associated with Pb and Zn sulphide mineralization, in a bid to identify the ore-forming fluids.

Sr, C and O isotope ratios were determined in samples from the entire Berg Aukas area. The samples analyzed in this study correspond to different petrographically defined groups or "fabric types", which have been defined in section 2.5 of the previous chapter. Particular attention was also given as to whether or not a particular dolomite type was observed to be associated with sulphide mineralization.

Extreme care was taken in separating the different dolomite types, and for those samples that are associated with sulphide mineralization, every effort was made to exclude any sulphides from the sample. Each sample was scanned by XRD to determine the level of homogeneity, and to semi-quantify the degree of mineral contamination, especially in terms if calcite as this would be significant when interpreting the C and O isotope data.

As regards to the samples submitted for Sr isotopic analysis it is important to note that there is a negligible input in terms of clay minerals or any other K-rich minerals. This was verified petrographically and with the aid of XRD, and hence it is assumed that there is essentially no Rb in the system. Following this premise, it is further assumed that the $^{87}Sr/^{86}Sr$ ratios presented in this study reflect the initial $^{87}Sr/^{86}Sr$ ratios of each of the dolomite types that were sampled.

Table 3.1: Carbonate samples from Berg Aukas used for isotope studies (lg = light grey; mg = medium grey; dg = dark grey; rec = recrystallized; min = mineralized).

Sample No.	Fabric Type	Description
BAD 14/3	A	light brown karst-fill mudstone
BAD 7/1a	A	lg/creamy dolomicrite
Q1-4a	A	lg dolomicrite
K1-1a	A	lg dolomicrite
K1-2a	A	lg dolomicrite
K1-3a	A	lg dolomicrite
BAD 14/2	A	lg dolomicrite (min)
BAD 15/13a	A	lg dolomicrite
BAD 2/1a	B	lg rec dolomite
Q2-1a	B	lg rec dolomite
Q2-1b	B	m-dg rec dolomite
K1-1e	B	lg rec dolomite
BAD 15/12	B	lg rec dolomite (min)
BAD 15/13b	B	lg rec dolomite
BAS-1a	B	lg rec dolomite
BAS-1b	B	lg rec dolomite (min)
BAS-2a	B	lg rec dolomite
BAS-2b	B	lg rec dolomite (min)
BAS-3a	B	lg rec dolomite
BAS-3b	B	lg rec dolomite (min)
HB-1a	B	lg rec dolomite
HB-1b	B	lg rec dolomite (min)
HB-2	B	lg rec dolomite (min)
BAD 2/8	B	lg laminated dolomite
BAD 2/3	B	dg laminated dolomite
BAD 2/2	B	dg dolomite
BAD 2/7a	B	dg dolomite (boundstone)
BAD 2/1b	C	coarse white dolospar
BAD 2/7b	C	coarse white dolospar
BAD 7/4b	C	white dolospar
Q1-4c	C	coarse white dolospar
Q1-10	C	coarse white dolospar + quartz
Q2-1c	C	coarse white dolospar
K1-1c	C	white dolospar
K1-2c	C	white dolospar
BAD 15/13c	C	coarse white dolospar
BAD 7/3	C	white dolospar (min)
BAD 7/1c	D	colloform vein
BAD 7/4a	D	coarsely-bladed colloform
BAD 7/2a	D	colloform
Q1-4b	D	colloform
K1-1b	D	colloform
K1-1d	D	colloform
K1-2b	D	colloform vein
K1-3b	D	colloform - lg
K1-3c	D	colloform - dg

Table 3.1 lists all the samples that were used for the isotope study, and includes a brief description of each of the samples.

Table 3.2: Results of AAS analyses on Berg Aukas samples (n/a = no assay).

Sample No.	Fabric type	Cu ppm	Pb ppm	Zn ppm	Mn ppm	Sr ppm	Fe %	Ca %	Mg %	SiO2 %
BAD 14/3	A	810	1700	1200	240	50	0.97	19.4	9.6	2.8
BAD 7/1a	A	3	28	135	150	170	n/a	22.5	13.2	0.7
Q1-4a	A	4	10	37	270	80	0.11	20.8	12.7	2.0
K1-1a	A	4	15	101	320	80	0.11	21.9	12.3	0.6
K1-2a	A	5	18	132	130	90	0.02	22.5	13.0	1.2
K1-3a	A	22	20	209	450	90	0.32	22.3	12.8	2.2
BAD 14/2	A	4	33	640	350	130	0.23	21.7	12.4	2.8
BAD 15/13a	A	3	14	124	340	110	0.11	21.4	12.8	1.8
BAD 2/1a	B	5	41	38	260	100	n/a	21.8	12.6	4.7
Q2-1a	B	3	11	14	440	150	0.04	21.4	12.5	2.2
Q2-1b	B	2	16	21	340	120	0.05	22.9	13.0	0.4
K1-1e	B	4	24	101	1760	130	0.12	22.4	12.2	1.0
BAD 15/12	B	6	533	594	430	90	0.07	21.0	12.6	0.2
BAD 15/13b	B	3	23	50	360	80	0.08	21.3	12.7	1.9
BAS-1a	B	5	277	780	400	120	0.16	21.8	12.8	0.5
BAS-1b	B	10	1600	1040	480	130	0.28	21.6	12.7	0.7
BAS-2a	B	3	87	560	370	150	0.09	21.5	13.2	2.3
BAS-2b	B	4	139	650	250	100	0.10	16.2	9.5	23.9
BAS-3a	B	7	23	317	570	170	0.12	21.1	12.8	1.9
BAS-3b	B	11	67	500	540	130	0.22	18.1	10.9	13.2
HB-1a	B	2	226	1380	450	60	0.05	20.5	12.6	3.2
HB-1b	B	7	940	2430	400	70	0.07	20.0	12.0	4.4
HB-2	B	3	192	2130	390	90	0.07	22.0	13.1	0.6
BAD 2/8	B	7	96	77	340	140	n/a	22.9	13.1	0.5
BAD 2/3	B	6	21	33	170	140	n/a	14.5	10.0	29.5
BAD 2/2	B	4	18	17	160	50	n/a	6.0	3.0	71.7
BAD 2/7a	B	8	14000	1630	530	180	n/a	19.7	11.2	10.8
BAD 2/1b	C	6	25	18	1250	140	n/a	20.6	11.7	10.3
BAD 2/7b	C	5	41	101	400	160	n/a	14.0	7.2	40.6
Q1-4c	C	8	20	108	1280	130	0.19	20.9	12.6	3.2
Q1-10	C	13	17	17	820	170	0.10	22.4	13.0	0.3
K1-1c	C	4	58	178	290	150	0.03	23.0	12.5	0.2
K1-2c	C	33	310	590	1670	130	0.11	21.7	12.4	3.8
BAD 15/13c	C	3	30	130	2110	150	0.11	21.9	13.0	1.2
BAD 7/3	C	3	15	152	80	30	n/a	3.3	1.9	80.1
BAD 7/1c	D	6	260	478	170	80	n/a	22.4	13.0	0.3
BAD 7/4a	D	6	62	76	380	100	n/a	22.2	13.0	0.1
BAD 7/2a	D	3	44	58	390	100	n/a	22.1	12.5	2.9
K1-1b	D	3	16	68	370	90	0.08	22.8	12.7	0.3
K1-1d	D	4	47	137	440	100	0.11	22.1	12.8	0.2
K1-2b	D	5	64	377	230	60	0.04	20.9	12.1	7.2
K1-3b	D	18	70	134	270	80	0.30	21.1	12.6	2.0
K1-3c	D	19	24	68	230	80	0.21	21.0	12.6	3.1

The prefix to the sample numbers has been devised to provide an approximate sample locality as follows:

BAD	-	Berg Aukas Diamond drillhole (near mine)
BAS	-	Berg Aukas Surface (near mine)
Q1,2	-	Quarry 1 or 2, respectively
K1,2	-	Kopje 1 or 2, respectively
HB	-	Heinrichsberg

3.2 Geochemistry of Carbonates

In all the carbonate samples used for isotopic investigations, the Sr contents were determined by AAS-analyses carried out by the TCL laboratory in Tsumeb, in addition to several other elements as listed in Table 3.2. A description of the analytical technique and likely errors is given in Appendix V.

Results show that the Sr content covers a fairly broad range of 50 to 180 ppm for both the micritic (A) and mosaic (B) dolomite types, whilst the white sparry dolomite (C) tends to have higher Sr concentrations of between 130 and 170 ppm. Colloform textured dolomite (D) typically shows lower Sr concentrations of between 60 and 100 ppm.

As regards to the other elements that were assayed, Cu has a particularly low concentration (Figure 3.1a) of between 1 and 35 ppm, with mosaic dolomite having the lowest concentration. Both Pb and Zn have similar concentrations and distribution patterns between the different dolomite types (Figures 3.1b and c). Unlike Cu, the concentration of Pb and Zn is highest in mosaic dolomite, with values exceeding 1600 ppm, whilst values less than 600 ppm are common for the remaining dolomite types. The concentration of Mn is highest in the white sparry dolomite (Figure 3.1d), with values exceeding 2000 ppm, whilst concentrations of less than 600 ppm are common for the other three dolomite types.

Concentrations of Ca and Mg remain constant for each of the different dolomite types, and the distribution of Fe shows no preference for any particular dolomite type.

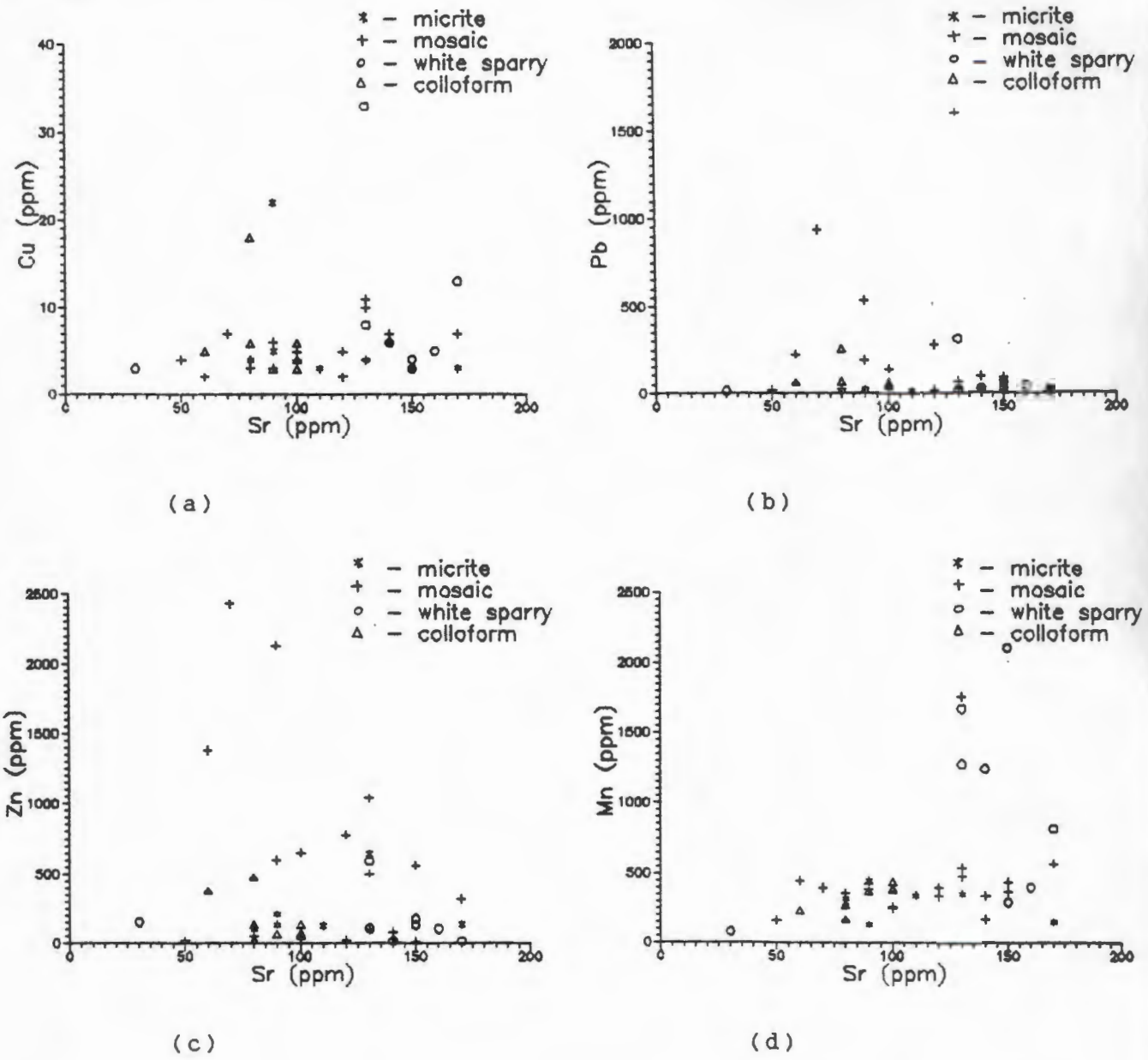

Figure 3.1: Selected element concentrations with respect to Sr concentration for different dolomite types.

3.3 Sr Isotope Studies

The results of the Sr isotope investigation are listed in Table 3.3, which also contains the Sr concentrations in ppm for all the samples that were analyzed. In Figure 3.2 $^{87}Sr/^{86}Sr$ ratios are displayed graphically as a function of the Sr concentration, subdivided into the different dolomite types A - D.

All the Sr isotope analyses were carried out at the Radiogenic Isotope Facility of the University of Cape Town, using a VG Sector Thermal Ionization Mass Spectrometer. Results have been

adjusted to the NBS standard SRM 987 (Mean $^{87}Sr/^{86}Sr$ = 0.710281, Standard Deviation = 0.000011, n = 14). A brief description of the technique is given in Appendix VI.

Table 3.3: Isotopic results (Sr, C, O) on dolomite samples from the Berg Aukas area.

Sample No.	Sr (ppm)	$^{87}Sr/^{86}Sr$	2σ std dev	$\delta^{13}C$ PDB °/₀₀	$\delta^{18}O$ PDB °/₀₀	$\delta^{18}O$ V-SMOW °/₀₀
BAD 14/3	50	0.711675	0.0011	-2.29	-6.16	24.56
BAD 7/1a	170	0.709040	0.0009	6.14	-2.64	28.18
Q1-4a	80	0.709131	0.0010	4.42	-4.72	26.04
K1-1a	80	0.709559	0.0009	2.87	-7.63	23.04
K1-2a	90	0.707822	0.0008	4.23	-4.21	26.57
K1-3a	90	0.709866	0.0009	2.85	-7.34	23.34
BAD 14/2	130	0.709924	0.0010			
BAD 15/13a	110	0.710417	0.0010	3.75	-5.90	24.82
BAD 2/1a	100	0.709535	0.0009	4.35	-1.08	29.79
Q2-1a	150	0.708809	0.0010	2.45	-4.90	25.86
Q2-1b	120	0.708955	0.0009	3.02	-3.50	27.30
K1-1e	130	0.713075	0.0010	1.51	-8.79	21.84
BAD 15/12	90	0.709520	0.0008	2.76	-7.36	23.32
BAD 15/13b	80	0.710189	0.0008	2.83	-6.50	24.21
BAS-1a	120	0.710261	0.0010	3.28	-6.00	24.72
BAS-1b	130	0.710417	0.0009	2.76	-6.50	24.21
BAS-2a	150	0.709962	0.0010	4.02	-5.63	25.10
BAS-2b	100	0.710112	0.0009	3.93	-5.81	24.92
BAS-3a	170	0.710380	0.0010	2.91	-7.75	22.92
BAS-3b	130	0.710397	0.0008	4.20	-5.62	25.11
HB-1a	60	0.712777	0.0008	2.23	-8.78	21.86
HB-1b	70	0.713932	0.0009	3.12	-8.45	22.20
HB-2	90	0.712936	0.0010	2.12	-9.10	21.53
BAD 2/8	140	0.708966	0.0008	2.99	-2.34	28.49
BAD 2/3	140			3.20	-5.96	24.76
BAD 2/2	50			2.73	-6.37	24.34
BAD 2/7a	180			2.43	-9.10	21.53
BAD 2/1b	140	0.714633	0.0009	4.15	-6.32	24.39
BAD 2/7b	160	0.716349	0.0009	1.32	-11.32	19.24
BAD 7/4b				3.16	-7.20	23.48
Q1-4c	130	0.714627	0.0008	3.61	-7.74	22.93
Q1-10	170	0.717375	0.0010	2.91	-9.99	20.61
K1-1c	150	0.708184	0.0013	3.16	-4.45	26.32
K1-2c	130	0.714426	0.0010	4.52	-5.66	25.07
BAD 15/13c	150	0.716034	0.0010	2.76	-10.73	19.84
BAD 7/3	30	0.713725	0.0024	4.10	-6.30	24.41
BAD 7/1c	80	0.708524	0.0008	3.96	-5.83	24.90
BAD 7/4a	100	0.709975	0.0009	3.95	-5.25	25.49
BAD 7/2a	100	0.710833	0.0009	3.61	-4.56	26.21
Q1-4b	100	0.710455	0.0008	3.69	-5.55	25.19
K1-1b	90	0.708958	0.0016	3.15	-9.38	21.24
K1-1d	100	0.709650	0.0010	4.16	-5.19	25.56
K1-2b	60	0.709200	0.0009	3.52	-8.48	22.16
K1-3b	80	0.708518	0.0011	4.12	-5.43	25.31
K1-3c	80	0.709651	0.0009	3.59	-7.89	22.77

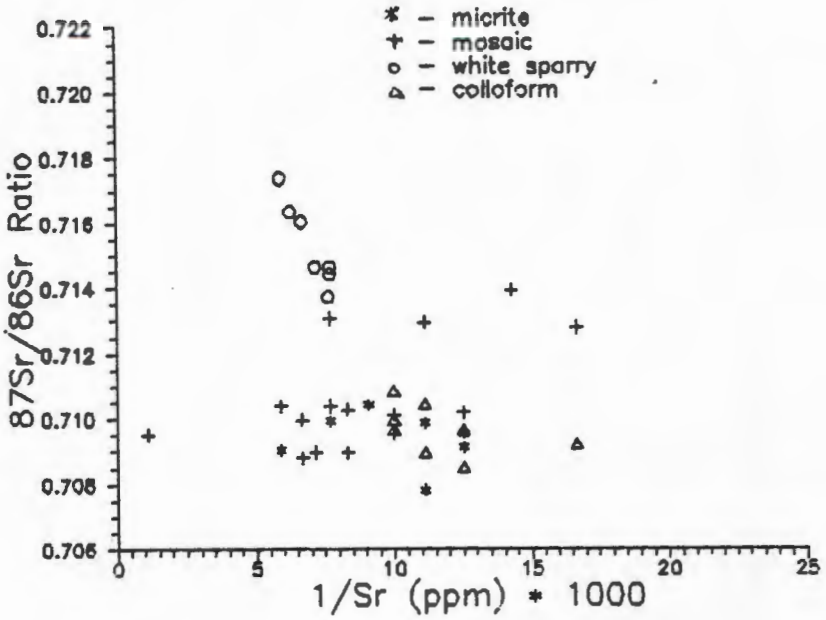

Figure 3.2: $^{87}Sr/^{86}Sr$ ratios with respect to Sr concentration for the different dolomite types in Berg Aukas.

It is clear that the majority of samples from all the different fabric types have been strongly enriched in radiogenic ^{87}Sr compared to seawater, which had an inferred $^{87}Sr/^{86}Sr$ ratio of the order of 0.709 during Precambrian times (Burke et al., 1982). Such a $^{87}Sr/^{86}Sr$ ratio also lies within the range of 0.7068 to 0.7091 at 800 ± 50 Ma, as published by Veizer et al. (1983).

The majority of micritic (type A), colloform (type D) and to a lesser extent mosaic (type B) dolomite types, have $^{87}Sr/^{86}Sr$ ratios between 0.708 and 0.711. The balance of the mosaic dolomite samples display a greater degree of enrichment in radiogenic Sr, with $^{87}Sr/^{86}Sr$ ratios ranging from 0.712 to 0.714. The greatest degree of enrichment is characterized by the white sparry dolomite, which has $^{87}Sr/^{86}Sr$ ratios between 0.714 and 0.718. The distribution of $^{87}Sr/^{86}Sr$ ratios with respect to each generation of dolomite is represented in Figure 3.3, and includes the range of $^{87}Sr/^{86}Sr$ ratios for gangue carbonate.

Such high isotopic signatures like those of the white sparry dolomite (fabric C), indicate that the fluids having precipitated these later carbonates were considerably enriched in radiogenic

^{87}Sr compared to seawater. It must once again be highlighted that there are no K-rich minerals in any of the dolomites which were sampled, and therefore it is assumed that contribution of radiogenic Sr brought about by the decay of radioactive ^{87}Rb, within the rock system is negligible. Therefore, the $^{87}Sr/^{86}Sr$ ratios presented in this study are assumed to reflect the initial $^{87}Sr/^{86}Sr$ ratios of each of the dolomite types that were sampled, and hence characterize the isotopic nature of the fluids which were responsible for the precipitation of the different dolomite types.

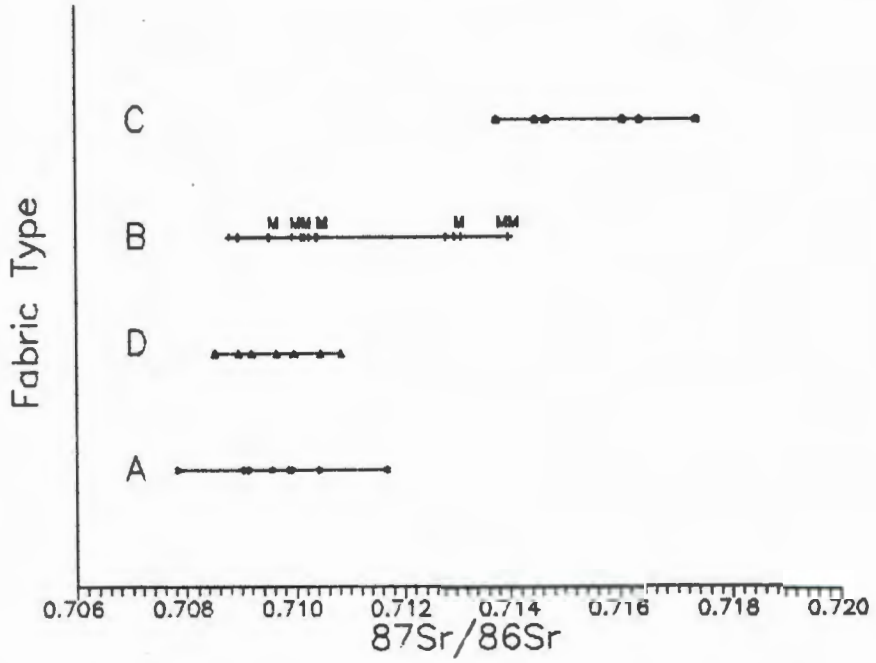

Figure 3.3: $^{87}Sr/^{86}Sr$ ratios with respect to fabric types in Berg Aukas carbonates (M = associated with Pb & Zn mineralization).

The $^{87}Sr/^{86}Sr$ ratios of gangue carbonate which appear spatially to be closely related to sulphide mineralization, are also plotted in Figure 3.2, and are almost identical to those ratios of the mosaic dolomite type. These are also strongly enriched in radiogenic Sr, with a mean of 0.711919 (n=6). It is of interest to note that the colloform dolomite (type D), has $^{87}Sr/^{86}Sr$ ratios within the range of the micritic dolomite, and differ greatly from the $^{87}Sr/^{86}Sr$ ratios of the gangue carbonate.

3.4 C and O Isotope Studies

The results of the C and O isotope analyses are listed in Table 3.3 and plotted in Figure 3.4.

The majority of samples analyzed have $\delta^{13}C$ values between +1 and +5 °/₀₀ with respect to the PDB standard, which are comparable with other sedimentary marine carbonates (Land, 1980). A single sample (BAD 14/3), which is a lithified karst-fill mud, is significantly depleted with a $\delta^{13}C$ value of -2.3 °/₀₀. Gangue carbonates associated with sulphide mineralization have similar values to the other fabric types that were sampled.

The $\delta^{18}O$ ratios of the different fabric types range from 19 to 30 °/₀₀ with respect to the Vienna - Standard Mean Ocean Water (V-SMOW) standard, and are generally depleted in the heavy isotope compared to modern carbonate sediments, but are within the typical range for ancient dolomites influenced by diagenetic modification (Veizer & Hoefs, 1976).

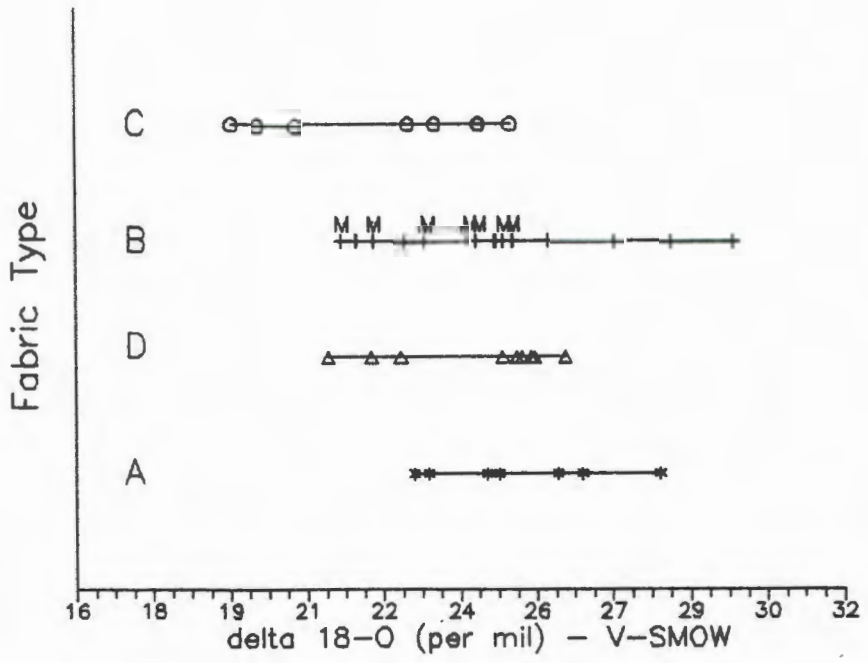

Figure 3.4a: Plot of $\delta^{18}O$ (per mil, V-SMOW) with respect to fabric type.

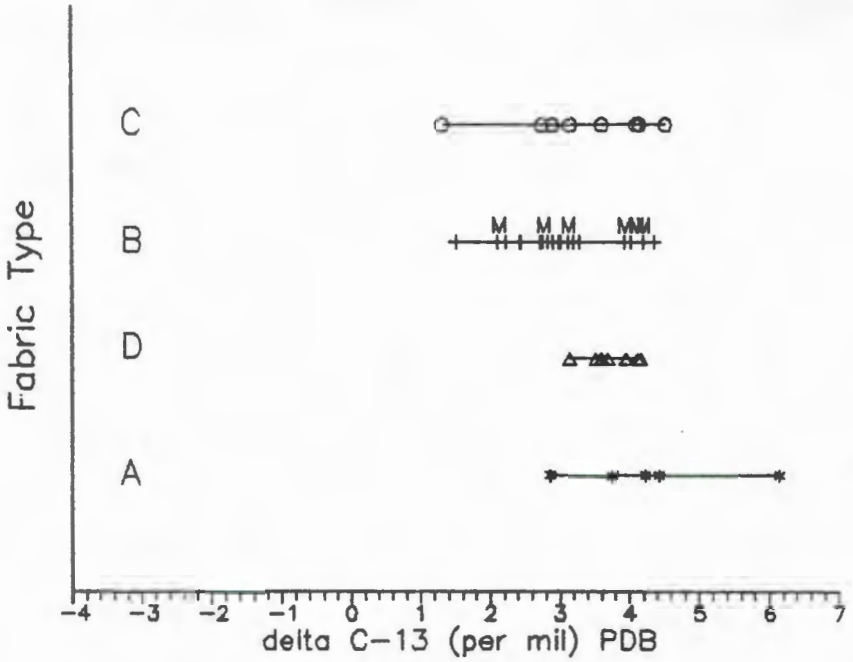

Figure 3.4b: Plot of $\delta^{13}C$ (per mil, PDB) with respect to fabric type.

In a broad sense, an isotopic trend with advancing diagenetic stage can be observed (Fig. 3.4b), with the fabric types becoming increasingly depleted in the heavy isotope, in the sequence A-D-B-C. A similar trend exists for $^{87}Sr/^{86}Sr$ ratios as depicted in Figure 3.2.

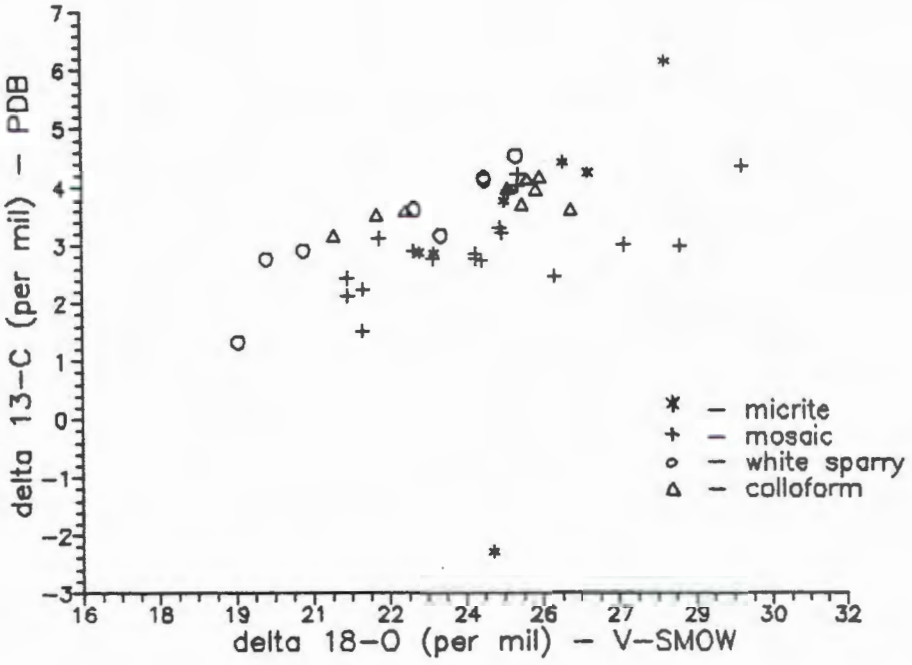

Figure 3.5: Plot of $\delta^{18}O$ (per mil - V-SMOW) versus $\delta^{13}C$ (per mil - PDB), for different fabric types at Berg Aukas.

The stable isotope results of Berg Aukas carbonates are summarized in Figure 3.5 where the $\delta^{13}C$ results are plotted against their accompanying $\delta^{18}O$ values.

The highest $\delta^{18}O$ value is of the order of 30 per mil (mosaic dolomite) which is in good agreement with syngenetic marine dolomite, as deduced from the fractionation curve at 30°C for a tropical sea (Friedman and O'Neil, 1977). The depletion in ^{18}O in subsequent generations as depicted in Figure 3.5, may well represent a combination of increasing temperature and changing fluid/rock ratios. A gradual decrease in $\delta^{13}C$ may be due to an increase in maturation of organic matter present in the host sediment.

The possibility does exist however, that when dealing with ancient dolomites the $\delta^{18}O$ ratios of these rocks are not those obtained during dolomitization, but have been altered to varying degrees during burial and neomorphism (Land, 1980). Hence, interpretation of O isotope ratios of dolomites does warrant a degree of caution.

4. COMPARATIVE ISOTOPE STUDY IN THE ODIN AND CLUBHEAD PROSPECTS

4.1 Introduction and Local Geology

Samples were collected from two other mineral occurrences in the OML, namely the Odin and the nearby Clubhead Prospects. Due to the close proximity of both these prospects, they will be assessed as a single entity, and will hence be referred to as the Odin Prospect.

The prospect lies within the dolomites of the Gauss Formation towards the stratigraphic middle of the Abenab Subgroup, on the northern limb of the locally dominant Uitkomst syncline. This Pb-Zn prospect bears many similarities to the significantly larger Berg Aukas deposit, and for this reason it was considered most suitable to collect a number of samples from this prospect, as part of a comparative study.

The following geological account of the Odin Prospect is a summary extracted from an unpublished company report on a routine exploration mapping and evaluation project (Deane, 1989).

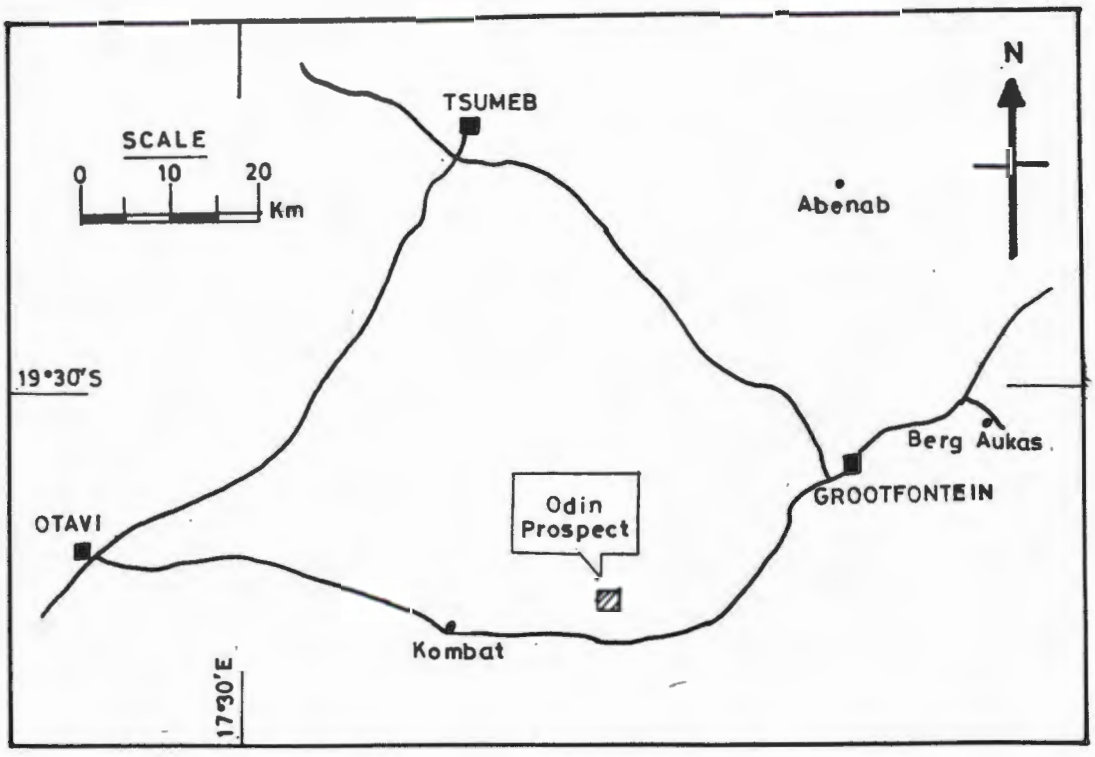

Figure 4.1: Locality map of the Odin Prospect.

The Odin Prospect is situated to the north east of Kombat, as illustrated in Figure 4.1. A geological map of the prospect, modified from the original map compiled by Deane, is presented in Figure 4.2.

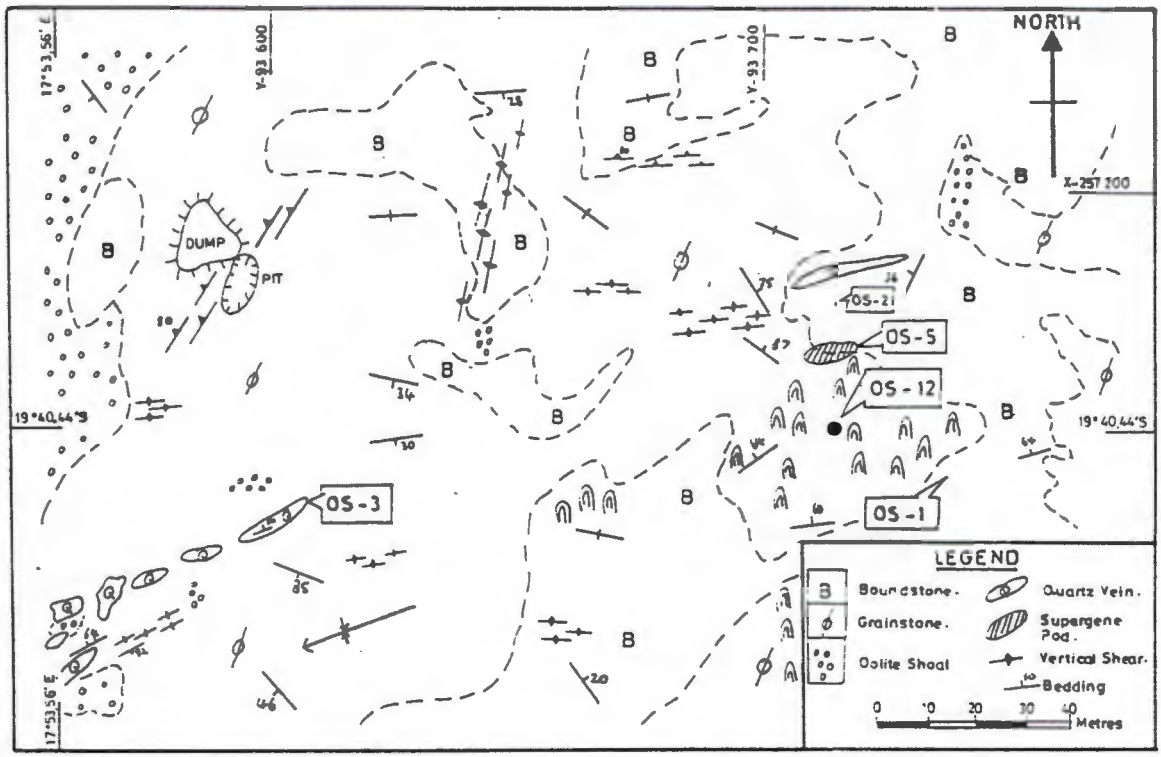

Figure 4.2: Geological plan of the Odin Prospect (modified after Deane, 1989).

4.1.1 Lithology

Two major facies were recognized by Deane (1989) at Odin: a Mega-domal Stromatolite Facies, and an Oolite Shoal Facies.

i) **Mega-Domal Stromatolite Facies:** This is, stratigraphically, the lowermost facies and consists of two interfingering sub-facies: i) a light to medium grey, massive to thickly bedded boundstone unit with abundant colloform development, and ii) a light to medium grey, massive to thickly bedded dolomitic grainstone. The colloforms in the former unit are mostly sub-rounded, exceed 5 mm in diameter, and consist of a coarse/bladed dolomite. Some colloforms are silicified, and thus display a

positive weathering. In the latter unit, colloform textures are developed only sporadically.

Apart from the colloforms being smaller (<5 mm), the stromatolitic build-up is not as prolific. However, the mega-domes themselves are much larger, ranging in basal diameter of 0,5 - 2 m with a distinctly low amplitude, and adopt a biohermal appearance. Occasional oolites may be found in this unit, which is interpreted as representing washed in material from a more proximal shoal.

ii) **Oolite Shoal Facies:** This facies directly overlies the Mega-domal Stromatolite Facies, and consists of a light to medium grey, well-sorted oolitic dolomite.

The two major facies described here have been interpreted by Deane (1989) as representing a sudden change from a relatively deep, sub-tidal environment (mega-dome facies), to a shallow sub-tidal setting above mean wave base, thus indicating a major regression.

4.1.2 Structure

The structural setting at Odin is dominated by the east-west trending Uitkomst syncline, on the northern limb of which the prospect is located. A series of shear events have been recorded at Odin. Those trending east-west (Figure 4.2), which have a strong vertical component of movement, are thought to have been associated with the development of the local syncline. Those shear zones trending northeast-southwest are thought to have developed later than the east-west shears, during periods of regional warping. Furthermore, it is believed that sulphide mineralization at Odin was concentrated along these later shear zones, one of them denoting the adjacent Clubhead Prospect.

Local faulting is also evident at Odin, which together with the excessive jointing, may have influenced karstification in the area.

4.1.3 Alteration

All the dolostones in the vicinity of the Odin Prospect have undergone varying degrees of recrystallization. The host grainstones appear to be coarsely crystalline in places, and the occurrence of a coarsely-crystalline, white dolospar is also common. The distribution of colloform textures within the dolostones has already been discussed, and irrespective of size, these consist mostly of a radial growth of coarsely crystalline/bladed dolomite. Silicification of some colloforms, especially the larger variety, is also quite common, resulting in these textures displaying a positive weathering.

Two phases of mineralization were observed at Odin: i) a primary hypogene phase and ii) secondary supergene enrichment. The former lead to the precipitation of galena and sphalerite, which occur as large euhedral crystals (up to 1 cm) in the host dolostone, in addition to the cores of some colloforms. This type of mineralization may also occur as disseminated blebs within the host rock.

Supergene mineralization is restricted to small karstic features, and accounts for localized high concentrations of galena, cerrusite and smithsonite.

4.2 Sample Description

As for Berg Aukas, petrographical studies of the Odin dolostones suggest a complex recrystallization history. To assist with any comparison with Berg Aukas samples, the different mineral generations or fabric types have been assigned the same alphabetic coding (A,B,C,D). A listing and brief description of the samples selected from the Odin area appear in Table 4.1. A similar sample identification code is used as for Berg Aukas, providing an approximate sample locality, as follows:

OD 12 - Odin Diamond drillhole (No. 12)
OS - Odin Surface
CH - Clubhead Surface

Table 4.1: Carbonate samples from the Odin and Clubhead Prospects used for isotope studies (lg = light grey; mg = medium grey; dg = dark grey; rec = recrystallized; min = mineralized).

Sample No.	Fabric Type	Description
CH-1a	A	lg/creamy dolomicrite
OD 12/4b	B	lg rec dolomite
OS-1	B	lg rec dolomite
OS-4b	C	white dolomitic microspar
OS-3b	C	coarse white dolospar
OD 12/4a	C	white dolospar (min)
OS-2b	C	white dolospar (min)
CH-1b	C	white dolospar (min)
CH-1c	D	colloform
OS-3a	-	quartz vein

Unlike at Berg Aukas, sulphide mineralization appears to have a distinct association with white sparry dolomite (fabric type C) at Odin. Furthermore, a single sample was collected from a quartz vein which is proximal to the mineralized sulphide zone at Odin.

4.3 Results

4.3.1 Petrographical Studies

For the petrographical investigation of the Odin area thin sections in addition to polished thin sections were examined. As in the case of the Berg Aukas dolostones, the same four dolomite crystal fabric groups were recognized, and are similarly designated fabric types A - D (refer to section 2.5).

Despite there being a broad similarity in terms of the general petrographical appearance between Berg Aukas and Odin dolostones, there are two differences which may be pertinent when comparing these two areas. Firstly, in the case of the Odin Prospect it was observed that sulphide mineralization appears to be directly associated with the white sparry dolomite (fabric type C), unlike the relationship with mosaic dolomite (fabric type B), as is the case at Berg Aukas. Secondly, the colloform textures common at both occurrences differ in terms of size. Whilst such features seldom exceed 10 mm at Odin, colloforms several centimeters in

width have been observed at Berg Aukas. Though the relevance of such observations may not be of immediate significance, it is worthwhile to bare these in mind.

4.3.2 Host Rock Mineralogy

XRD analyses were performed on finely ground powder of all the fabric types, in addition to a single specimen collected from a silica vein. A semi-quantitative evaluation of each sample presented as peak height proportions, is presented in Table 4.2.

Table 4.2: Semi-quantitative evaluation of Odin and Clubhead samples determined by XRD.

Sample No.	Fabric Type	Peak Intensity c/s Qtz (101)	Cal (104)	Dol (104)	Qtz %	Cal %	Dol %
CH-1a	A	-	-	19729	-	-	100
OS-1	B	-	-	22663	-	-	100
OS-4b	C	7584	314	172	94	4	2
OS-2b	C	-	-	18428	-	-	100
OD 12/4a	C	-	-	20979	-	-	100
CH-1b	C	877	-	21437	4	-	96
CH-1c	D	1097	-	47087	23	-	77
OS-3a	*	63579	-	9557	87	-	13

Note: * = dolomite sample associated with a quartz vein

With the exception of a single specimen, all of the samples are free of calcite. In the case of sample OS-4b, which resembles a white sparry carbonate in hand specimen, there is a high level of silica contamination in addition to a relatively minor calcite component.

Similarly, the white sparry dolomite (CH-1b) and the colloform dolomite (CH-1c) sampled from the nearby Clubhead Prospect, have a distinctly siliceous component. It is of interest to note that the silica vein which was sampled (OS-3a) yielded some 13% of dolomite, thus a portion of this sample was retained for Sr isotope analysis.

To allow for comparison with Berg Aukas dolomite fabric types, the degree of crystallinity of Odin specimens was determined by XRD, the results appearing in Table 4.3.

Table 4.3: Dolomite crystallinity of Odin and Clubhead samples based on XRD peak intensity ratios.

Sample No.	Fabric Type	Peak Intensity c/s Dol (115)	Dol (110)	$I_{(115)}/I_{(110)}$
CH-1a	A	958	1228	0.78
OS-1	B	1105	1604	0.69
OS-4b	C	200	240	0.83
OS-2b	C	298	197	1.51
OD 12/4a	C	206	256	0.80
CH-1b	C	809	1014	0.79
CH-1c	D	823	943	0.87
OS-3a	*	314	261	1.20

Note: * = dolomite sample associated with a quartz vein

The same data has been combined with that of Berg Aukas samples and presented graphically in Figure 4.3.

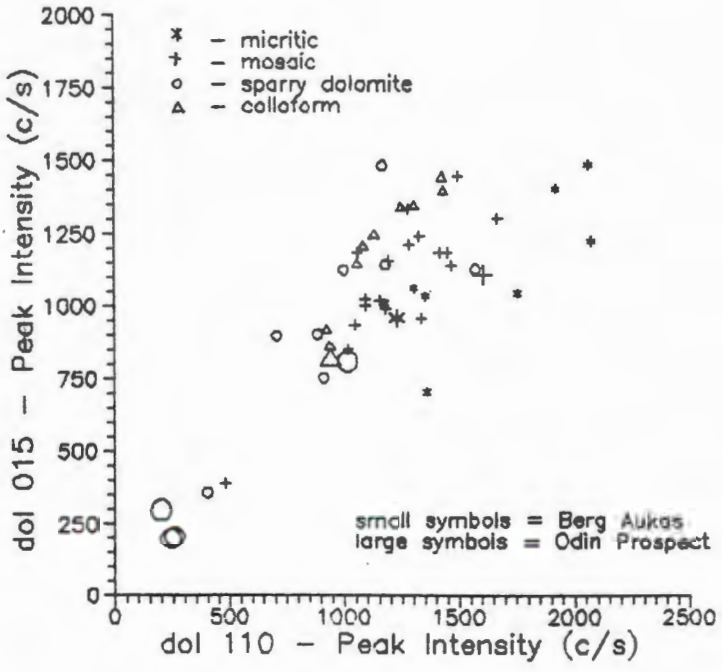

Figure 4.3: Dolomite crystallinity as determined by XRD for both Odin and Berg Aukas.

The few dolomite crystallinity data of the different fabric types collected from Odin samples show a good correlation with similar fabric types sampled from Berg Aukas.

4.3.3 Isotope - Geochemical Studies (Sr, C, O)

The results of the Sr, C and O isotope investigation are listed in Table 4.4, which also contains the Sr concentration in ppm, as determined by AAS, for all the samples that were analyzed.

Table 4.4: Isotopic results (Sr, C, O) on dolomite samples from the Odin and Clubhead Prospects.

Sample No.	Sr (ppm)	$^{87}Sr/^{86}Sr$	2σ std dev	$\delta^{13}C$ PDB °/₀₀	$\delta^{18}O$ PDB °/₀₀	$\delta^{18}O$ V-SMOW °/₀₀
OD 12/4b	90	0.712178	0.0008	2.05	-7.35	23.33
OS-1	70	0.710773	0.0008	1.02	-4.96	25.79
OS-4b	100	0.711164	0.0009	1.12	-8.59	22.05
OS-3b	130	0.716334	0.0009	2.61	-6.99	23.70
OD 12/4a	100	0.710627	0.0008	2.41	-8.44	22.21
OS-2b	100	0.711631	0.0009	2.20	-5.91	24.81
OS-3a	30	0.721393	0.0008	(insufficient CO_2)		
CH-1a	110	0.707765	0.0009	3.51	-2.66	28.16
CH-1c	80	0.714804	0.0010	2.73	-8.83	21.80
CH-1b	80	0.715924	0.0011	3.26	-8.12	22.54

A plot of $^{87}Sr/^{86}Sr$ ratio versus Sr concentration for each of the fabric types is presented in Figure 4.4, and compares values of Odin samples with those of Berg Aukas. A similar plot is presented in Figure 4.5, which illustrates $^{87}Sr/^{86}Sr$ ratios with respect to fabric types for both Odin and Berg Aukas samples, in addition to highlighting which of the samples were gangue dolomite.

A single $^{87}Sr/^{86}Sr$ ratio of the micritic dolomite (type A) sampled at Odin has a value of 0.7078, which is a little lower compared to the Berg Aukas equivalents. A $^{87}Sr/^{86}Sr$ ratio of 0.710 for a sample of mosaic dolomite (type B) from Odin is comparable with those at Berg Aukas. A relatively broader range of $^{87}Sr/^{86}Sr$ ratios is evident for the sparry dolomite (type C) sampled from Odin compared with those of Berg Aukas, with values ranging from

0.711 to 0.717. A single colloform specimen (type D) sampled at Odin had a significantly higher $^{87}Sr/^{86}Sr$ ratio of approximately 0.715, compared to the equivalent samples collected at Berg Aukas.

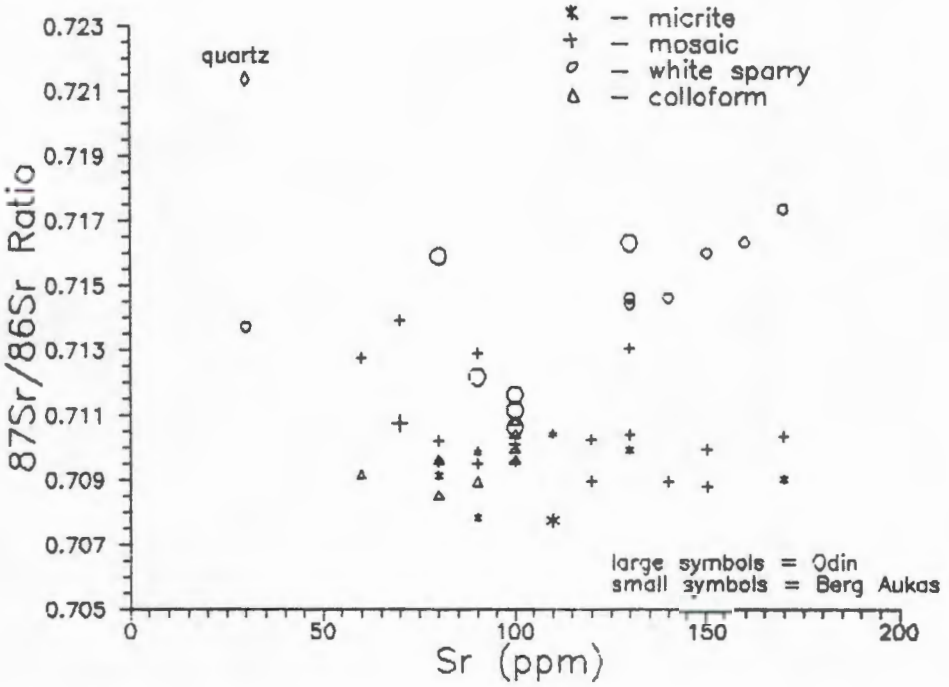

Figure 4.4: $^{87}Sr/^{86}Sr$ ratios with respect to Sr concentration for different dolomite types at Odin, compared to Berg Aukas data.

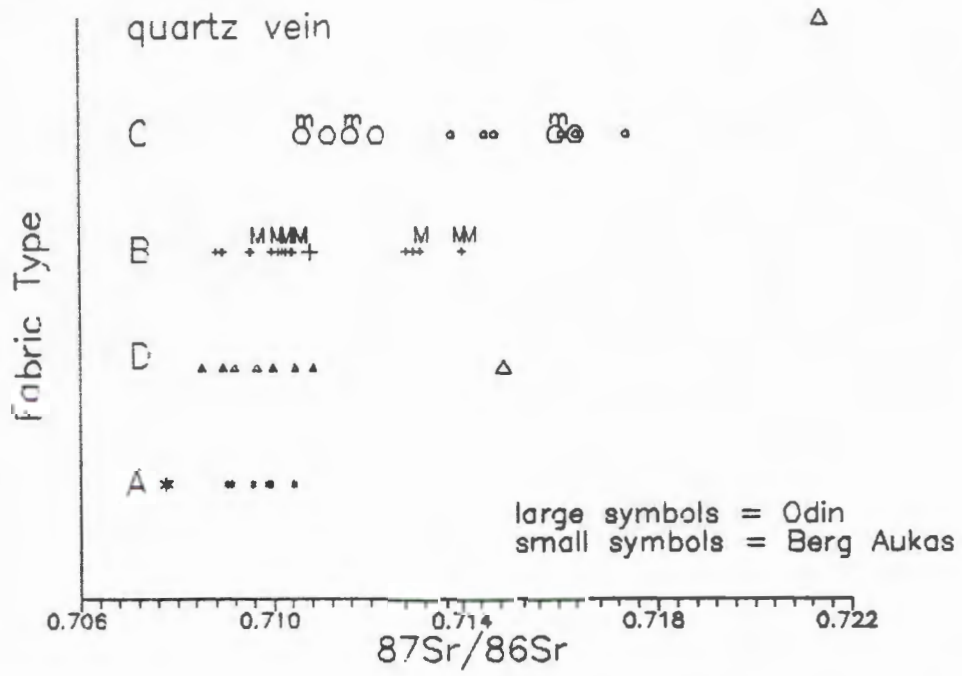

Figure 4.5: $^{87}Sr/^{86}Sr$ ratios with respect to fabric types at Odin, compared to Berg Aukas data (M = gangue dolomite at Berg Aukas; m = gangue dolomite at Odin).

As regards to the dolomite which is associated with a quartz vein which was sampled at the Odin Prospect, a comparatively high $^{87}Sr/^{86}Sr$ ratio of the order of 0.721 was measured.

As is the case for Berg Aukas Sr isotope data, there are no K-bearing minerals in any of the dolomites which were sampled from the Odin Prospect, and therefore it is assumed that the contribution of radioactive ^{87}Rb is negligible.

The $^{87}Sr/^{86}Sr$ ratios of the gangue dolomite sampled from the Odin Prospect range from 0.711 to 0.715, which is similar to the $^{87}Sr/^{86}Sr$ ratios of the gangue dolomite sampled from Berg Aukas.

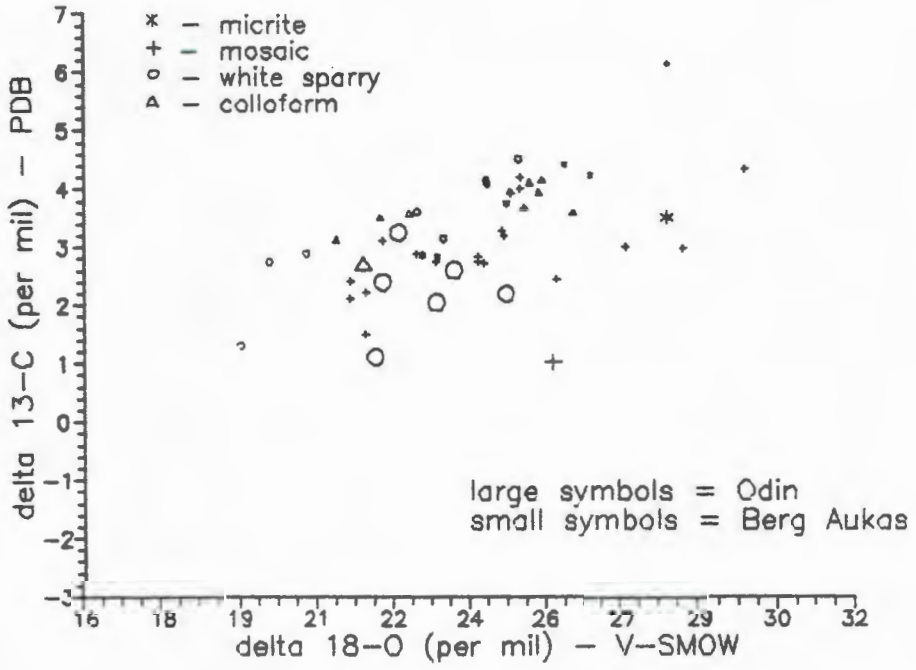

Figure 4.6: Plot of $\delta^{18}O$ (per mil - V-SMOW) versus $\delta^{13}C$ (per mil - PDB) for different fabric types at Odin, compared to Berg Aukas data.

Results of C and O isotope analyses (Figures 4.6 and 4.7) carried out on Odin samples show little variation when compared to similar samples collected at Berg Aukas. However, the single $\delta^{18}O$ for the Odin colloform dolomite (fabric type D), is noticeably depleted in the heavy isotope compared to its Berg Aukas analogues.

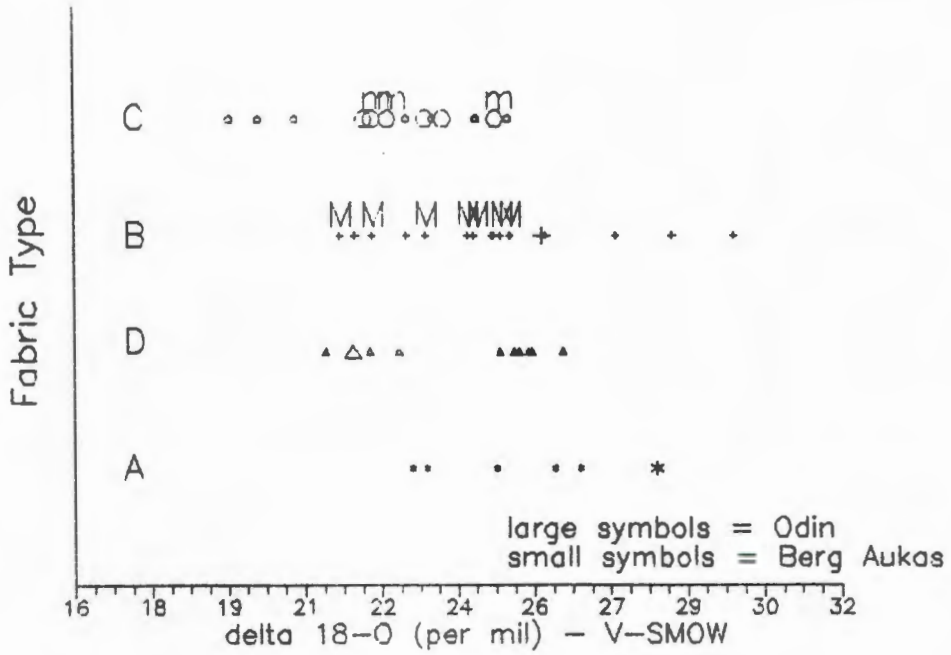

Figure 4.7a: Plot of $\delta^{18}O$ (per mil, V-SMOW) with respect to fabric type at Odin, compared to Berg Aukas data (M = gangue dolomite at Berg Aukas; m = gangue dolomite at Odin).

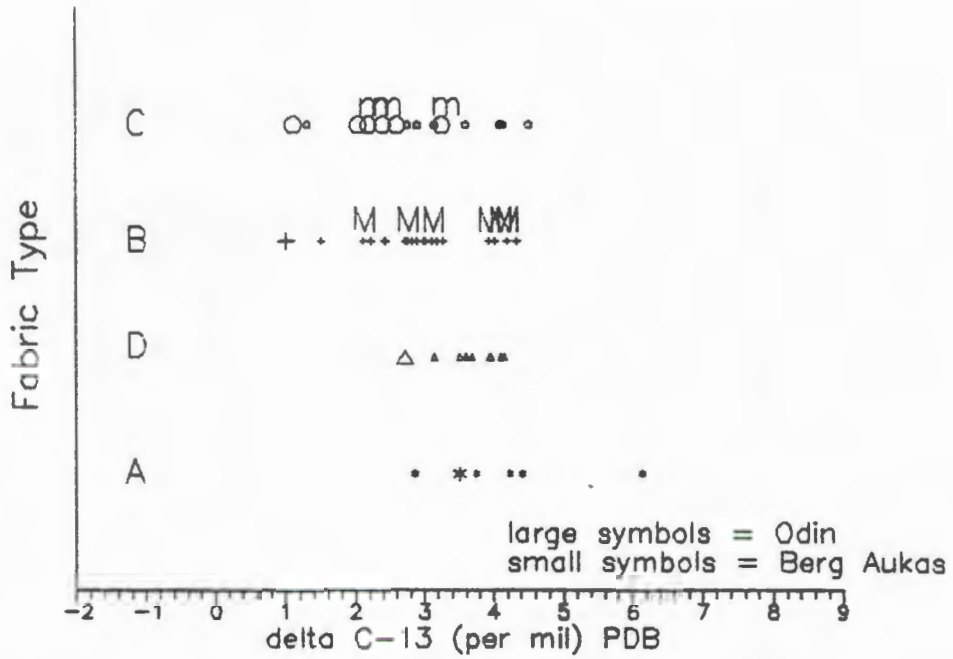

Figure 4.7b: Plot of $\delta^{13}C$ (per mil - PDB) with respect to fabric type at Odin, compared to Berg Aukas data (M = gangue dolomite at Berg Aukas; m = gangue dolomite at Odin).

The trends to higher $^{87}Sr/^{86}Sr$ ratios and lower $\delta^{13}C$ and $\delta^{18}O$ values from type A - D - B - C, as observed for the Odin Samples, is similar to that found at Berg Aukas.

It would appear that the noticeable differences between the Odin Prospect and Berg Aukas deposits, is that the sulphide mineralization is hosted by sparry dolomite at Odin unlike the mosaic dolomite host which is the case at Berg Aukas. Furthermore, it would appear that the colloform dolomite at Odin is more enriched in radiogenic Sr, compared to the Berg Aukas equivalents, whilst the micritic dolomite at Odin is less enriched in radiogenic Sr compared to those sampled at Berg Aukas.

5. POST DEPOSITIONAL ALTERATION

Having presented the results of detailed petrographic and isotope-geochemical investigations in the previous chapters, an attempt will be made to reconcile and interpret this data in terms of post depositional alteration. This shall include probable models for dolomitization and colloform development, in addition to physico-chemical conditions leading to the formation of the Zn-Pb sulphide deposits at Berg Aukas.

5.1 Dolomitization

Controversy continues over the relative responsibility of dolomitization models in accounting for extensive ancient dolomites (Zenger and Dunham, 1988). In determining the origin of a particular dolomite type at Berg Aukas, it is necessary to examine the collective evidence from the field to the laboratory, as rarely do one or a few criteria prove to be reliable.

Average concentration and isotopic values for the four principal dolomite types described in this study, are listed in Table 5.1.

Table 5.1: Average concentration of Sr and mean values of C, O and Sr isotopes for Berg Aukas dolomites.

	Dolomite Type	Sr (ppm)	$\delta^{13}C$ PDB	$\delta^{18}O$ PDB	$\delta^{18}O$ V-SMOW	$^{87}Sr/^{86}Sr$
A	Micritic	100	+4.1	-5.3	+25.4	0.709679
B	Mosaic	115	+2.9	-6.2	+24.4	0.710638
C	White sparry	147	+2.8	-7.7	+22.9	0.714419
D	Colloform	86	+3.7	-6.4	+24.3	0.709529

In Figure 5.1, Berg Aukas dolomites are compared with various genetic types of dolomite.

C and C isotopic values for Berg Aukas dolomites are compared with fields of values for other varieties of dolomite from the geologic record, as shown in Figure 5.2.

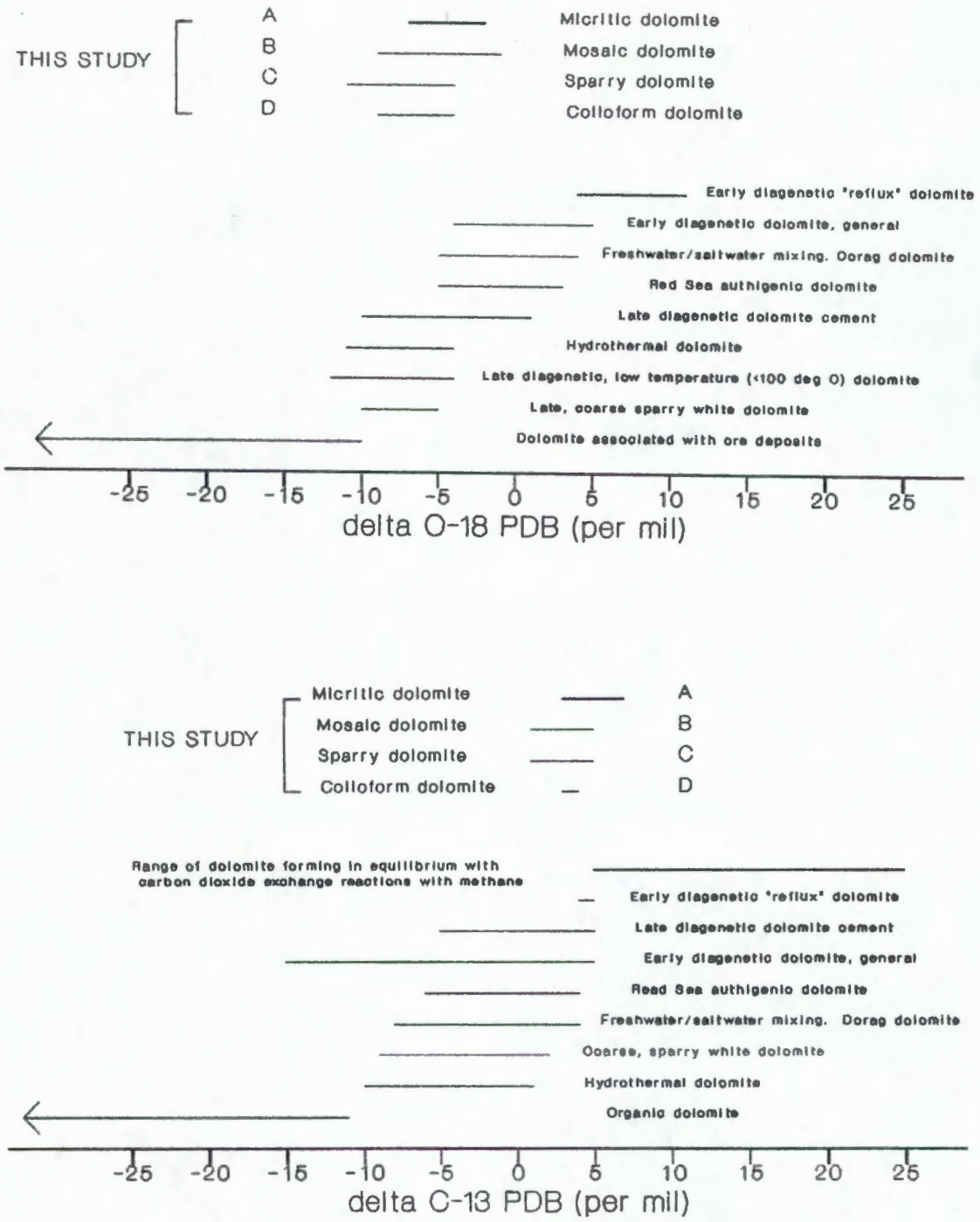

Figure 5.1: Bar graphs for $\delta^{13}C$ and $\delta^{18}O$ comparing Berg Aukas dolomites with various genetic types of dolomite (after Mattes and Mountjoy, 1980).

It has already been described in Chapters 2 and 3, that all of the dolomites found at Berg Aukas have undergone varying degrees of

recrystallization or neomorphic alteration. It is of relevance to note, however, that the Otavi Mountain Land is a metamorphic terrain (Miller, 1983), and though a very low-grade one, it is

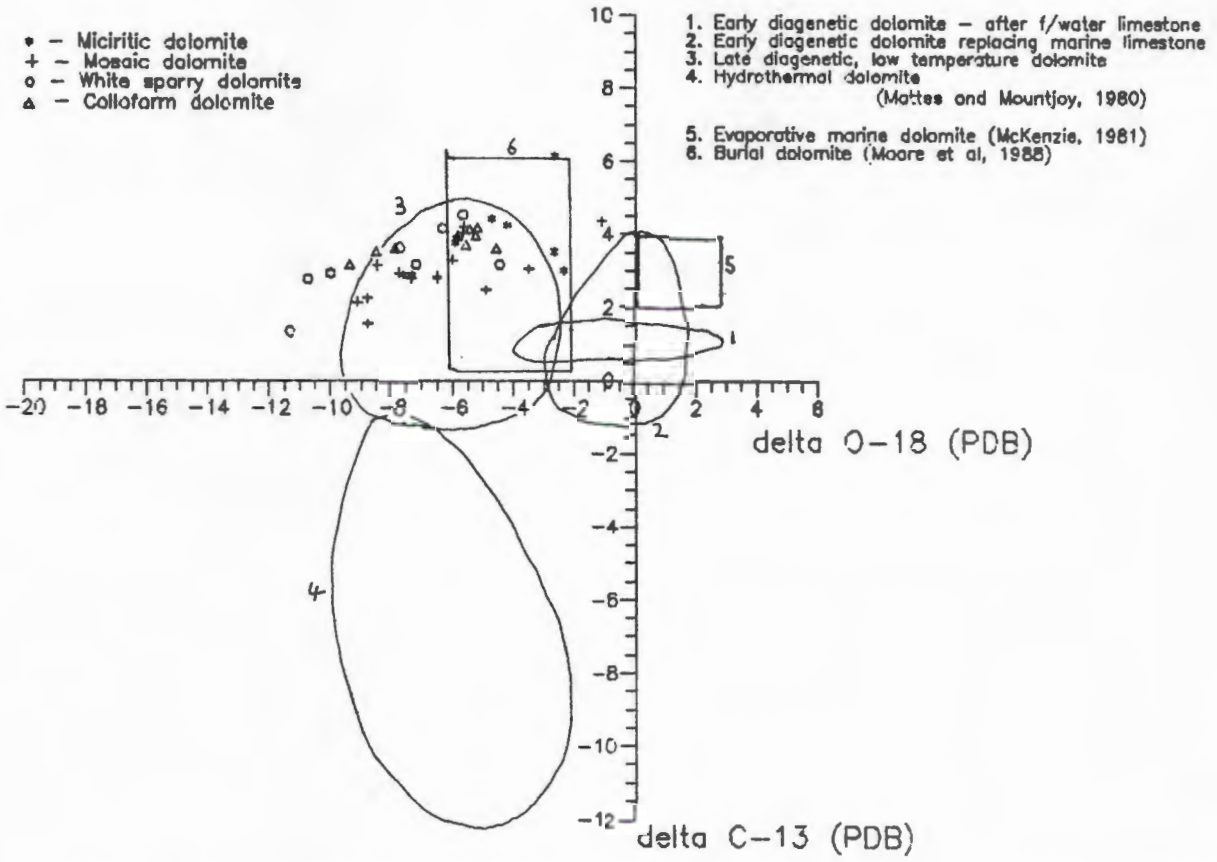

Figure 5.2: Carbon and oxygen isotope values for Berg Aukas dolomites compared with fields of values for various genetic types of dolomite (Mattes and Mountjoy, 1980; McKenzie, 1981; Moore et al., 1988).

logical that even the oldest dolomite generation must have been of neomorphic/metamorphic origin. It is not surprising therefore, that the stable isotope data should plot into the field for late-diagenetic/burial dolomite, as depicted in Figures 5.1 and 5.2.

Although petrographic and field evidence suggest a platform shelf environment, with depth of carbonate precipitation and sedimentation inferred to be moderately shallow, it would be misleading to make any inference as to the precise origin of the dolomite as such.

Results of O and C isotope analyses for the four dolomite types defined in this study, are given in Chapter 3. They indicate that carbonates from Berg Aukas are remarkably homogeneous in their stable isotope composition, but show a noticeable though slight isotopic trend with paragenesis (Fig. 5.1).

The $\delta^{18}O$ values of all the dolomite generations plot in the range of 19 to 29.5 per mil. Dolomite samples of generation B vary in a similar range as the oldest generation A. However, with advancing diagenesis, consistent differences in the oxygen isotopic composition are recognized. The dolomite of generation D is slightly depleted in ^{18}O compared to generation B, and similarly generation C is slightly depleted compared to D.

A similar situation exists with the C isotopic composition of the same samples (Fig 5.1). The host rock (generation A) yield $\delta^{13}C$ values which vary within a narrow range from approximately +3 to +6 per mil. The other samples analyzed from Berg Aukas range in a similar order of $\delta^{13}C$. A clear trend is visible once again, with both generations B and C being slightly depleted in ^{13}C in comparison to generation A.

Summarizing the results obtained one can state that despite the fact that the variation ranges in the isotopic compositions of C and O are relatively small, consistent trends are observed. In such a case, there is a significant evolution towards lighter isotopic composition with advancing diagenesis. This trend is independent of any association with ore minerals in the samples analyzed.

The relatively narrow range of O isotope variation is indicative of the lack of significant meteoric influence, as discussed by Allan & Matthews (1982) and Gorzawski (1989).

In a burial environment, changing temperature conditions may become an important factor for isotope fractionation processes. Crystallization of the different dolomite generations at progressively increasing temperatures would result in a progressive depletion of ^{18}O in the crystallizing dolomite. This could also account for a depletion in ^{13}C, but since the equilibrium isotopic fractionations between dolomite and water at low temperatures still

have to be exactly determined, the rise in temperature expected with advancing diagenesis is difficult to quantify from the isotopic data.

A mixing effect is necessary to explain the stable isotope composition of the dolomites presented in this study. The C and O isotopic ratios of the fluid, from which the dolomites precipitate, change in composition due to changing mixing ratios with the host rock, and due to the contribution of an incoming fluid with probably a different and possibly depleted isotopic composition. However, even an influxing brine enriched in ^{18}O would be possible, providing the temperature of crystallization was high enough. It should be noted, however, that high temperatures are unlikely, bearing in mind the temperature normally associated with relatively shallow burial. A possible source of light C is by the oxidation of organic matter dispersed in the host rock or from other parts of the basin, within which the sediments were precipitated.

The effect of mixing is also reflected in the $^{87}Sr/^{86}Sr$ ratios, (Chapter 3, Fig. 3.3) whereby equilibration took place between an incoming fluid which is relatively rich in radiogenic ^{87}Sr, and the Sr contained in the dolomite host rocks. As discussed in Chapter 3, the host rocks (generation A) display a Sr isotopic composition very close to seawater, which had a $^{87}Sr/^{86}Sr$ ratio of the order of 0.709 during the Precambrian (Veizer et al., 1983).

Subsequent generations of dolomite (types D, B and C) become progressively enriched in radiogenic ^{87}Sr compared to the host rock, and this is probably brought about as a result in increasing brine/host rock ratios (Gorzawski, 1989). As will be discussed in Section 5.4 of this chapter, it can be assumed that with an advancing diagenetic stage, the basinal brine became progressively more radiogenic by exchange reactions with detrital material which formed part of the host sediment, or basement rocks.

5.2 Formation of Colloforms

In this study, the term "colloform" refers to a rounded, more or less spherical texture, consisting of radial fibrous, acicular, or

columnar crystals that have grown approximately perpendicular to sets of lithological bands (Plate 5.1).

A proposed mechanism for colloform formation and development in sphalerite ores is presented by Roedder (1968), the principle of which may well be applicable to the formation of similar structures in dolomites. In brief, Roedder refutes earlier suggestions that colloform textures are the result of crystallization of colloidal gels, and may even may been transported as colloidal sols. Roedder did show that colloform textures in sphalerite ores revealed crystal growth features, that cannot have formed by crystallization from gels. He further suggests that most, and perhaps all these textures, grew directly as minute druses of continuously euhedral crystals projecting into an ore fluid or any other source fluid.

During this study, numerous colloform-textured dolomites were sampled and cut for polishing. Furthermore, discrete samples were collected from as many of the individual colloform bands as possible, in addition to any other dolomitic components which may constitute the rock. An example of this is illustrated in Plate 5.1, which shows a polished slab, having been cut perpendicular to the oblate colloform textures. A list of isotopic values for the material sampled is presented in Table 5.2.

Various isotopic trends for colloformal dolomite, in addition to the other dolomitic components found at Berg Aukas, have already been discussed in Chapter 3. A brief summary as to the pertinent characteristics of colloform-textured dolomite as found at Berg Aukas follows:

a) Tend to be found in areas of tectonic instability and are often associated with solution breccias.

b) Radial structures consisting of fibrous/bladed, acicular, or columnar crystals, which are white to pink in colour, which develop approximately perpendicular to fracture walls or void linings.

c) Crystals often exhibit undulose extinction, similar to "saddle" dolomite.

d) Alternating lighter- and darker-red bands when viewed in cathodoluminescence, and is often associated with micritic dolomite (Plate 5.2).

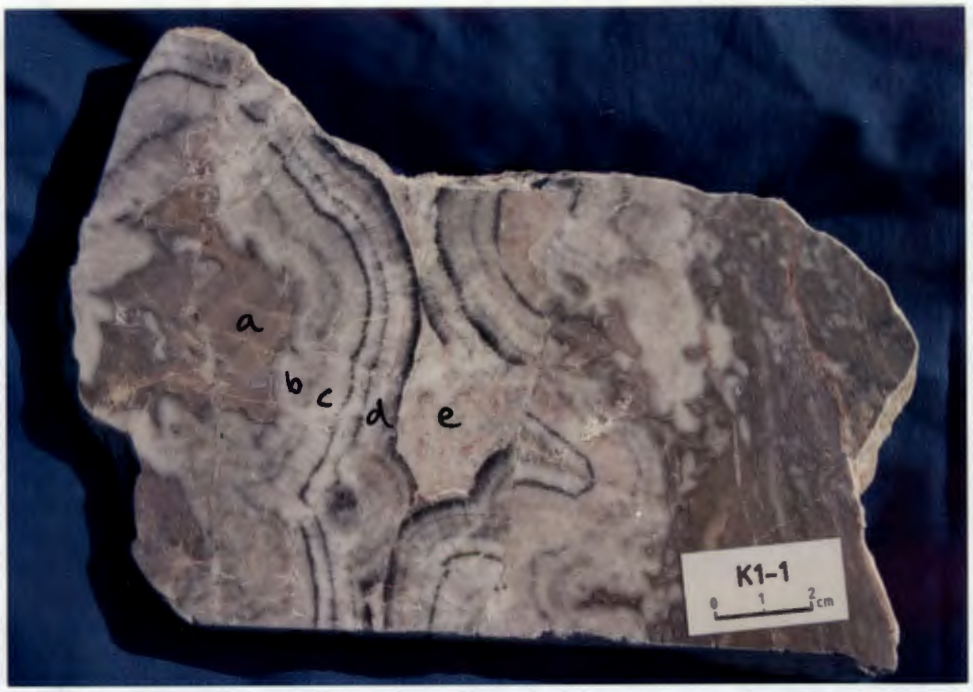

Plate 5.1: A polished surface showing colloform texture in dolomicrite of the Gauss Formation, in the vicinity of Kopje 1. For isotopic analyses of spots (a) to (e), see Table 5.2.

e) Sr concentrations are generally lower compared to the other dolomite types.

f) Sr, O and C isotopic data are similar to those values reported in the host rock (micritic dolomite - type A).

Table 5.2: Isotopic analyses of sample spots (a) to (e) taken from a colloform texture (specimen K1-1).

Sample	Dolomite Type	Sr (ppm)	$^{87}Sr/^{86}Sr$	$\delta^{18}O$ °/oo (V-SMOW)	$\delta^{13}C$ °/oo (PDB)
a	dolomicrite	80	0.709559	23.04	+2.87
b	colloform I	90	0.708958	21.24	+3.15
c	colloform II	150	0.708184	26.32	+3.16
d	colloform III	100	0.709650	25.56	+4.16
e	mosaic dol.	130	0.713075	21.84	+1.51

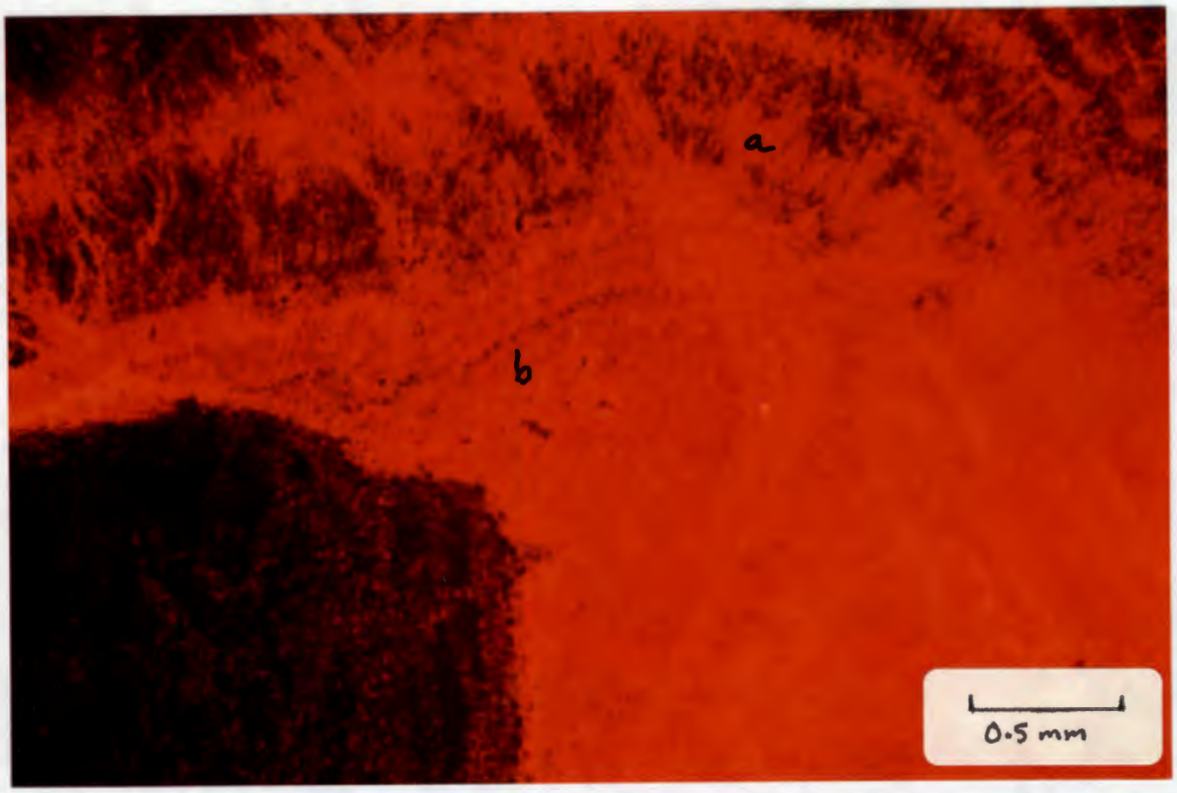

Plate 5.2: A photomicrograph of part of a colloform texture (a) in contact with micritic dolomite (b), as seen in cathodoluminescence.

Isotopic evidence suggests that the dolomite which comprises the colloforms crystallized relatively early in the diagenetic history of the rock, predating both the mosaic and white sparry dolomite types. Whilst sharp crystal contact exist between colloform crystals and both coarse white spar and mosaic dolomite, the contact with micritic dolomite is interpenetrant. Furthermore, close examination of the micritic dolomite ("a" in Plate 5.1), shows how the colloform banding mimics the outline of the micrite. This may suggest that precipitation of colloform dolomite developed in response to the dissolution of the micritic dolomite. The same can be said when viewing the contact between the host micritic dolomite and colloform dolomite in cathodoluminescence (Plate 5.2). Once again the colloform banding mimics the outline of the micrite, and furthermore the characteristic colour of the colloform bands due to luminescence, is similar to that of the host micrite.

The opinion of Roedder (1968) is shared in this study, in that the dominant parameter controlling the formation of colloform textures is a relatively high degree of supersaturation, which results in high rates of nucleation and crystallization. All crystallization from solutions indicates some degree of supersaturation. If the degree of supersaturation is low, crystal growth rates will also be

low, but as spontaneous nucleation is then insignificant or completely absent, all precipitated material may collect on only a few nuclei present. The average size of the individual crystals would vary with the rates of precipitation.

A question the reader may well ask is "what initiates colloform development, and what causes their distinct texture"?

In response to the first part, it is likely that the initial rock had undergone a period of structural deformation which may have involved sedimentary slumping at a very early stage, which may certainly have been pre-burial and possibly whilst the rock was not yet fully lithified. This is verified by $^{87}Sr/^{86}Sr$ ratios which are close to seawater values. Whatever the structural mechanism, the initial carbonate was fractured to invoke a secondary porosity, which would provide likely conduits for the migration of locally derived connate marine water.

This would have been followed by the local dissolution of the micrite, and the later re-precipitation of the more coarsely crystalline colloform dolomite, derived from a supersaturated carbonate solution.

Relatively high degrees of supersaturation are easy to achieve in solutions of materials of low solubility (Roedder, 1968), and carbonates would certainly be no exception to this.

The near-spherical appearance of colloforms is considered to be attributed towards a surface tension phenomena. An alternative process for the formation of these spherical forms would be the radial diffusion from point sources, and subsequent precipitation of substances in concentric (Liesegang) shells (Roedder, 1968).

However, the fact that colloform banding can imitate the outline of the host carbonate (Plate 5.1), has led the author to believe that these spherical structures are formed by replacement processes. Whereby the host micrite is subject to dissolution induced by the early formation of a secondary porosity, and subsequently re-precipitated into the space generated by the dissolution process. Furthermore, the inherent secondary porosity is mostly preserved to

be occluded by latter dolomite generations, such as mosaic dolomite and sparry dolomite.

The individual bands which constitute the colloform texture are considered to be the product of element partitioning. Searl (1990) described a similar phenomena in dolomitized limestones, whereby void-filling ankerite displays well developed sector zonation, analogous to the banding which constitutes the colloform texture described in this study.

According to Searl (1990), sector zonation is a consequence of the non-equivalence of surface cation sites on growing crystal faces, and is preserved where crystal growth was faster than the rate of cation diffusion in the lattice. However, Searl also reports that lattice diffusion in carbonates is negligible at diagenetic temperatures, and hence an alternative explanation is sort.

Searl (1990) proposed that sector zonation is a function of pCO_2. As pCO_2 builds up as a result of the maturation of organic matter in the surrounding sediment, dolomite will approach equilibrium with the surrounding fluid. The subsequent release of fluid along fault planes and/or fractures within the host rock, will lead to a reduction in pCO_2 and the subsequent re-adjustment of the pH to match the new equilibria with dissolved CO_2. Such a situation will thus generate dolomite supersaturation, and the subsequent precipitation of dolomite, until such time as equilibrium is re-attained and the pCO_2 starts to build up prior to the next structural/tectonic event. Searl (1990) believes that it is the continued oscillation in pCO_2 and therefore the CO_3^{2-} concentration levels, which give rise to highly competitive sector boundaries.

Such a scenario may well account for the distinct sector zonation or banding in colloform textures as sampled from Berg Aukas, and the fact that such textures are found to be associated with inferred areas of structural deformation, may further reinforce Searls' model for sector zonation.

5.3 Fluid/Rock Ratio During Mineralization

Studies of carbonate diagenesis have endeavoured to determine how processes of water-rock interaction have controlled the textural and geochemical evolution of the diagenetic products (Banner et al., 1988). Quantitative models are developed to determine the simultaneous variations in several isotopic and elemental parameters as a function of water-rock interaction. This study employs the method described by Blattner (1985), that of the calculation of fluid/rock (F/R) ratios on the basis of simple mass-balance equations by modelling Sr, C, and O isotopic shifting capacities.

In this section F/R ratios have been calculated for the mineralized Berg Aukas dolomite, and will be used to examine the significance, if any, of Sr, O and C isotopic ratios for quantifying fluid-rock interaction in such a carbonate system.

The theoretical rationale of this study is based on the assumption that any fluid with an isotopic composition which differs from that of the infiltrated rock, has the potential to be modified during interaction with the host rock (Frimmel, 1991). Since there must be an exact balance between the amount of an isotope gained by the fluid and the same isotope species lost by the rock, the relative isotope shifts in any zone of interaction can provide a quantitative measure of the interacting masses of fluid and rock. The respective F/R ratio can be calculated in terms of a simple mass-balance equation governing any fluid-rock interaction in a closed system, described by Blattner (1985) as follows:

$$F/R = - c_R.\sigma_R/c_F.\sigma_F \qquad (1)$$

where: c_R, c_F = concentration by weight of the isotopic element (C, O, Sr) in the rock and fluid, respectively.

σ_R, σ_F = the isotope shift for completely reacted or exchanged rock and fluid, respectively.

F, R = cumulative fluid throughput and the infiltrated rock, in mass units, respectively.

The expressions $F.c_F.\sigma_F$ and $R.c_R.\sigma_R$ are known as isotopic shifting capacities (Blattner, 1985), and must be of opposite sign.

Fluid that may have passed through without reacting would not show an isotope shift. Consequently, a mass of isotopically exchanged rock determines a minimum mass of fluid with which it must have reacted with, regardless of reaction kinetics or flow patterns (Frimmel, 1991). In actual systems, such as those described for Berg Aukas, the quantitative use of mass balance is limited by difficulties in measuring the composition of the passed fluid. It will be shown, however, that this limitation may be overcome by modelling fluid-rock interaction with respect to different elements.

Furthermore a "closed-system" behaviour, where all fluid simultaneously equilibrates with the rock, can be distinguished from an "open-system" behaviour where a series of infinitely small aliquots of fluid equilibrates and then leaves the system. In the latter case fluid-rock interaction can be quantified by the relation:

$$F/R = \ln[(F/R)_{cs} + 1] \qquad (2)$$

where $(F/R)_{cs}$ is calculated for a "closed-system" from equation 1 (Taylor, 1977; Valley, 1986; Frimmel, 1991). In the case of Berg Aukas, Sr^{2+} has been introduced into the system as there are insufficient phyllosilicates and other Sr-rich minerals within the Berg Aukas dolostones to explain the amount of Sr present. Furthermore, the mere presence of a significantly sized ore body at Berg Aukas can only be explained by the infiltration of an external fluid.

It is logical therefore, that F/R ratios be presented for an "open-system" situation. To facilitate the comparison between F/R ratios calculated for different species, they will be calculated as volume ratios.

5.3.1 Sr Isotope Shift

Within the Berg Aukas deposit the mosaic dolomite (fabric type B), which appears to host the sulphide mineralization, displays $^{87}Sr/^{86}Sr$ ratios in the range 0.7095 and 0.7139 (Fig. 5.3b).

Other data groupings include the colloform dolomite (fabric type D), which ranges from 0.7085 to 0.7108 and the white sparry dolomite (fabric type C) whose $^{87}Sr/^{86}Sr$ ratios have the highest values of between 0.7137 and 0.7173.

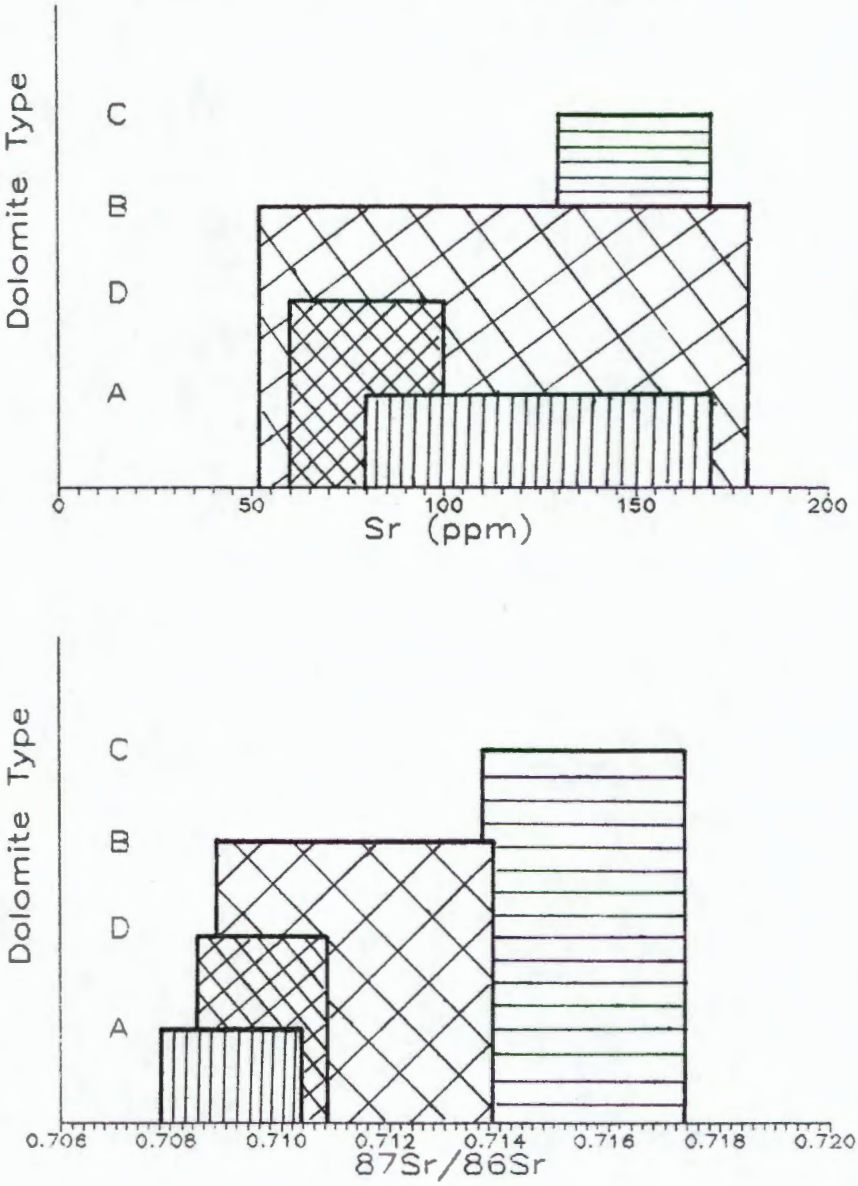

Figure 5.3: Ranges of $^{87}Sr/^{86}Sr$ ratios and Sr concentrations for Berg Aukas dolomites.

In view of Sr concentrations between 30 and 180 ppm (Fig. 5.3a) and an extremely low Rb/Sr ratio, the measured isotopic ratios are effectively initial ratios, and in the case of the mineralized mosaic dolomite this can be regarded as reflecting that of the mineralizing fluid.

The micritic dolomite (fabric type A), which appears petrographically to be the least altered of the dolomite types found at Berg Aukas, has $^{87}Sr/^{86}Sr$ ratios which range from 0.7078 to 0.7105. Though the range is reasonably broad, the mean value compares well to that of Pre-Cambrian seawater, which is approximately 0.709 (Veizer et al., 1983).

Equation 2 has been applied to calculate F/R ratios for an "open system" situation. For the case of mineralizing fluid, σ_R is the difference between the most altered rock immediately adjacent to the sulphide mineralization which has precipitated out of that fluid, and the unaltered original host rock composition. The isotopic shift of the fluid σ_F, represents the isotopic variation for each of the fluids which had infiltrated the host rock. For such a case the host rock is represented by the micritic dolomite (type A), whilst separate calculations will be attempted for the mineralizing fluid (type B) and that fluid which had precipitated the coarse dolospar (type C).

The variation in $^{87}Sr/^{86}Sr$ ratios of the different dolomite types, as depicted in Figure 5.3, can be attributed to two factors: 1) the variation is a function of the distance to the cause of the alteration, such as the site of mineralization or any other fluid source, and 2) the variation may reflect a random regional trend.

Based on petrographic studies using cathodoluminescence as described in Chapter 2, it will be assumed that the variation of $^{87}Sr/^{86}Sr$ ratios is a function of the distance to the cause of the alteration and not a random regional variation. Potential fluids that have altered the dolomicrite (type A) isotopically are those which precipitated dolomite types B and C. However, as described in Chapter 2, sulphide mineralization appears to be directly related to the mosaic dolomite (type B), and not the coarser dolospar (type C). As the colloforms (type D), do not appear to bear any relationship with a mineralizing fluid, and neither do they show any significant isotopic difference with the host dolomite, they shall be excluded from further consideration in this context.

Two separate fluids have been studied here, which are considered to be directly related to the following dolomite types:

B - mineralizing fluid associated with mosaic dolomite

C - fluid responsible for the precipitation of white sparry dolomite

The following calculation applies to deduce the volumetric F/R ratio for closed and open systems. An illustration depicting the various isotopic shifts is presented in Figure 5.4.

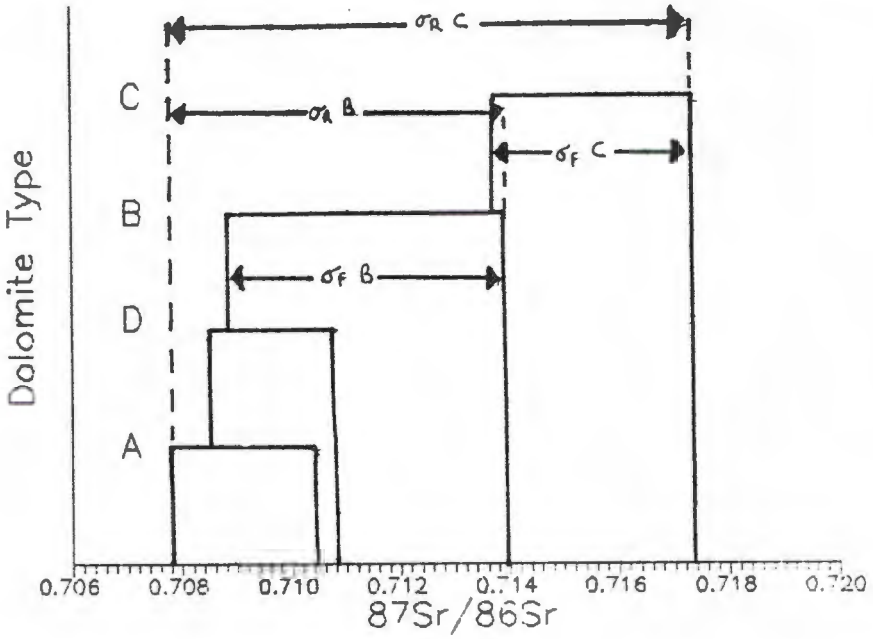

Figure 5.4: Ranges of $^{87}Sr/^{86}Sr$ ratios showing the isotopic shifts.

Given the following parameters, where "*" denotes an average value as listed in Table 5.1:

Assumed density of rock (δ_R)	=	2.85 gcm^{-3}
Assumed density of fluid (δ_F)	=	1.2 gcm^{-3}
Initial [Sr] in host rock (c_R) in ppm	=	100 *
Initial [Sr] in fluid (c_F) in mg/l	=	assign values
Initial [Sr] in fluid (c_F) in ppm	=	(mg/l)/density
Isotope shift for fluid B ($\sigma_{F\ B}$)	=	0.7140 - 0.7090
	=	0.0050
Isotope shift for fluid C ($\sigma_{F\ C}$)	=	0.7175 - 0.7137
	=	0.0038
Isotope shift for rock ($\sigma_{R\ B}$)	=	0.7140 - 0.7078
	=	0.0062

Isotope shift for rock ($\sigma_{R\ c}$) = 0.7175 - 0.7078
= 0.0097

Hence, for a closed system:

$$F/R \text{ ratio (in mass units)} = -(c_R.\sigma_R)/(c_F.\sigma_F) \quad (3)$$

Using (3) and density values for δ_R and δ_F:

$$\text{Volumetric } F/R_{c.} \text{ ratio (closed system)} = [-(c_R.\sigma_R)/(c_F.\sigma_F)].\delta_R/\delta_F \quad (4)$$

Using (4) for an open system:

$$\text{Volumetric } F/R_{o.} \text{ ratio (open system)} = \ln(\text{vol } F/R_{c.} + 1) \quad (5)$$

To plot a volumetric $F/R_{o.}$ ratio versus Sr concentration graph, known values (c_R, σ_R, σ_F, δ_R, δ_F) are substituted into the aforementioned expressions. Assumed values of c_F (in mg/l) are

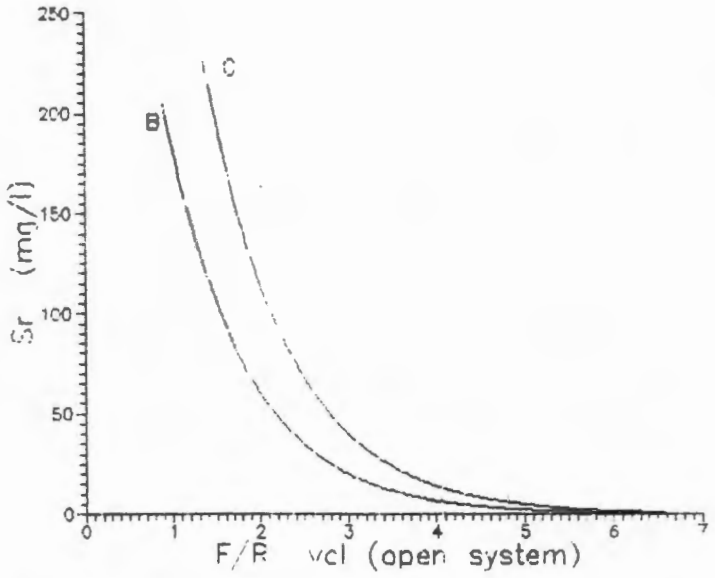

Figure 5.5: Relationship between Sr-content in 2 different fluids (B = mineralized; C = white sparry dolomite) and calculated F/R ratio for an open system.

repeatedly substituted into the same expressions, and a note was made of the corresponding volumetric $F/R_{o.}$ ratios.

The least known factor is the Sr concentration of the reacting fluid (c_F) which cannot be measured directly. Taking a relatively high salinity into account, as it can be expected in ore-forming fluids reacting with shallow marine carbonates, a c_F-value between 10 and 200 mg/l is considered to be realistic. A graphical presentation of the calculated volumetric F/R ratios (open system) as a function of initial Sr concentration appears in Figure 5.5.

Assuming a c_F-value between 10 and 200 mg/l, the corresponding F/R volume ratios (open-system) for the mineralized fluid (B) and the colloform-forming fluids (D) are quite similar, ranging from 1.0 to 4.1, and 1.0 to 4.0, respectively. The F/R volume ratio for sparry dolomite precipitating fluids (C), have significantly higher F/R ratios which range between 1.5 and 4.8.

5.3.2 O and C Isotope Shift

As with Sr isotopes, equations 1 and 2 can be solved for stable isotopic shifting capacities as well. In this case the ratio σ_R/σ_F is usually expressed as:

$$\frac{\sigma_R}{\sigma_F} = \frac{\delta_f(\text{rock}) - \delta_i(\text{rock})}{\delta_i(\text{fluid}) - \delta_f(\text{rock}) + \Delta} \qquad (6)$$

where: σ_R, σ_F = isotope shift (C,O) for rock and fluid respectively.

δ_i, δ_f = initial and final isotopic values (in standard per mil notation), respectively.

$\Delta = \delta_f(\text{rock}) - \delta_f(\text{fluid})$

The micritic dolomite samples which remained relatively unaltered with respect to their Sr isotope composition (corresponding to contemporaneous seawater), are characterized by higher $\delta^{13}C$ and $\delta^{18}O$ values; with $\delta^{13}C_{PDB}$ values of +2.8 to +4.4 per mil and $\delta^{18}O_{V\text{-}SMOW}$ values of +23 to +28 per mil. A similar isotopic alteration with respect to C and O is noted for the mosaic dolomite samples, which have been effected by the mineralizing fluids; with $\delta^{13}C_{PDB}$ values of +2 to +4 per mil and $\delta^{18}O_{V\text{-}SMOW}$ values of +21.6 to +25.2 per mil. These ranges of $\delta^{18}O$ and $\delta^{13}C$ values for Berg Aukas dolomites are represented graphically in Figure 5.6.

Thus, the values δ_i and δ_f for the rock can be measured from outside of (micritic dolomite) and from within the aureole (mosaic dolomite) as an average +25.5 and +23.4 per mil for O, and +3.6 and +3.0 per mil for C, respectively.

It is unfortunate that unlike the $^{87}Sr/^{86}Sr$ ratios presented in this study, the isotopic variation of both O and C isotopes within the various dolomite types is too large, and that between them too small to calculate meaningful F/R ratios. Despite this, an attempt has been made in determining the limits of the initial $\delta^{18}O$ value of the fluid, which may subsequently be used to set constraints on the temperature of fluid reaction with the host rock.

A major uncertainty in deducing the physical conditions during fluid-rock interaction is the lack of direct measurements of the fluid's isotopic composition before reacting. Furthermore, the O isotope fractionation between dolomite and water is strongly dependent on temperature (Friedman & O'Neil, 1977), thus providing a reasonable thermometer, assuming the isotopic composition of the fluid is known. This is illustrated in Figure 5.7, which is a plot of $\delta^{18}O_i$ (fluid) as a function of temperature, as calculated using expression (7).

Given the following parameters:

Temperature of equilibration (T_{eq}) in K	=	assign value
^{18}O of host rock ($^{18}O_{hr}$)	=	25.5 °/₀₀
^{18}O of mineralized fluid ($^{18}O_{mf}$)	=	calculated

Hence,

$$^{18}O_{mf} = {}^{18}O_{hr} - ((2.58*10^6/T_{eq}/T_{eq})-4.3) \qquad (7)$$

A similar calculation was made for the white sparry dolomite (generation C), whereby $^{18}O_{hr}$ assumes an average value for type C dolomite.

An upper limit for the temperature of equilibration (T_{eq}) is given by the homogenization temperature for primary fluid inclusions as measured in sphalerite. Misiewicz (1988) concluded that the homogenization temperature ranges from 97° to 205°C for sphalerite,

whilst Ypma (1984) had obtained higher values, whose results from sphalerite determinations range from 230° to 250°C.

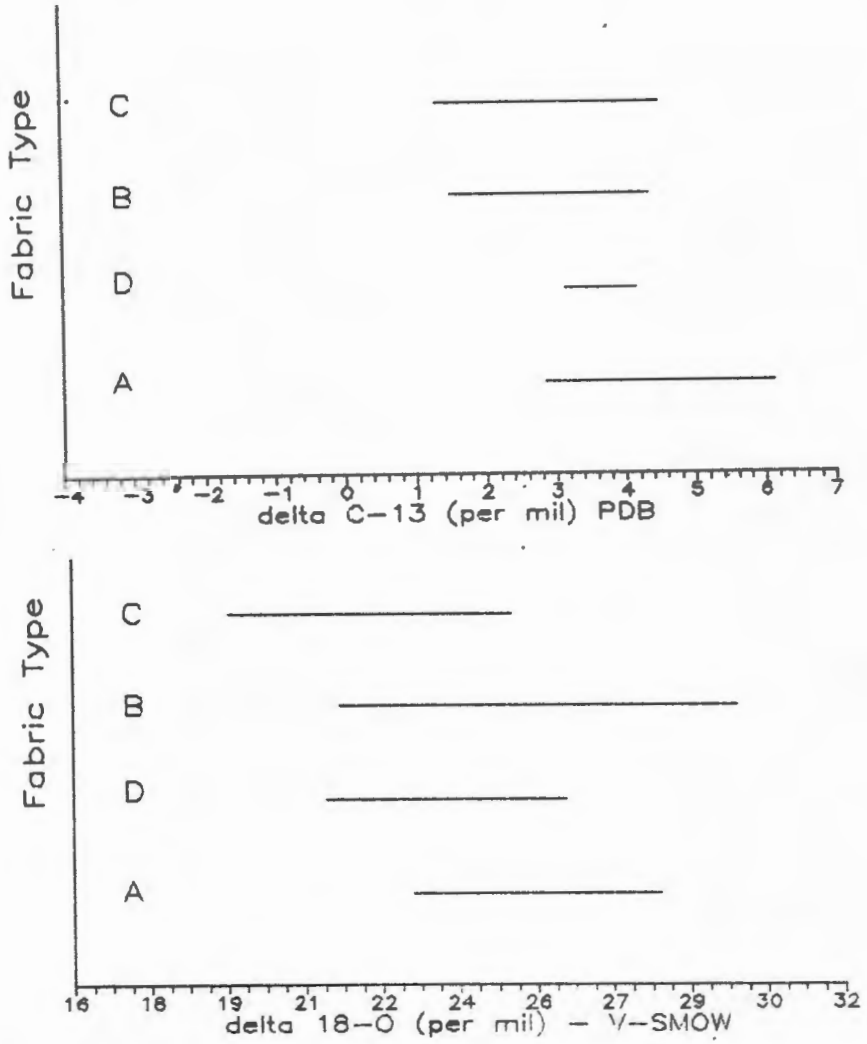

Figure 5.6: Ranges of $\delta^{18}O$ and $\delta^{13}C$ values for Berg Aukas dolomites (A - micritic; B - mosaic; C - white sparry; D - colloform).

Based on the $^{87}Sr/^{86}Sr$ ratios presented earlier in this chapter for the mineralized dolomite (type B), it is proposed that the mineralized fluids had been derived from a metamorphic origin. Sheppard (1986) reports that metasediments typically have $\delta^{18}O$ values within the range +3 to +20 with respect to the SMOW standard, after having applied the H- and O-isotope fractionation factors. The relatively large $^{18}O/^{16}O$ variations reflect the wide range of compositions of the sedimentary (authigenic and detritic minerals) and meta-igneous parent rocks, and the range of temperatures where isotopic fractionation factors tend to be quite variable.

With reference to Figure 5.7, $\delta^{18}O_1$ values of the mineralizing fluid of between +3 and +20 would correspond to a temperature range of between 50 and 300°C, respectively.

The observed isotopic shifts for both O and C can be attributed to the activity of CO_2 and/or CH_4, and H_2O. As regards to this, the presence of graphite and sulphides is greatly significant. Likely fluid components which could coexist with graphite includes CO_2, H_2O, CH_4 and H_2. According to Holloway (1984), these species will mix to form a single homogeneous fluid, at temperatures above 400°C, whilst at lower temperatures they will unmix into carbonic fluid (CO_2 or CH_4) and an H_2O-rich liquid.

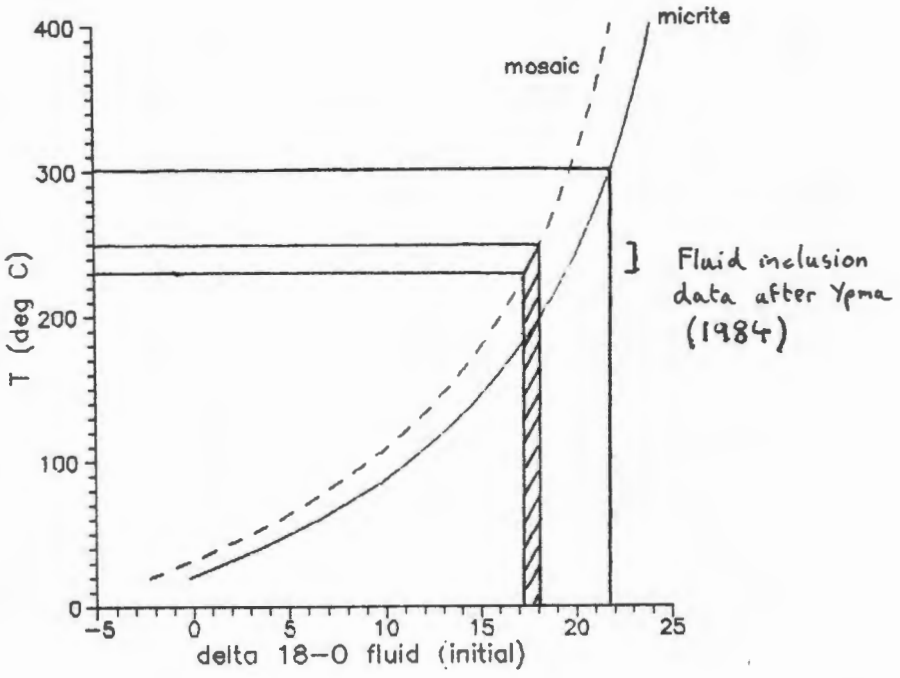

Figure 5.7: Changes in $\delta^{18}O_1$ (fluid) as a function of temperature.

Holloway further calculated that the fluid composition coexisting with graphite at $T_{eq} < 400$°C and $P_{eq} > 0.3$ kb, will be either CO_2 - H_2O or CH_4 - H_2O, depending on the fO_2.

Needless to say, sulphides were present in the mineralizing fluid in the form of galena and sphalerite, and graphitic material has been documented in numerous Berg Aukas borehole logs. Furthermore, the presence of initially sulphides as opposed to sulphates would

suggest a low fO_2 was evident at the time of mineralization. For this reason, it will further be assumed that H_2O was the important fluid species responsible for the observed O isotope shift.

5.4 Source of Mineralizing Fluid

Sulphide mineralization appears to be directly related to the mosaic dolomite (generation B), and hence the isotopic data obtained places some constraints on the possible type of fluid causing the sulphide mineralization at Berg Aukas. Of the various types of metal-transporting waters, the only ones which could be characterized by $^{87}Sr/^{86}Sr$ ratios around 0.712 are either meteoric, certain magmatic, or metamorphic waters (Frimmel and Papesch, 1990).

Meteoric waters typically have $\delta^{18}O$ of less than 0 per mil, and hence dolomite that had recrystallized solely in the presence of fluids derived from a meteoric origin, should exhibit a more distinct shift to lower $\delta^{18}O$ than is observed. Similarly, magmatic waters can be excluded as a likely source of mineralizing fluid, as they generally have $^{87}Sr/^{86}Sr$ ratios much lower than 0.712 (Kessen et al., 1981), with the exception of waters derived from an S-type granitoid magmatism with considerable crustal contamination (Frimmel and Papesch, 1990). However, there is no evidence for any such intrusion younger than the Berg Aukas dolomites.

An $^{87}Sr/^{86}Sr$ ratio of 0.712 can well be accounted for by the presence of regional metamorphic fluids, enriched in radiogenic ^{87}Sr due to the interaction with Rb-bearing rocks. Such rocks would include the metasediments of the underlying Nosib Group. It is quite likely that the isotopic ratios derived from the mineralized mosaic dolomite, strongly suggests that metamorphic fluids were a major component of the ore-forming solutions.

As regards to the subsequent recrystallization of the different dolomite types, such as the coarse white dolospar, there is a distinct shift toward slightly lower $\delta^{13}C$ and more substantially lower $\delta^{18}O$ values (Figure 5.6). This shift would suggest that the mineralizing fluids must have been derived from an external source,

as would be expected for an open-system behaviour for the Berg Aukas dolomites during recrystallization.

6. GENETIC MODEL

The main features which should be considered for a genetic model can be summarized as follows:

Berg Aukas occurs in dolomitic units deposited in peritidal environments during the period 830 - 760 Ma (Kröner, 1982), and is located on the eastern margin of the Northern Platform Zone of the Damara Oregon, and so constitutes the eastern extremity of the OML. Subsequent uplift in the central belt of the orogen resulted in the deposition of Mulden Group clastic sediments at approximately 640 - 560 Ma (Kröner, 1982), which produced burial exceeding 3.6 km (SACS, 1980).

Sedimentological observations suggest in Berg Aukas a strong association between the occurrence of ore and sedimentological facies of the host rock. The dolomitic horizons hosting the ore body is made up mainly of barrier dolomitic grainstones (dolarenites). The ore lenses, however, do not occur randomly in all parts of the host grainstones. They show a clear link to intercalations of micritic dolomite, with accompanying algal mats and stromatolitic horizons attributed to tidal flat and lagoonal facies.

The ore paragenesis (Zn-Pb) is very simple, it is pyrite poor and typical for MVT deposits, as will be discused later on in this chapter. It differs significantly from other major carbonate-hosted deposits in the OML, which are predominantly Cu rich, and are situated in close proximity to a major unconformity which separates the Tsumeb Subgroup from the overlying Mulden Group sediments. For the case of the deposits at Tsumeb and Kombat, there is a close association with feldspathic sandstones.

Abundant, megascopically visible, diagenetic textures and structures reflect a complex diagenetic history. Widespread dolomite dissolution is observed, especially in breccia structures. In terms of primary mineralization, the paragenetic sequence is simple and constant throughout the deposit. It can be summarized in the following three generations: 1) a fine grained micritic dolomite (and associated colloform textures) which is free of sulphide mineralization, 2) medium- to coarse-grained mosaic

dolomite associated with sphalerite and/or galena, and 3) a coarse sparry dolomite which is barren of sulphide mineralization. The presence of a single paragenetic sequence, in terms of primary sulphide mineralization, is an argument favouring a single ore-forming event.

The diagenetic evolution of the Berg Aukas deposit has been traced combining petrographic and isotopic data. Significant isotopic trends were found, and physico-chemical constraints concerning the genesis of the deposit are derived.

The Sr isotope analyses of host rocks and gangue reveal important characteristic features. An examination of the data presented in Chapters 3 and 5, shows that the $^{87}Sr/^{86}Sr$ ratios obtained for the host rock average at 0.709, which is close to the assumed Sr isotopic composition of seawater during the Precambrian. Small but significant isotopic trends are recognized and reflect the evolution history of the fluids during the formation of the ore deposit. The later generations or dolomite types are always slightly enriched in radiogenic ^{87}Sr compared to the earlier ones.

The results reveal the introduction of a fluid relatively enriched in radiogenic ^{87}Sr, which is probably due to circulation through Rb-bearing detrital material. It is considered likely that the underlying Nosib Group meta-sediments is the most probable source of radiogenic ^{87}Sr.

The O and C isotope ratios of the dolomites sampled, lie within a very narrow range, but show a trend towards lighter isotopic composition in the later crystallization generations. Such a trend is more pronounced for the $\delta^{18}O$-values compared to $\delta^{13}C$-values. Such isotopic shifts can be explained in part by increasing temperature, and as significant meteoric influence can be excluded, metamorphic waters should be considered as a likely cause for the isotopic shifts.

6.1 Genetic Model for Berg Aukas

The model proposed here for Berg Aukas is similar to that described by Gorzawski (1989) in his study of the San Vicente Pb-Zn deposit

in Central Peru. This model is based on the introduction of Zn- and Pb-bearing metamorphic water, having formed in response to a regional metamorphism. In particular, according to this model the Berg Aukas deposit had been formed during late stages of diagenesis under considerable burial.

The upper temperature limit indicated by O isotopes (240 to 300°C) is similar to the fluid inclusion data presented by Misiewicz (1988) and Ypma (1984), which ranges from 97° to 205°C and 230° to 250°C, respectively. Abiogenic reduction of sulphates at or near the ore site, and the subsequent introduction of metamorphic waters characterized by Sr isotopic ratios slightly higher than contemporaneous seawater, is likely to be the main factor controlling ore formation. Leaching of detrital material derived from Precambrian meta-sediments of the Nosib Group, would explain such Sr ratios.

The ore-forming process at Berg Aukas is envisaged as a single stage event, characterized by a definite ore-fluid evolution as determined by various physico-chemical constraints (T, eH, pH etc). Such processes would control the precipitation and/or dissolution of minerals, in addition to influencing changes in isotopic ratios of the ore fluid.

Some constraints can be mentioned concerning the time and dynamics of the migration of the Pb- and Zn-bearing fluid. If a temperature of ore formation is assumed to be of the order of 250°C, it is most unlikely that such high temperatures alone can be the product of burial. A major tectonic event (F3) took place between 580 and 550 Ma, which resulted in the folding of the Molasse sediments of the overlying Mulden Group (Kröner, 1982). Kröner also reports that the peak of metamorphism occurred in the northern part of the Damara Orogen shortly after, at 550 to 540 Ma.

Movements related to the uplift in the central belt of the Damara Orogen at 640 to 560 Ma (Kröner, 1982), could have indirectly influenced the fluid dynamics. This would have taken the form of a fluid expulsion, whereby the initial metal reservoir would have been the clastics sediments of the lower Nosib Group, which infilled rift grabens.

Subsequent tectonic activity was responsible for providing structural conduits, which assisted in directing the movement of hydrothermal fluids. The basal unconformity with the underlying Nosib Group at Berg Aukas, behaved as an aquiclude surface, which guided the metaliferous fluids towards structurally, lithologically and chemically favourable traps, in the overlying porous and permeable carbonate rocks.

Subsequent oxidation by circulating meteoric waters would have concentrated the sulphides and deposited V, which was transported as calcium metavanadate complexes (Misiewicz, 1988). It is thought by Misiewicz, that the V had been derived either from the weathered components of the underlying gabbros in the basement complex, or from sediments which were derived from the basement.

Mineralization is intimately associated with an intricate karst network, and the ore is hosted by breccia bodies. Supergene enrichment has been responsible for a varied ore mineralogy which includes descloizite, willemite, smithsonite, cerussite, sphalerite and galena.

6.2 Comparison with MVT Deposits

A detailed presentation of Sr isotope trends during diagenesis in a variety of ore-bearing carbonate basins thought to be MVT in origin, is presented by Gorzawski et al. (1989). It has been mentioned in earlier chapters that isotope studies can provide important constraints on the diagenetic evolution of carbonate rocks, and the ore minerals associated with them. Specifically the study of $^{87}Sr/^{86}Sr$ ratios has proved to be extremely successful in order to pin down the timing of diagenetic events (Gorzawski et al., 1989).

This section will compare the results of Sr isotope analyses carried out on a variety of MVT ore-bearing carbonates, with those obtained from the Berg Aukas deposit. Furthermore, similarities and differences as regards to other geological features will also be discussed.

In Figure 6.1 the results of Sr isotopes analyses obtained in this study, are displayed together with those obtained for several MVT

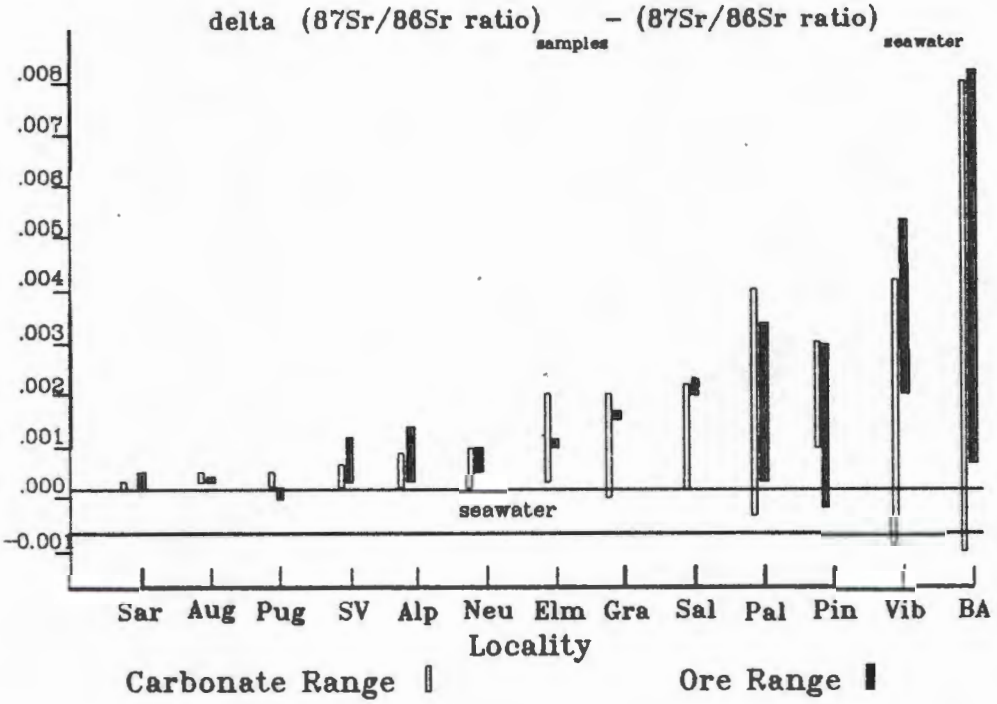

Figure 6.1: Variation ranges of Sr isotope compositions in Berg Aukas (BA) compared to data for other MVT districts. Sar = Sardinia, SV = San Vicente/Peru, Alp = Alpujarrides/Spain, Neu = Neuquén/Argentina, Pal - Pallières/France (Gorzawski et al., 1989). Aug = Auglaize quarry, Pug = Pugh quarry, Elm = Elmwood, Gra = Gratz-Lockport, Sal = Salem (MVT deposits, USA, Kessen et al., 1981). Pin = Pine Point/Canada (Medfor et al., 1983), Vib = Viburnum Trend/Missouri, USA (Lange et al., 1983). The values are normalized to the assumed contemporaneous strontium isotope composition of seawater after Burke et al. (1982).

deposits in both North and South America as well as Europe. The figure distinguishes between the various ranges in gangue (open bars) and ore minerals (including carbonates clearly associated with ore minerals, solid bars). In order to facilitate the comparison, the results have been normalized to the assumed value of the respective seawater composition.

The variation range comprises values from close to zero (Sardinia, Auglaize) to very strong increases (Viburnum Trend, Berg Aukas), with respect to the $^{87}Sr/^{86}Sr$ ratios of their respective seawater compositions. In a first approximation (Gorzawski et al., 1989),

Table 6.1: Comparison of Berg Aukas with other MVT deposits (+ = in agreement with MVT deposits).

Mississippi Valley-type deposits	Berg Aukas
Host rock character and alteration	
A. Shallow water carbonates	+
B. Certain stratigraphic horizons are the principal producers, but mineralization extends over a large stratigraphic interval	Ore is hosted by a single stratigraphic horizon
C. Unconformities beneath and within the mineralized stratigraphic interval controls facies patterns	A single major unconformity exists beneath the deposit
D. Most ore deposits are confined to dolomitized areas	Ore deposit occurs exclusively in dolomite
E. Recrystallization is common	+
F. Silicification has developed to varying degrees	+
Region Structure and ground preparation	
A. Districts occur proximal to domal features	No major domal features have been recorded
B. Major faults and fault breccias are important in localizing ore	+
C. Permeable horizons allow extensive lateral movement of ore solutions	No extensive lateral movement can be observed
D. Ground prepared by minor faults and fractures	+
E. Ground further prepared by solution and collapse through the action of groundwaters related to unconformities	Ground preparation by dissolution important in concentrating secondary mineralization
Local structural controls	
A. **Sedimentary structures**	
1) Ridges or bars	Not observed
2) Reefs and reef-like structures	Bioherms are present - effect on mineralization is unknown
3) Submarine slide breccias	May have given rise to solution breccias
4) Lateral facies changes	Ore deposit restricted to a grainstone unit
B. **Tectonic structures**	
1) Folds	Flexing has been of use in creating fractures
2) Minor faults and fractures	Fractures play a major part in the plumbing

Table 6.1: (continued)

Mississippi Valley-type deposits	Berg Aukas
	system, in localizing the ore deposit
3) Fault breccias	Not directly associated with mineralization
C. Solutional structures 1) Solution collapse breccias provide transport and host mechanism for ore fluids. Collapse structures may occur near or parallel to major faults; a great variety of shapes is exhibited by the resultant breccia bodies	Solution collapse appear to be the dominant ore-bearing structures
Ore character	
A. Open space filling of vugs, fractures, and breccias is the principal manner of ore occurrence	Much of the primary ore is deposited within irregularly shaped vugs in breccias and host rock
B. Veins are locally associated with predominantly stratiform ore	True veins have not been reported
C. Size of ore deposit is controlled by the size of the local controlling structure	+
D. Most deposits are relatively low grade	Grade is high - often exceeds 15% combined Zn and Pb
Mineralogy	
A. Principal minerals are restricted to a small number	Principal primary minerals are sphalerite and galena. Numerous secondary minerals are found
B. Principal ore minerals have simple chemical compositions	Primary ore minerals are simple sulphides

it appears that for those deposits characterized by a predominantly stratiform geometry and a clear facies control (left part of Figure 6.1), the absolute difference of the $^{87}Sr/^{86}Sr$ ratios are significantly smaller than in non-stratiform ore deposits (right part of Figure 6.1). This trend can be explained in terms of early versus late diagenetic timing of the ore forming processes.

However, other factors, such as the hydrodynamics of the basin, the lithological characteristics such as the amount of Rb-bearing minerals, and the paleogeographic position within the basin, including the vicinity to the basement, should also be considered (Gorzawski et al., 1989).

It would appear from Figure 6.1, that Berg Aukas has reached an advanced evolutionary stage, and hence the broad range of the Sr isotope ratios for both ore-bearing fluids and the host carbonate. Such a trend is similar to the data reported for the Viburnum Trend deposits in the USA. However, it is possible that some of the samples analyzed did contain traces of Rb, hence causing higher $^{87}Sr/^{86}Sr$ ratios.

A comparison of the Berg Aukas deposit with other MVT deposits is presented in Table 6.1. As can be seen in this table, the Berg Aukas deposit offers many similarities to "typical" MVT deposits, and despite differences in grade and lateral extent of the ore body, it may well be incorporated into the family of MVT deposits.

6.3 Implications for Further Prospecting

One of the prime objectives of this study was to recognize possible isotopic alteration haloes around sites of mineralization. Furthermore, it was anticipated to establish spatial distances over which fluid-rock interaction had taken place, by means of modelling the kinetics of fluid flow, and subsequently attempt to measure the proximity to an ore body.

It is unfortunate that this aspect of the study was not possible due to the following reasons: 1) Inaccessibility to underground workings and limited surface and borehole core samples, failed to provide an adequate three-dimensional coverage of the existing ore body; 2) The broad range of isotopic data within sample types, and the comparatively narrow range of values between sample types, proved too unreliable to attempt any meaningful modelling of the kinetics of fluid flow.

However, most of the techniques described here can indirectly be applied to exploration, allowing for some constraints to be made.

It must be emphasized that none of the techniques described here will give any indication as to the size and grade of a potential ore body. The techniques will merely provide an indication as to whether or not the necessary ore-bearing fluids had infiltrated a particular site of interest, assuming of course that the mineralization is of Berg Aukas type.

Results of this study have shown that by means of cathodoluminescence, it is possible to distinguish the different generations of dolomite, and by careful examination, it is further possible to associate any sulphide mineralization with a particular generation of dolomite. In a similar fashion, it has also been demonstrated that $^{87}Sr/^{86}Sr$ variation ranges also constitute a sensitive tool for determining the different generations of the host carbonate. This in itself, also provides a means of approximating the stage of basin evolution. This method has the disadvantage that the increase of radiogenic ^{87}Sr depends on the amount of Rb-bearing minerals present in the basin. However, this method has the important advantage that within a given basin or local depositional center, this last parameter can be modelled. Therefore, each evolution stage is "finger-printed" in its' cement or crystallization generations by the Sr isotopic signatures, which generally tend toward increased values with advancing diagenesis.

Assuming that petrographic and cathodoluminescence studies succeed in identifying the particular carbonate generation associated with sulphide mineralization, it would then be possible to place an approximate age of the mineralizing event, with respect to the diagenetic history of the host rock.

On a regional scale, it would then be possible to compare the various sulphide-bearing carbonates within the OML, based on their individual isotopic signatures. Armed with the necessary isotopic information concerning the host dolomite, and its relative diagenetic age, the exploration geologist would then be in a position to determine whether or not the necessary mineralizing fluids had infiltrated the area of interest or not. This would all assume, of course, the correct classification of the ore-bearing fluid has been made, and that any likely input of Rb-bearing minerals within the area of interest is negligible.

Owing to the excessive costs of using some of the more traditional geophysical and geochemical techniques, the study of Sr isotope ratios provides a comparatively cheap means of identifying and recognizing ore-bearing fluids. To use this method objectively, would require strict control as to the sampling of the different carbonate generations, using the techniques described in this study, as opposed to the standard whole-rock geochemical sampling currently practiced.

As regards to the usefulness of O and C isotopes, though significantly cheaper to analyze compared to the Sr method, results presented in this study have shown that the use of stable isotopes, for the purpose of differentiating between the different carbonate generations, is less effective.

7. SUMMARY AND CONCLUSIONS

The present study focuses on geochemical aspects of the crystallization processes in carbonate-hosted Zn-Pb-(V) deposits, during the diagenetic evolution of the enclosing sedimentary basin. The application of isotopic methods as a tool in order to constrain mechanisms and timing of ore-forming processes, was especially emphasized. For this purpose, detailed petrographic and (isotope-) geochemical investigations have been carried out in two carbonate-hosted deposits displaying similarities (stratigraphy, diagenetic fabrics), but also subtle diversities concerning mainly the facies-bound character. Whilst the principal study centered on the Berg Aukas deposit; a minor comparison was made with the Odin/Clubhead Prospects.

The main characteristics can be summarized as follows:

i) Geology, paleogeography, and facies - Both ore deposits occur in Upper Precambrian (830 - 760 Ma) dolomitic units of the Gauss Formation of the Abenab Sub-group. Though the sedimentary units of both areas were deposited on a peritidal platform along a rift margin, the ore is bound to a dolomitized grainstone facies for the case of Berg Aukas, whilst at Odin both oolitic grainstone and stromatolitic facies play host to primary sulphide mineralization. In terms of tectonic framework, both ore bodies are similar as regards to their association with synformal features and high-angled shears. A major basal unconformity is evident at both localities, which separates the basal Nosib Group meta-sediments, and the overlying carbonates.

As the sulphide mineralization is situated within the uppermost part of the Gauss Formation (boundstones and oolitic grainstone facies) at Odin, unlike the underlying grainstone facies at Berg Aukas, the degree of burial at Odin is inferred as being marginally less compared to Berg Aukas.

ii) Petrography, ore textures and structures - From a macroscopic point of view, both Odin and Berg Aukas rock types are dominated by complex diagenetic textures, comprising intense dissolution-precipitation phenomena, solution cavities, impregnation of pore space and colloform structures.

Petrographical studies resulted in identifying several phases of dolomitization, recrystallization, and to a lesser extent silicification, which appear closely associated with ore formation. For the case of Odin, the white sparry dolomite (generation C) would appear to be the host rock of the ore minerals, unlike Berg Aukas, where the mosaic dolomite (generation B) is the gangue rock. As regards to the colloform structures, it is of interest to note that the size distribution of these textures differ between Berg Aukas and Odin, with those found at Berg Aukas being significantly larger and more intensely developed, compared to their Odin equivalents. Furthermore, evidence of sulphide mineralization occluding the cores of colloform textures has been noted at Odin, unlike Berg Aukas, where such a phenomena has not been observed.

As regards to the white sparry dolomite (generation C), this dolomite type appears petrographically to be more coarsely grained, compared to their Odin counterparts, and this feature is reflected when comparing the dolomite crystallinity data as determined by X-ray diffraction.

The ore paragenesis is simple for both Odin and Berg Aukas deposits, dominated by Zn- and Pb-sulphides and poor in Cu, which appears typical for MVT deposits.

iii) Sr isotope studies - This turned out to constitute an excellent tool in order to constrain the relative timing of the evolution of the carbonate host rocks. $^{87}Sr/^{86}Sr$ analyses were carried out on samples collected from both Berg Aukas and Odin. Consistent trends are observed in the data, and a distinction will be made between relative and absolute variations between the two ore deposits.

The relative trends are similar in both of the areas studied. In both cases the later crystallization generations are enriched in radiogenic ^{87}Sr compared to earlier ones. This consistent trend towards increasing $^{87}Sr/^{86}Sr$ ratios with advancing diagenetic stages is one of the main results of this study. By comparing these results with similar studies carried out in France and Peru (Gorzawski, 1989), it may be concluded that the trend observed in this study corresponds to the general rule that minerals forming at

the end of the diagenetic crystallization sequence are, in general, more radiogenic than those forming at the beginning.

The increasing Sr ratios in the subsequent diagenetic generations are explained by equilibration during crystallization with the Sr isotopic composition of the fluids involved. The results indicate that the diagenetic evolution of each dolomite generation was determined by fluids with different isotopic composition.

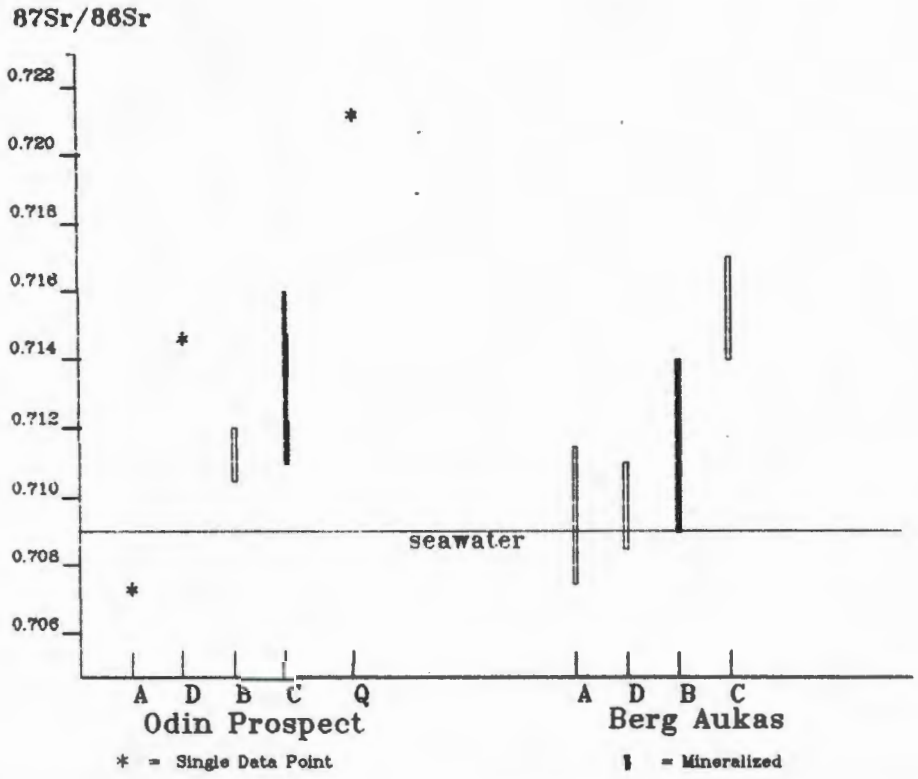

Figure 7.1: Comparison of the variation ranges of the Sr isotope ratios for the different dolomite generations, as sampled from Berg Aukas and Odin. (A = micritic dol., B = mosaic dol., C = sparry dol., D = colloform dol., Q = carbonate in quartz vein)

The $^{87}Sr/^{86}Sr$ ratios measured in single samples reflect a certain mixing proportion between the Sr contained in the host rock, and the strontium contained in the circulating fluid. In the last generations, the fluid/host rock ratio is significantly higher and therefore the values are increasingly more radiogenic.

The absolute variations, which involves the magnitude of the Sr isotope ratios for each of the dolomite generations, are well

documented for Berg Aukas samples. However, due to the limited data available for Odin samples, only approximate differences between the two deposits can be attempted. The results obtained are summarized in Figure 7.1, in which for both localities studied, the ranges of $^{87}Sr/^{86}Sr$ ratios of the different carbonate generations (highlighting those associated with sulphide mineralization), are compared with the Sr isotope composition of contemporaneous seawater (after Burke et al., 1982).

Despite the limited data for the Odin Prospect, an intense enrichment in radiogenic ^{87}Sr can be observed in both areas. Two factors may be considered to be mainly responsible for the differences in the increase of the $^{87}Sr/^{86}Sr$ ratios: 1) the amount of detrital material in the basin, and 2) time (in terms of the evolution stage of the basin and its fluids).

It appears that the magnitude of the variation range of the $^{87}Sr/^{86}Sr$ ratios in a given area provides information on the diagenetic stage and on the provenance of the participating fluids. In general, the process of diagenetic evolution is accompanied by an increase in the $^{87}Sr/^{86}Sr$ ratio which is related to the exchange with detrital material in situ, and/or to the influx of fluids displaying more radiogenic compositions.

Finally, it can be said that $^{87}Sr/^{86}Sr$ variation ranges constitute a sensitive tool for determining the stage of basin evolution, assuming the amount of Rb-bearing minerals is negligible. Furthermore, providing one is able to recognize a particular carbonate generation to be directly associated with sulphide mineralization, one could thus approximate the relative age of mineralization, with respect to the evolutionary history of the basin.

*iv) C isotopic compositions - These vary in a narrow range, which is typical for most marine carbonate rocks. However, despite subtle variations between the different generations of dolomite, results indicate an almost general trend towards lighter isotopic composition in the later crystallization generations. This trend is observed at Odin as well as Berg Aukas. The C isotope compositions must therefore be regarded in terms of an evolving fluid, slightly but continuously changing its composition during

crystallization, under conditions of burial diagenesis and a steady increase in temperatures.

v) O isotopic compositions - As with the C isotope compositions, a similar but more pronounced trend is observed with the O isotope compositions from the different areas studied. Depleted $\delta^{18}O$ values are typical of ancient dolomitic rocks, and with advancing diagenesis a clear trend is recognized. The later crystallization generations are generally depleted in ^{18}O compared to the earlier ones. Such a trend would be in agreement with decreasing isotope fractionation due to increasing temperatures, as the host sediments are subjected to progressive burial and compaction. In addition, the introduction of isotopically lighter basinal fluids and different mixing ratios, may also influence the isotopic composition of diagenetic carbonates.

Significant meteoric influence can be excluded, since the extended range of the O isotope compositions which would have been expected is not recognized.

In summary, the isotopic investigations on consecutive crystallization generations succeeded in recognizing differences in the isotopic composition, according to the position of the sample analyzed, with respect to the diagenetic crystallization sequence. With advancing diagenesis, the $^{87}Sr/^{86}Sr$ ratios show an increasing radiogenic trend and, to a lesser extent, the isotopic compositions of C and O become progressively lighter.

As an aid to exploration, the interpretation of these isotopic evolution trends, in combination with petrographic data may allow one to place constraints on the relative timing and mechanism of ore formation in the Berg Aukas and Odin areas, assuming the crystallization generation which is associated with mineralization has been successfully recognized. In both the areas studied, ore formation is viewed in close relationship with the circulation of metal-rich basinal fluids, during the late stages of diagenesis, under the influence of a regional metamorphism. These fluids were enriched in radiogenic ^{87}Sr, due to the interaction with detrital sediments within the basement rocks.

Though this study failed to provide a means of quantifying the proximity of mineralization in a given three-dimensional space, it would be possible to deduce whether or not the fluid responsible for mineralization, had infiltrated a particular area of interest.

ACKNOWLEDGMENTS

I am indebted to a great number of persons and institutions who have either directly or indirectly influenced the course of this study. In particular, I acknowledge the following:

Gold Fields South Africa Limited and Gold Fields Namibia Limited are thanked for their generous financial assistance and logistical support, without which this study would not have been possible. In particular, I am most grateful to Dr Richard Viljoen, and Messrs Basil van Tonder and Louis Krüger who found me worthy of support.

A sincere thanks is extended to Dr Hartwig Frimmel who supervised the thesis. Despite numerous personal difficulties, the encouragement and willing feedback of this dedicated earth scientist, kept me going through such difficult times. Furthermore, I am most grateful to Dr Chris Harris for his interest and assistance with the stable isotope analyses, and to Drs Richard Armstrong and Steve Richardson for their assistance with the Sr isotope analyses. Chandra Harris is particularly thanked for having helped in the sample preparation for the Sr isotope studies.

I am also especially thankful to my colleagues in Namibia, whose enthusiasm and companionship have been inspirational. I am indebted to John Deane for his willing help regarding the Odin Prospect, and for his companionship and exchange of ideas whilst on the numerous study visits to Cape Town. Messrs Clive King and Hammish McLaren are thanked for their stimulating views concerning the Berg Aukas story, and lastly to Andreas Palfi and Buks and Lilet Lubbé who made working in Berg Aukas a most worthwhile experience.

My wife Sabine is sincerely thanked for having meticulously drafted most of the illustrations.

Last but most of all, I thank my wife Sabine and young son Tim for their patience, support and understanding without which nothing would have been possible. To my late son James, who passed away tragically during the onset of this study, I dedicate this thesis to you.

REFERENCES

Adams, J.E. & Rhodes, M.G. (1960). Dolomitization by seepage refluxion. *Bull. Amer. Assoc. Petrol. Geol.*, **44**, 1912-1920.

Ahrent, H., Hunziker, J.C., & Weber, K. (1978). Age and degree of metamorphism and time of nappe emplacement along the southern margin of the Damara Orogen. *Geol. Rdsch*, **67**, 719-742.

Al-Aasm, I., Taylor, B.E. & South, B. (1990). Stable isotope analysis of multiple carbonate samples using selective acid extraction. *Chem. Geol.*, **80**, 119-125.

Allan, J.R. & Matthews, R.K. (1982). Isotope signature associated with early meteoric diagenesis. *Sedimentology*, **29**, 797-817.

Allsopp, H.L. & Ferguson, J. (1970). Measurements relating to the genesis of the Tsumeb Pipe, South West Africa. *Earth Planet. Sci. Lett.*, **9**, 448 -453.

--- Welke, H.J., & Hughes, M.J. (1981). Shortening the odds in exploration. *Nuclear Active*, **24**, 8-12.

Anderson, G.M. & Macqueen, R.W. (1982). Ore deposit models - 6: Mississippi Valley-type lead-zinc deposits. *Geoscience Canada*, **9**, 108-117.

Banner, J.l., Hanson, G.N., & Meyers, W.J. (1988). Water-rock interaction history of regionally extensive dolomites of the Burlington-Keokuk Formation (Mississippian): Isotopic evidence. *In: Sedimentology and Geochemistry of Dolostones*. Soc. Econ. Paleontologists Mineralogists Spec. Publ. No. 43, 97-113.

Bathurst, R.G.C. (1971). *Carbonate sediments and their diagenesis*. Elsevier, Amsterdam, 620 pp.

Beukes, N.J. (1989). *Report on a stratigraphic reconnaissance of the Otavi Mountain Land, and a strategy for future sedimentological work*. Gold Fields Namibia Limited unpubl. report, 13 pp.

Blattner, P. (1985). Isotope shift data and the natural evolution of geothermal systems. *Chem. Geol.*, **49**, 187-203.

Boles, J.R. (1981). Clay diagenesis and effects on sandstone cementation (case histories from the Gulf Coast Tertiary). *In:* Longstaffe, F.J. (Ed.), *Clays and the Resource Geologist*. Mineral. Assoc. Canada, Short Course Handbook, 7, 148-168.

Burke, W.H., Denison, R.E., Hetherington, E.A., Koepnick, R.B., Nelson, H.F. & Otto, J.B. (1982). Variation of seawater $^{87}Sr/^{86}Sr$ throughout Phanerozoic time. *Geology*, **10**, 516-519.

Bush, P. (1973). Some aspects of the diagenetic history of the sabkha in Abu Dhabi, Persian Gulf. *In:* Purser, E.H. (Ed.), *The Persian Gulf - Holocene Carbonate Sedimentation and Diagenesis in a Shallow Epicontinental Sea*. New York, Springer Verlag, 471 pp.

Callahan, W.A. (1964). Paleogeographic premises for prospecting for strata-bound base metal deposits in carbonate rocks. *CENTO Symposium on mining geology and base metals, Ankara, Turkey*, 191 -248.

Chilingar, G.V. (1956). Ca/Mg ratio and geologic age. *Bull. Amer. Assoc. Petrol. Geol.*, **40**, 2256-2266.

Clauer, N. & Kröner, A. (1979). Strontium and argon isotopic homogenization during low-grade regional metamorphism of pelitic sediments: the Pan-African upper Damara sequence of Northern Namibia (South West Africa). *Earth Planet. Sci. Lett.*, **43**, 117-131.

Coplen, T.B., Kendall, C. and Hopple, J. (1983). Comparison of stable isotope reference samples. *Nature*, **302**, 236-238.

Emrich, K., Ehalt, D.H. & Vigel, J.C. (1970). Carbon isotope fractionation during the precipitation of calcium carbonate. *Earth Planet. Sci. Lett.*, **8**, 363-371.

Emslie, D.P. (1980). The mineralogy and geochemistry of the copper, lead, and zinc sulphides of the Otavi Mountain Land. *National Institute for Metallurgy*, **Report 2056**, 47 pp.

Fairbridge, R.W. (1957). The dolomite question. *In:* LeBlanc, R.J. and Breeding, J.G. (Eds.). *Regional Aspects of Carbonate Deposition*. Spec. Publ. Soc. Econ. Palaeont. Mineral., 5, 125-178.

Faure, G. (1986). *Principles of Isotope Geology*. Wiley, New York, 589 pp.

--- & Powell, J.L. (1972). *Strontium isotope geology*. Springer-Verlag, Berlin, 188 pp.

Folk, R.L. (1965). Some aspects of recrystallization in ancient limestones. *In:* Pray, L.C. & Murray, R.C. (Eds.), *Dolomitization and limestone diagenesis: A symposium*. Spec. Publ. Soc. Econ. Palaeont. Mineral., 13, 14-48.

--- & Land, L.S. (1975). Mg/Ca ratio and salinity: two controls over crystallization of dolomite. *Bull. Amer. Assoc. Petrol. Geol.*, **59**, 60-68.

Friedman, I. & O'Neil, J.R. (1977). Compilation of stable isotope fractionation factors of geochemical interest. *In:* Fleischer, M. (Ed.). *Data of geochemistry*. USGS Prof. Paper, 440 pp.

Frimmel, H.E. (1988). Strontium isotopic evidence for the origin of siderite, ankerite and magnesite mineralizations in the Eastern Alps. *Mineral. Deposita*, **23**, 268-275.

--- (1991). Isotopic constraints on fluid/rock ratios in carbonate rocks: barite-tetrahedrite mineralization in the Schwarz Dolomite, Tyrol (Eastern Alps, Austria). *Chem. Geol.*, **90**, 195-209.

--- & Niedermayer (1991). Strontium isotopes in magnesites from Permian and Triassic strata, Eastern Alps. *Appl. Geochemistry*, **6**, 89-96.

--- (1992). Isotopic fronts in hydrothermally mineralized carbonate rocks. *Mineral. Deposita*, **27**, 257-267.

Frimmel, H.E. & Papesch, W. (1990). Sr, O, and C isotope study of the Brixlegg Barite deposit, Tyrol (Austria). *Econ. Geol.*, **85**, 1162-1171.

Garven, G. (1985). The role of regional fluid flow in the genesis of the Pine Point deposit, Western Canada Sedimentary Basin. *Econ. Geol.*, **80**, 307-324.

Gavine, G.H. (1979). *Aspects of the geology of the Berg Aukas Zn-Pb-V deposit*. B.Sc. Honours thesis (unpubl.), Univ. Cape Town, 37 pp.

Gregg, J.M. and Sibley, D.F. (1984). Epigenetic dolomitization and the origin of xenotopic dolomite texture. *J. Sedim. Petrol.*, **54**, 908-931.

Goodell, H.G. & Garman, R.K. (1969). Carbonate geochemistry of Superior deep test well, Andros Island, Bahamas. *Bull. Amer. Assoc. Petrol. Geol.*, **53**, 513-536.

Gorzawski, H. (1989). *Isotopic, Geochemical, and Petrographic Characterization of the Diagenetic Evolution in Carbonate-Hosted Stratabound Zn-Pb-(F-Ba) Deposits*. Heidelberg, 250 pp.

---, Fontboté, L., Sureau, J.F. & Calvez, J.Y. (1989). Strontium isotope trends during diagenesis in ore-bearing carbonate basins. *Geol. Rdsch.*, **78**, 269-290.

Grobler, N.J. (1961). *The geology of the Western Otavi Mountain Land, S.W.A.* M.Sc. thesis (unpubl.), Univ. Orange Free State, 119 pp.

Hanshaw, B.C., Back, W. & Deike, R.G. (1971). A geochemical hypothesis for dolomitization by groundwater. *Econ. Geol.*, **66**, 710-724.

Hartnady, C.J. (1978). The stratigraphy and structure of the Naukluft Nappe Complex. *14th and 15th Ann. Reps. Precambrian Res. Unit, Univ. Cape Town*, 163-170.

Hayward, A.B. and Graham, R.H. (1989). Some geometrical characteristics of inversion. *In:* Cooper, M.A. and Williams, G.D. (eds.), *Inversion Tectonics*. Geol. Soc. Spec. Publ. 44, 17-39.

Hedberg, R.M. (1979). Stratigraphy of the Owamboland Basin, South West Africa. *Bull. Precambrian Res. Unit, Univ. Cape Town*, **24**, 325 pp.

Hedge, C.E. (1974). Strontium isotopes in economic geology. *Econ. Geol.*, **69**, 823-825.

Hoagland, A.D. (1976). Appalachian zinc-lead deposits. *In:* Wolf, K.H. (Ed.). *Handbook of Strata-bound and Stratiform Ore Deposits*, **6**. Elsevier, Amsterdam, 495-534.

Holloway, J.R. (1984). Graphite-CH_4-H_2O-CO_2 equilibria at low-grade metamorphic conditions. *Geology*, **12**, 455-458.

Horton, R.A. & De Voto, R.H. (1990). Dolomitization and diagenesis of the Leadville Limestone (Mississippian), Central Colorado. *Econ. Geol.*, Monograph 7, 86-107.

--- & Geissman, J.W. (1990). Geochemistry of the Leadville Dolomite (Mississippian), Central Colorado. *Econ. Geol.*, Monograph 7, 66-85.

Jodry, R.L. (1969). Growth and dolomitization of Silurian reefs, St. Clair County, Michigan. *Bull. Amer. Assoc. Petrol. Geol.*, 52, 957-981.

Kessen, K.M., Woodruff, M.S. & Grant, N.K. (1981). Gangue mineral $^{87}Sr/^{86}Sr$ ratios and the origin of Mississippi Valley-type mineralizations. *Econ. Geol.*, **76**, 913-920.

Kröner, A. (1981). Precambrian Plate Tectonics, 57-90. *In*: Kroner, A. (Ed.). *Precambrian Plate Tectonics*. Elsevier Scientific Publishing Company, 781 pp.

--- (1982). Rb-Sr geochronology and tectonic evolution of the Pan-African belt of Namibia, southwestern Africa. *Amer. J. Sci.*, **282**, 1471-1507.

Kyle, J.R. (1981). Geology of the Pine Point lead-zinc district. *In:* Wolf, K.H. (Ed.). *Handbook of Strata-bound and Stratiform Ore Deposits*, **9**, *Regional Studies and Specific Deposits*. Elsevier, Amsterdam, 643-741..

Land, L.S. (1980). The isotope and trace element geochemistry of dolomite: the state of the art. Spec. Publ. Soc. Econ. Palaeont., **28**, 87-110.

--- (1985). The origin of massive dolomite. *J. Geol. Educ.*, **33**, 112-125.

Lange, S., Chaudhuri, S. & Clauer, N. (1983). Strontium isotopic evidence for the origin of barites and sulfides from the Mississippi Valley-type ore deposits in South-east Missouri. *Econ. Geol.*, **78**, 1255-1261.

Lippman, R. (1973). *Sedimentary Carbonate Minerals*. New York, Springer-Verlag, 228 pp.

Lombaard, A.F., Günzel, A., Innes, J. & Krüger, T.L. (1986). The Tsumeb lead-copper-zinc-silver deposit, South West Africa/Namibia, 1761-1787. *In:* Anhaeusser, C.R., and Maske, S., (Eds.). *Mineral Deposits of Southern Africa, II*. Geol. Soc. S.Afr., 2335 pp.

Lumsden, D.N. (1988). Characteristics of deep-marine dolomite. *J. Sedim. Petrol.*, **58**, 1023-1031.

--- & Chimahusky, J.S. (1980). Relationship between dolomite non-stoichiometry and carbonate facies parameters. *In:* Zenger, D.H., Dunham, J.B., and Ethington, R.L. (Eds.). *Concepts and models of dolomitization*. Soc. Econ. Paleontologists Mineralogists Spec. Publ. No. 28, 123-137.

Martin, H. (1965). The precambrian geology of South West Africa and Namaqualand. *Precambrian Res. Unit, Univ. Cape Town*, 159 pp.

--- (1978). The mineralization of the ensialic Damara orogenic belt, 405-415. *In*: Verwoerd, W.J. (Ed.). *Mineralization in metamorphic terrains*. Spec. Publ. Geol. Soc. S. Afr., **4**, 551 pp.

--- (1983a). Overview of the geosynclinal, structural and metamorphic development of the intracontinental branch of the Damara Orogen, 473-502. *In*: Martin, H. & Eder, F.W. (Eds.). *Intracontinental Fold Belts: Case Studies in the Varsican Belt of Europe and the Damara Belt of Namibia*. Springer-Verlag, Berlin, 945 pp.

--- (1983b). Alternative Geodynamic Models for the Damara Orogeny, 913-945. *In*: Martin, H. & Eder, F.W. (Eds.). *Intracontinental Fold Belts: Case Studies in the Varsican Belt of Europe and the Damara Belt of Namibia*. Springer-Verlag, Berlin, 945 pp.

Martin, H. & Porada, H. (1977). The intracratonic branch of the Damara orogen in South West Africa, 1. Discussion of geodynamic models. *Precambrian Res.*, **5**, 311-338.

Mason, R. (1981). The Damara mobile belt in South West Africa/Namibia, 745-788. *In*: Hunter, D.R. (Ed.). *Precambrian of the Southern Hemisphere*. Elsevier Scientific Publishing Company, 882 pp.

Mattes, B.W. & Mountjoy, E.W. (1980). Burial dolomitization of the Upper Devonian Miette Buildup, Jasper National Park, Alberta. *In:* Zenger, D.H., Dunham, J.B. & Ethington, R.L. (Eds.), *Concepts and Models of Dolomitization*. Spec. Publ. Soc. Econ. Palaeont. Mineral., 28, 259-297.

McKenzie, J.A., Hsü, K.J. & Schneider, J.F. (1980). Movement of subsurface waters under the sabkha, Abu Dhabi; UAE, and its relation to evaporative dolomite genesis. *In:* Zenger, D.H., Dunham, J.B. & Ethington, R.L. (Eds.), *Concepts and Models of Dolomitization*. Spec. Publ. Soc. Econ. Palaeont. Mineral., 28, 11-30.

--- (1981). Holocene dolomitization of calcium carbonate sediments from the coastal sabkhas of Abu Dhabi, U.A.E.: a stable isotope study. *J. Geol.*, **89**, 185-198.

Medfor, G.A., Maxwell, R.J. & Armstrong, R.L. (1983). $^{87}Sr/^{86}Sr$ ratio measurements on sulfides, carbonates, and fluid inclusions from Pine Point, North-west Territories, Canada: An $^{87}Sr/^{86}Sr$ ratio increase accompanying the mineralization process. *Econ. Geol.*, 78, 1375-1378.

Meyers, W.J. & Lohmann, K.C. (1985). Isotope geochemistry of regionally extensive calcite cements zones and marine components in Mississippian limestones. *In:* Schneidermann, N. & Harris, P.M. (Eds.). *Carbonate Cements*. Spec. Publ. Soc. Econ. Palaeont. Mineral., **36**, 223-240.

Miller, R. McG. (1979). The Okahandja Lineament, a fundamental tectonic boundary in the Damara Orogen of South West Africa/Namibia. *Trans. Geol. Soc. S. Afr.*, **82**, 349-361.

--- (1983). The Pan African Damara orogen of South West Africa/Namibia. *Spec. Publ. Geol. Soc. S. Afr.*, **11**, 431-515.

--- & Hoffmann, C. (1981). Geology of the Damara Belt. *Excursion Guide, Geocongress '81, Geol. Soc. S. Afr.*, 115 pp.

Misiewicz, J.E. (1985). *The classification, genesis, and geological and tectonic setting and exploration potential of the Berg Aukas Zn -Pb-V deposit*. Gold Fields Namibia Limited unpubl. report, 32 pp.

--- (1988). *The geology and metallogeny of the Otavi Mountain Land, Damara orogen, SWA/Namibia, with particular reference to the Berg Aukas Zn-Pb-V deposit - a model of ore genesis*. M.Sc. thesis (unpubl.), Rhodes Univ., 143 pp.

Moore, C.H. (1985). Upper Jurassic subsurface cements: A case history. *In:* Schneidermann, N. & Harris, P.M. (Eds.). *Carbonate Cements*. Spec. Publ. Soc. Econ. Palaeont. Mineral., **36**, 291-308.

---, Chowdhury, A. & Chan, L. (1988). Upper Jurassic Smackover platform dolomitization northwestern Gulf of Mexico: a tale of two waters. *In:* Shukla, V. & Baker, P.A. (Eds.). *Sedimentology and Geochemistry of Dolostones*,. Spec. Publ. Soc. Econ. Palaeont. Mineral., 43.

--- (1989). *Carbonate Diagenesis and Porosity*. Developments in Sedimentology 46. Elsevier Scientific Publishing Company, 338 pp.

Morrow, D.W. (1982a). Dolomite - Part 1: The Chemistry of Dolomitization and Dolomite Precipitation. *In:* McIllreath, I.A. (Ed.), *Diagenesis*. Geoscience Canada, 9, 5-13.

--- (1982b). Dolomite - Part 2: Dolomitization Models and Ancient Dolostones. *In:* McIllreath, I.A. (Ed.), *Diagenesis*. Geoscience Canada, 9, 95-107.

Muir, M., Lock, D. & Von der Borch, C. (1980). The Coorong Model for penecontemporaneous dolomite formation in the Middle Proterozoic McArthur Group, Northern Territory, Australia. *In:* Zenger, D.H., Dunham, J.B. & Ethington, R.L. (Eds.), *Concepts and Models of Dolomitization*. Spec. Publ. Soc. Econ. Palaeont. Mineral., 28, 51-68.

Ohle, E.L. (1959). Some considerations in determining the origin of ore deposits of the Mississippi Valley-type - part I. *Econ. Geol.*, **54**, 769-789.

--- (1980). Some considerations in determining the origin of ore deposits of the Mississippi Valley-type - part II. *Econ. Geol.*, **75**, 161-172.

--- (1985). Breccias in Mississippi Valley-type deposits. *Econ. Geol.*, **80**, 1736-1752.

Patterson, R.J. & Kinsman, D.J.J. (1981). Hydrologic framework of a sabkha along Arabian Gulf. *Bull. Amer. Assoc. Petrol. Geol.*, **65**, 1457-1475.

Porada, H. (1979). The Damara-Ribeiro orogen of the Pan-African Brasiliano cycle in Namibia (South West Africa) and Brazil as interpreted in terms of continental collision. *Tectonophysics*, **57**, 237-265.

--- (1983). Geodynamic model for the geosynclinal development of the Damara Orogen, Namibia, South West Africa, 503-541. *In:* Martin, H. & Eder, F.W. (Eds.), *Intracontinental Fold Belts: Case Studies in the Varsican Belt of Europe and the Damara Belt of Namibia*. Springer-Verlag, Berlin, 945 pp.

--- (1985). Stratigraphy and facies in the upper Proterozoic Damara Orogen, Namibia, based on a geodynamic model. *Precambrian Res.*, **29**, 235-264.

Radke, B.M. and Mathis, R.L. (1980). On the formation and occurrence of saddle dolomite. *J. Sedim. Petrol.*, **50**, 1149-1168.

Ricketts, B.D. (1983). The evolution of a Middle Precambrian dolostone sequence - a spectrum of dolomitization regimes. *J. Sedim. Petrol.*, **53**, 565-586.

Roedder, E. (1968). The noncolloidal origin of colloform textures in sphalerite ores. *Econ. Geol.*, **63**, 451-471.

Roering, C. (1989). *A summary of observations from a structural reconnaissance of the Otavi Mountain Land – a strategy for future structural work in the area.* Gold Fields Namibia Limited unpubl. report, 7 pp.

Sanford, B.V. (1962). Sources and occurrences of oil and gas in the sedimentary basins of Ontario. *Proc. Geol. Assoc. Canada*, **14**, 59-89.

Sangster, D.F. (1988). Breccia-hosted lead-zinc deposits in carbonate rocks. *In:* James, N.P. & Choquette, P.W. (Eds.). *Paleokarst*. Springer, New York, 102 -116.

--- (1990). Mississippi Valley-type and sedex lead-zinc deposits: A comparative examination. *Trans. Instn. Min. Metall.*, **99**, 21-42.

Searl, A. (1990). Complex sector zonation in ankerite: geochemical controls on crystal morphology and intersector element partitioning. *Mineral. Mag.*, **54**, 501-507.

Sheppard, S.M.F. (1986). Characterization and isotopic variations in natural waters. *In:* Valley, J.M., Taylor, H.P. & O'Neil, J.R. (Eds.). *Stable Isotopes in High Temperature Geological Processes*. Rev. Min., 16, 165-181.

South African Committee for Stratigraphy (SACS), (1980). The Damara Sequence, 415-438. *In:* Kent, L.E. (Compiler). *The Stratigraphy of South Africa, Part 1, Litho-stratigraphy of the Republic of South Africa, South West Africa/Namibia, and the Republics of Bophuthatswana, Transkei and Venda*. Handb. Geol. Surv. S.Afr., **8**, 690 pp.

Söhnge, P.G. (1957). *The geology of the Otavi Mountain land*. Tsumeb Corporation Limited unpubl. report, 116 pp.

--- (1964). The geology of the Tsumeb Mine, 367-382. *In:* Haughton, S.H. (Ed.). *The geology of some ore deposits in Southern Africa*. Geol. Soc. S.Afr., **2**, 739 pp.

Sverjensky, D.A. (1986). Genesis of Mississippi Valley-type lead-zinc deposits. *Ann. Rev. Earth Planet Sci.*, **14**, 177-199.

Taylor, H.P. (1977). Water/rock interactions and the origins of H_2O in granitic batholiths. *J. Geol. Soc. Lond.*, **133**, 509-558.

Tucker, M.E. (1982). Precambrian dolomites: petrographic and isotopic evidence that they were different. *Geology*, **10**, 7-12.

Turner, F.J. (1968). *Metamorphic Petrology*. McGraw-Hill, New York, 403 pp.

Valley, J.M. (1986). Stable isotope geochemistry of metamorphic rocks. *In:* Valley, J.M., Taylor, H.P. & O'Neil, J.R. (Eds.). *Stable Isotopes in High Temperature Geological Processes*. Rev. Min., 16, 165-181.

Van der Westhuizen, W.A. (1984). *The nature, genesis and geochemistry of the supergene vanadium ores of the Otavi Mountain Land*. Ph.D. thesis (unpubl.), Univ. Orange Free State, 196 pp.

Veizer, J. & Compston, W. (1974). $^{87}Sr/^{86}Sr$ composition of seawater during the Phanerozoic. *Geochim. Cosmochim. Acta.*, **38**, 1461-1484.

--- & Hoefs, J. (1976). The nature of O^{18}/O^{16} and C^{13}/C^{12} secular trends in sedimentary carbonate rocks. *Geochim. Cosmochim. Acta.*, **40**, 1387-1395.

---, Compston, W., Clauer, N. & Schidlowski, M. (1983). $^{87}Sr/^{86}Sr$ in Late Proterozoic carbonates: evidence for a "mantle" event at ~900 Ma ago. *Geochim. Cosmochim. Acta.*, **47**, 295-302.

Von der Borch, C.C. (1976). Stratigraphy and formation of Holocene dolomitic carbonate deposits of the Coorong area, South Australia. *J. Sedim. Petrol.*, **46**, 952-966.

Wanless, H.R. (1979). Limestone response to stress: Pressure solution and dolomitization. *J. Sedim. Petrol.*, **49**, 437-462.

Ypma, P.J.M. (1984). *Fluid inclusions and ore genesis in the Otavi Mountains, South West Africa. Part I: Geothermometry and barometry.* Unpubl. report, Department of Economic Geology, University of Adelaide, Australia, 84 pp.

Zenger, D.H. & Dunham, J.B. (1988). Dolomitization of Siluro-Devonian limestones in a deep core (5,350 m), Southeastern New Mexico. *In: Sedimentology and Geochemistry of Dolostones.* Spec. Publ. Soc. Econ. Palaeont. Mineral., 43, 161-173.

APPENDIX III

Detailed Sample Localities

1. BOREHOLE SAMPLES

Abbreviations:

Pd	=	Powder
P/B	=	Polished Briquette
T/S	=	Thin Section
P/T/S	=	Polished Thin Section
*	=	Local Gold Fields Namibia grid

Sample No.	Borehole No.	Collar Position Northing X-	Easting Y+	Depth (m) below collar	Type
		(Local Origin 22°S, 19°E)			
Berg Aukas Mine					
BAD 2/1	BAD 2	274456.2	77221.5	15.5	T/S, P/T/S
BAD 2/1a,b	"	"	"	"	Pd
BAD 2/2	"	"	"	58.2	Pd, T/S, P/B
BAD 2/3	"	"	"	69.2	Pd, T/S
BAD 2/5	"	"	"	110.0	T/S
BAD 2/7	"	"	"	150.0	P/T/S
BAD 2/7a,b	"	"	"	"	Pd
BAD 2/8	"	"	"	167.5	Pd, T/S
BAD 7/1	BAD 7	274031.9	77868.2	1.0	P/T/S
BAD 7/1a,b,c	"	"	"	"	Pd
BAD 7/2	"	"	"	11.5	T/S, P/T/S
BAD 7/2a	"	"	"	"	Pd
BAD 7/3	"	"	"	59.5	Pd
BAD 7/4	"	"	"	111.5	T/S, P/T/S
BAD 7/4a,b	"	"	"	"	Pd
BAD 7/5	"	"	"	170.0	P/T/S
BAD 7/6	"	"	"	201.0	T/S
BAD 7/7	"	"	"	225.0	P/T/S
BAD 7/8	"	"	"	256.0	P/T/S
BAD 7/9	"	"	"	257.0	T/S
BAD 7/10	"	"	"	282.0	"
BAD 14/2	BAD 14	274527.1	78490.8		Pd, P/T/S
BAD 14/3	"	"	"		Pd
BAD 15/12	BAD 15	274472.5	78527.2		Pd, P/T/S
BAD 15/13	"	"	"		P/T/S
BAD 15/13a,b,c	"	"	"		Pd
		(Kombat Mine grid)			
Odin Prospect					
OD 12/1	OD 12	X-257150.0	Y-93715.0	3.5	P/B, P/T/S
OD 12/2	"	"	"	26.4	"
OD 12/3	"	"	"	32.1	T/S
OD 12/4a,b	"	"	"	41.8	Pd, P/T/S
OD 12/5	"	"	"	43.6	T/S
OD 12/6	"	"	"	67.3	P/T/S

2. SURFACE SAMPLES

Sample No.	Locality Name	Northing X-	Easting Y+	Type
		(Local Origin 22°S, 19°E)		
Berg Aukas				
BAS-1	Mine Kopje - trench	274672.5	78218.1	P/T/S
BAS-1a,b	" " "	"	"	Pd
BAS-2	" " "	274636.2	78163.6	P/T/S
BAS-2a,b	" " "	"	"	Pd
BAS-3	Mine Kopje - S. adit	274663.4	78472.6	P/T/S
BAS-3a,b	" " "	"	"	Pd
Q1-1	Quarry 1	272763.6	83108.9	P/T/S
Q1-2	"	"	"	"
Q1-4	"	"	"	"
Q1-4a,b,c	"	"	"	Pd
Q1-5	"	"	"	P/T/S
Q1-6	"	"	"	"
Q1-7	"	"	"	"
Q1-10	"	"	"	Pd, P/T/S
Q2-1	Quarry 2	272818.2	83163.5	P/T/S
Q2-1a,b,c	"	"	"	Pd
K1-1	Kopje 1	273381.7	79436.2	P/T/S
K1-1a,b,c,d,e	"	"	"	Pd
K1-2	"	"	"	P/T/S
K1-2a,b,c	"	"	"	Pd
K1-3	"	"	"	P/T/S
K1-3a,b,c	"	"	"	Pd
HB-1	Heinrichsberg	277927.1	79390.7	P/T/S
HB-1a,b	"	"	"	Pd
HB-2	"	"	"	Pd, P/T/S
GS-15	Grootfontein Syncline	276781.6	79508.9	T/S
		(Kombat Mine grid)		
Odin Prospect				
OS-1	Odin	X-257140.0	Y-93738.0	Pd,P/T/S
OS-2	"	X-257173.0	Y-93715.0	P/B, P/T/S
OS-3a,b	"	X-257138.0	Y-93607.0	Pd, T/S
OS-4b	"	X-257320.0	Y-93820.0	Pd, T/S
OS-5	"	X-257166.0	Y-93720.0	T/S
Clubhead Prospect				
CH-1	Within shear zone	Grab sample		P/T/S
CH-1a,b,c	" " "	" "		Pd

APPENDIX IV

X-Ray Diffraction - Analytical Techniques

1. REFERENCE DATA

The following table lists the peak reflections for quartz, calcite and dolomite, as taken from the Joint Committee for Powder Diffraction (JCPD) cards 5-0490, 5-586 and 11-78 respectively.

Quartz			Calcite			Dolomite		
dÅ	2θ	(hkl)	dÅ	2θ	(hkl)	dÅ	2θ	(hkl)
4.26	20.85	100	3.86	23.04	102	4.03	22.06	101
3.34	26.66	101	3.03	29.43	104	3.69	24.12	012
2.46	35.22	110	2.84	31.44	006	2.88	30.99	104
2.28	39.48	102	2.49	36.00	110	2.67	33.56	006
2.23	40.31	111	2.28	39.48	113	2.54	35.34	015
2.12	40.78	200	2.09	43.18	202	2.40	37.39	110
1.98	45.82	201	1.93	47.16	204	2.19	41.18	113
1.82	50.21	112	1.91	47.53	108	2.06	43.82	021
1.80	50.72	003	1.87	48.55	116	2.01	44.99	202
			1.63	56.60	211	1.85	49.31	024
			1.60	57.45	212	1.80	50.60	018
						1.79	51.14	116
						1.78	51.30	009

Note: Conversion tables from unit Å to °2θ, based on the CuKα$_1$ sub-peaks were used in the compilation of this table.

2. MACHINE PARAMETERS

The following machine parameters were used for each of the 3 tasks that were performed by XRD:

i) Task A: General scan to record the homogeneity of each sample.

Generator Voltage	:	40 kV
Generator Current	:	30 mA
Radiation Source	:	CuKα
Filter Type	:	graphite monochromator
Slits	:	½° divergent slit
		½° receiving slit
		1° anti-scatter slit
Recording Mode	:	step-scan

Step Size	:	0.02 °2θ
Count Period	:	1 sec
Range	:	20 - 53 °2θ

ii) Task B: A short scan was performed on a few randomly selected samples, to determine the degree of non-stoichiometry (see text for details).

Generator Settings	:	(as for Task A)
Recording Mode	:	step-scan
Step Size	:	0.02 °2θ
Count Period	:	4 sec
Range	:	30.50 - 32.00 °2θ

iii) Task C: To determine the degree of dolomite crystallinity (see text for details).

Generator Settings	:	(as for Task A)
Recording Mode	:	step-scan
Step Size	:	0.02 °2θ
Count Period	:	4 sec
Range	:	$dol_{(015)}$ 35.10-35.60 °2θ
		$dol_{(110)}$ 37.20-37.60 °2θ

APPENDIX V

AAS - Analytical Technique

The following points briefly describe the laboratory procedures for the determination of selected element concentration, by means of Atomic Absorption Spectrometry (AAS).

a) Rock samples were pulverized and 100g of sample were retained.

b) Analysis of the elements Cu, Pb, Zn, Mn, Fe and Sr required a single digestion, where 0.3g of sample was dissolved in 60% perchloric acid. Matrix matching (stabilizer) was done with a combined oxalic acid mixture of 0.5% oxalic acid, 3.5% perchloric acid, 0.7% potassium chloride and 0.3% aluminium nitrate to make up a specific volume.

c) After mixing, the solution was aspirated and the various concentrations of elements were determined by atomic absorption using a Perkin Elmer 2830/PE 3030 Atomic Spectrometer. These results were compared according to the calibrated standards for each of the elements.

d) Regular check samples (duplicates) were assayed. A 95% confidence limit was considered acceptable. High range standards were used to check the instrument.

APPENDIX VI

Sr Isotopes - Analytical Techniques

1. EXTRACTION OF STRONTIUM

The following points briefly describe the sequence of events for the extraction of the Sr component of the carbonate samples that were submitted for analysis. Sample preparation took place in a clean, dust-free environment, as part of the Radiogenic Isotope Facility at the University of Cape Town.

a) Split approximately 100mg of the required sample.

b) Add distilled 0.62N HCl to the sample, and heat at 70°C overnight.

c) Centrifuge the sample to remove any undissolved material.

d) Dry solution on a hotplate.

e) Add 1ml 2.5N distilled HCl, and centrifuge.

f) Pass the solution through cation exchange columns, calibrated for the removal of Sr.

g) Dry sample.

h) Add a single drop of 7N distilled HNO_3 and dry down.

2. MASS SPECTROMETRY

Individual Sr samples were taken up into solution using a mixture of 0.48N H_3PO_4 (to enhance ionization) and 2% HNO_3, and were loaded onto single de-gassed tantalum filaments.

Analyses were carried out on a VG Sector Thermal Ionization Mass Spectrometer, with data corrected for mass fractionation using a $^{86}Sr/^{88}Sr$ ratio of 0.1194.

The following is a summary of the standard values obtained during the analysis period:

Standard used	=	NBS Standard SRM 987
Values compiled for period	=	02/02/91 to 14/03/91
Number of analyses	=	14
Mean $^{87}Sr/^{86}Sr$	=	0.710281
Standard deviation	=	0.000011
Minimum value	=	0.710263
Maximum value	=	0.710305

APPENDIX VII

Stable Isotopes - Analytical Techniques and Terminology

1. ANALYTICAL TECHNIQUES

For C and O isotope measurements of carbonates, the carbon dioxide requested for the analyses was liberated from powdered samples by reaction with 100% phosphoric acid.

X-ray diffraction analysis of each sample had revealed varying degrees of calcite contamination in the predominantly dolomitic samples. For this reason, the method of Al-Aasm et al. (1990) was employed, which involves the method of selective acid extraction at different reaction temperatures.

The powdered carbonate samples were reacted at 25°C for 2 hours, after both sample and acid had been degassed under vacuum and left to equilibrate for 2 hours at a temperature of 25.2°C. The evolved CO_2 was collected and analyzed for $\delta^{18}O$, $\delta^{13}C$ (calcite). The reaction was allowed to continue for a further 22 hours at 25°C, after which the CO_2 was discarded. The sample was then reacted for 24 hours at 50°C, the CO_2 produced during this time would then be collected and analyzed for $\delta^{18}O$, $\delta^{13}C$ (dolomite).

The O isotopic composition of the CO_2 extracted was determined using a VG Micromass 602E double collector ratio mass spectrometer. O isotope data are reported relative to the V-SMOW (Vienna - Standard Mean Ocean Water) standard, whilst a Namaqua marble was used as an in-house laboratory standard.

The following expressions were used to correct the "raw" data (δ45 and δ46 peak positions) collected from the mass spectrometer, to $\delta^{18}O$ and $\delta^{13}C$ values:

i) For samples reacted at 25°C:

$$\delta^{18}O_{V\text{-}SMOW} = [0.99679 * (\delta 46 + 0.009 * \delta 45)] + 6.095$$

$$\delta^{13}C_{PDB} = [1.03795 * (\delta 45 - 0.0338 * \delta 46)] - 22.109$$

ii) For samples reacted at 50°C:

calcite

$\delta^{18}O_{V\text{-}SMOW} = [0.9980 * (\delta 46 + 0.009 * \delta 45)] + 7.346$

dolomite

$\delta^{18}O_{V\text{-}SMOW} = [0.9964 * (\delta 46 + 0.009 * \delta 45)] + 5.701$

$\delta^{13}C_{PDB}$ = (the same equation as for 25°C)

The results are expressed using the "per mil" (‰) notation.

The relationship between the PDB and V-SMOW scales has been established by Coplen et al. (1983) as:

$$\delta^{18}O_{V\text{-}SMOW} = 1.03091\ \delta^{18}O_{PDB} + 30.91$$

or

$$\delta^{18}O_{PDB} = 0.97002\ \delta^{18}O_{V\text{-}SMOW} - 29.98$$

2. STABLE ISOTOPE TERMINOLOGY

The terminology and mathematical rationale of stable isotope geochemistry is briefly summarized below.

2.1 The Isotope Exchange Reactions

Isotope exchange reactions are equilibrium reactions in which the isotopes of a single element are exchanged between two substances. For the general case of an isotope exchange reaction between two substances A and B, where the subscripts 1 and 2 refer to the molecules totally substituted by the light and heavy isotope, respectively:

$$aA_1 + bB_2 = aA_2 + bB_1 \qquad (1)$$

The equilibrium constant for this reaction is written in the usual way:

$$K = \frac{(A_2/A_1)^a}{(B_2/B_1)^b} \qquad (2)$$

2.2 The Fractionation Factor α

The isotopic fractionation factor between two substances A and B is defined as:

$$\alpha_{A-B} = R_A/R_B \qquad (3)$$

where = $^{18}O/^{16}O$, $^{13}C/^{12}C$

In terms of δ values this expression becomes from (1):

$$\alpha_{A-B} = \frac{(1000 + \delta_A)}{(1000 + \delta_B)} \qquad (4)$$

The δ value is defined as:

$$\delta_x = [(R_x - R_{std})/R_{std})] * 10^3 \ ^o/_{oo} \qquad (5)$$

and R_x = $^{18}O/^{16}O$, $^{13}C/^{12}C$

R_{std} = corresponding ratio in standard
e.g. SMOW, V-SMOW, PDB

The fractionation factor α is related to the equilibrium constant in the following way:

$$K = \alpha = \frac{(^{18}O/^{16}O)_A}{(^{18}O/^{16}O)_B} \qquad (6)$$

It is a useful mathematical fact that $10^3 \ln (1.0X)$ is approximately equal to X. Values of α are normally very close to unity, for example 1.0025. Therefore where $\alpha = 1.0025$, $10^3 \ln\alpha = 2.5$. That is, $10^3 \ln\alpha$ is the "per mil fractionation" or the $^o/_{oo}$ fractionation. For perfect gases, lnα varies as $1/T^2$ and $1/T$ in high- and low-temperature limits respectively. In addition to this, smooth and often linear curves have been obtained when $10^3 \ln\alpha$ is plotted against $1/T^2$, for experimentally determined fractionation factors between mineral pairs or mineral-water pairs (e.g. Friedman and O'Neil, 1977). This $10^3 \ln\alpha$ is very well approximated by the value:

$$\Delta_{A-B} = \delta_A - \delta_B = 10^3 \ln\alpha_{A-B} \qquad (7)$$

please make pocket at back of thesis for maps.

135

please use lower case b r w in title

A STUDY OF THE BERG AUKAS-TYPE Pb-Zn-V DEPOSITS IN THE OTAVI MOUNTAIN LAND, NAMIBIA

by

Peter J Chadwick

Submitted in fulfillment
for the degree of Master
of Science (Geology) at the
University of Cape Town.

January. 1993

GEOLOGY OF THE BERG AUKAS AREA

SCALE 1 : 10 000

0 200 400 600 800 1000 metres

LEGEND

Major Lithotypes

- calcrete pan
- DOLOMICRITE
  - pale/light grey
  - medium-to dark grey
- LAMINATED/RYTHMITIC DOLOSTONE
  - light-to medium-grey
  - dark grey
- DOLOMITIC BOUNDSTONE/ CRYPTALGAL LAMINATE
  - medium grey
  - dark grey
- LIMESTONE
  - brown

NOTE No stratigraphic sequence is implied in this lithological column.

GEOLOGY BY P.J. CHADWICK, JUNE 1991

- definite lithological contact
- inferred lithological contact
- tectonic breccia
- solution breccia
- matrix-supported pebble conglomerate
- oolitic shoal
- cryptalgal lamination
- mega-domal stromatolites
- domal/columnar stromatolites
- finely-laminated/rythmitic mudstone/siltstone
- recrystallized dolostone (white dolospar common)
- development of colloform textures

Structural Symbols

- strike and dip of sedimentary lamination
- vertical sedimentary lamination
- strike and dip of shear (no sense of movement)
- strike-slip shear
- planar fracture/joint set
- fault with unknown sense of movement
- inferred fault
- strike-slip fault
- up-strata shear (thrusting)
- down-strata shear (sliding)

Miscellaneous Symbols

- main road
- farm road
- farm boundary fence
- major power line
- Kalkfontein 732 — farm name and number
- quarry
- dump
- mine shaft
- homestead
- Aukas — survey beacon
- Kopje 1 — exploration reference beacon

x-84 000 x-82 000 x-80 000 x-78 000 x-76 000

x-277 000 x-275 000 x-273 000

TO RUNDU

TO BERG AUKAS

TO GROOTFONTEIN

calcrete ridge

dense thorn bush

cultivated lands

Heinrichsberg

Berg Aukas 593

Kalkfontein 732

Strydfontein 1

Quarry 2

Strydfontein

Quarry 1

Kopje 1

Kopje 2

Nose Area

Nose Kopje

Aukas

mine housing

mine hostel

slimes dam

power station

slag dump

waste dump

#1 shaft

#2 shaft

electrical sub-station

A A'

B B'

C C'

D D'

N

REGIONAL LOCALITY

Ongarangombe 808 · Gaffe 713 · Venterspost 111 · Strydfontein 1 · Kalkfontein 732 · Berg Aukas Mine · Feisenquell 2 · Kranzfontein 753 · Berg Aukas 593 · GROOTFONTEIN · Ackerbau 3 · Norfolk 734 · Nyborg 733 · Philadelphia 214

19°30'S 19°30'S 18°50'E 18°50'E

0 1 2 3 4 5 Kilometres

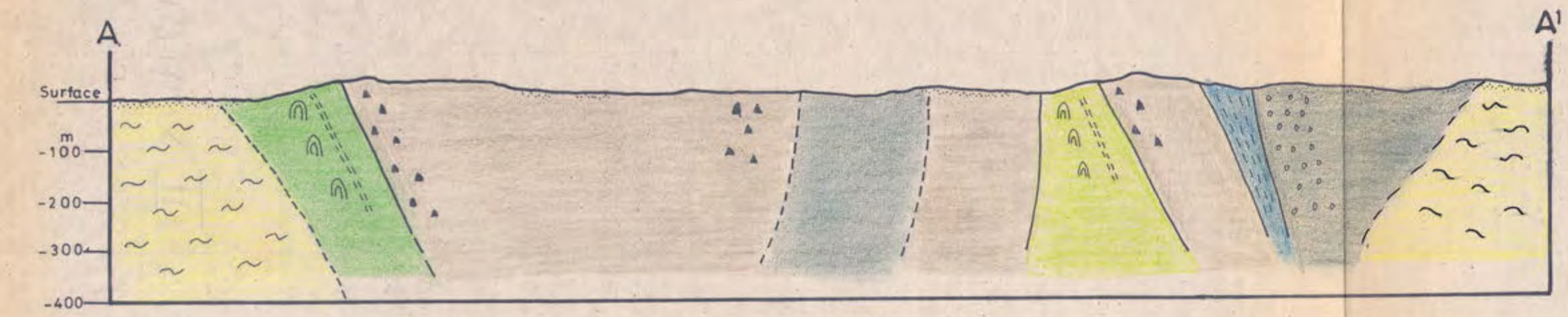

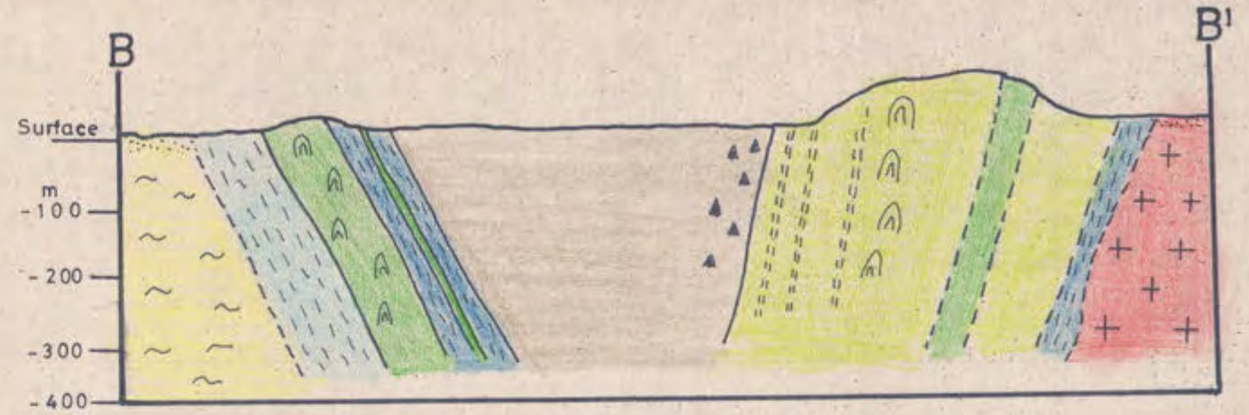

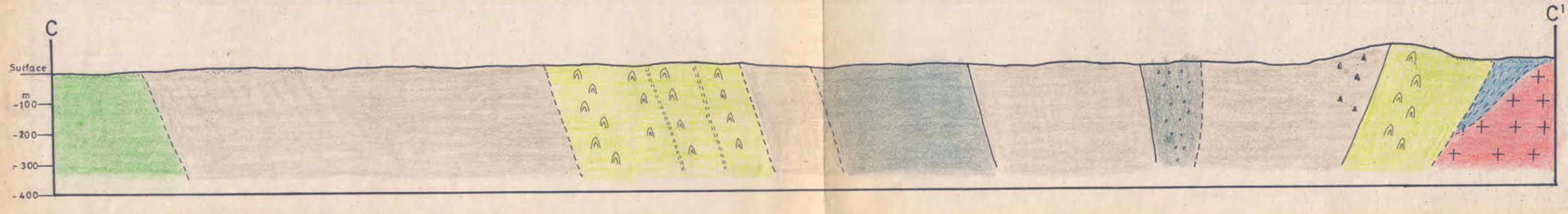

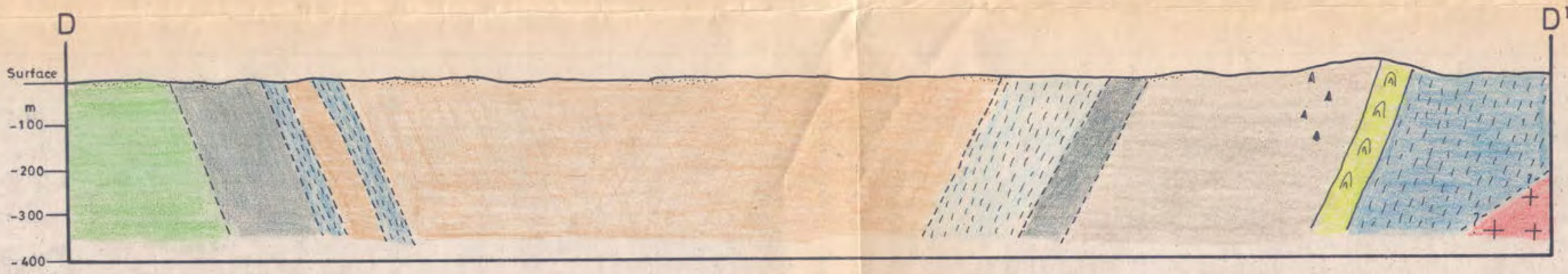

Note: No stratigraphic sequence has been inferred. The colour coding used here is based solely on the lithology.

BERG AUKAS – CROSS-SECTIONS BASED ON SURFACE GEOLOGY

SCALE 1:1 000

DOLOMICRITE:	LAMINATED DOLOSTONE:	DOLOMITIC BOUNTONE:
Pale/Light Grey.	Light to Medium Grey.	Medium Grey.
Medium to Dark Grey.	Dark Grey.	Dark Grey.
Limestone	Nosib Metasediments	Grootfontein Mafic Body